UCRL-19653

c. 2

MICROWAVE PHOTON ASSISTED TUNNELING IN SUPERCONDUCTING TUNNEL JUNCTIONS

James Newton Sweet
(Ph. D. Thesis)

August 1970

AEC Contract No. W-7405-eng-48

LAWRENCE RADIATION LABORATORY
UNIVERSITY of CALIFORNIA BERKELEY

UCRL-19653 c.2

DISCLAIMER

TABLE OF CONTENTS

and the response compared to the theoretical predictions of Werthamer. In this case, quantitative agreement with the theory is generally poor and does not appear to be correlated with sample resistance. In particular, the quasiparticle and Josephson currents do not see the same value of microwave voltage at the fundamental frequency ω.

I. INTRODUCTION

The steady state currents in a superconducting tunnel junction can be greatly altered when time varying electromagnetic fields are present in the junction barrier region. On a microscopic scale this phenomena may be thought of as an inelastic tunneling process in which one or more photons are absorbed or emitted by the tunneling electrons. On a macroscopic scale, the net effect of the inelastic photon-assisted tunneling process is to modify the dc volt-amp characteristic of the tunnel junction. The exact form of the modified characteristic depends on the spatial distribution, magnitude, and frequency of the electromagnetic field and also on the physical characteristics of the junction such as its effective area and barrier thickness. It is the purpose of this work to describe the results of some low frequency (3.8-4 Ghz) microwave-photon assisted tunneling experiments and to examine in detail how the experimental results in this frequency range compare with the various microscopic theories which have been proposed to describe photon assisted tunneling.

The tunneling of quasiparticles in the presence of a microwave field is usually designated as photon-assisted tunneling (PAT). This process was first observed experimentally by Dayem and Martin[1] and later discussed theoretically by Tien and Gordon.[2] In the Tien-Gordon (TG) Theory, the energies of the electrons in the metal electrodes are assumed to be varied adiabatically by the microwave field. This variation of electron energies results in modification of the electron energy density of states in one electrode relative to the other, and

this modification in turn affects the dc quasiparticle tunneling current. The exact form of the modified quasiparticle tunneling characteristics, in this theory, depends only on the applied microwave frequency ω and the quantity $\alpha \equiv eV/\hbar\omega$, where V_{rf} is the magnitude of the effective microwave voltage appearing across the junction. Quantitative discrepancies between theory and experiment have stimulated additional experimental studies of PAT by Cook and Everett[3] and others.[4,5] In an attempt to obtain a closer agreement between theory and experiment, Cook and Everett (EC) modified the original TG theory by assuming that the electron energy levels in each electrode were modulated in phase with the applied field but independently in magnitude, with the magnitude of the difference in electron energies being given by eV_{rf}. The resultant theory agrees more closely with some experimental data,[4,5] especially in the limit of high microwave frequencies ($\gtrsim$ 40 GHz), but is difficult to justify theoretically and does not predict the exact form of the measured current voltage (I-V) characteristic when large fields are present.

The interaction of an applied field with the Josephson[6] tunneling currents can also produce a modification of the dc I-V characteristic. This effect was predicted by Josephson in his original theoretical work on supercurrent tunneling[6,7] and subsequently semiquantitative experimental agreement with theory was obtained by Shaprio.[8] The coupling of Josephson currents to an applied rf field is complicated by the presence of self-generated ac fields and by the basic nonlinearity of the governing equations. However, the response of the Josephson current should be correlated with the quasiparticle PAT response, as both have a functional dependence on α as V_{rf} is varied, and this correlation provides a basis for extracting information about the detailed nature of the interaction of the Josephson currents with the electromagnetic fields.

We have made a series of detailed photon-assisted tunneling measurements utilizing microwave electric fields with "low" frequencies (3.8-4.0 GHz); i.e. frequencies such that $\hbar\omega/e$ is much smaller than the voltage corresponding to either the sum of the electrode energy gaps, $(\Delta_1 + \Delta_2)$ or the voltage width of the tunneling current rise at this voltage. These measurements with Sn-SnO-Pb and Sn-SnO-Sn high vacuum evaporated thin film tunnel junctions are the first detailed experimental study of photon assisted quasiparticle tunneling using low microwave frequencies and a wide range of values for the parameter α. Our results are in good agreement withthe theoretical predictions of Tien and Gordon when our junction resistances are $\gtrsim$ 1 ohm. Using the single adjustable parameter α, an excellent detailed fit can be made to the theoretical power dependence of the tunneling current as a function of bias voltage for a wide range of microwave power levels. Systematic deviations from the theory, which are observed for lower resistance junctions, can be explained quantitatively by a lumped circuit model which includes the effects of junction capacitance. Similar studies of the interaction of Josephson currents with the rf field show much worse agreement with theory. In particular, values of α derived from the quasiparticle tunneling data do not correspond to those necessary to fit the rf power dependence of the dc Josephson current.

In the next section of this paper the basic properties of superconducting tunnel junctions are reviewed with emphasis on the properties of thin film junctions. The theories of photon-assisted tunneling are discussed in Section III and the details of the experimental measurements

are described in Section IV. Experimental results and comparison with theory are presented in Section V followed by a discussion of these results and our conclusions in Section VI.

II BASIC PROPERTIES OF JUNCTIONS

A. Quasiparticle Tunneling

Evaporated film tunneling junctions are composed of two relatively thick ($\gtrsim$ 1000Å) metallic strip electrodes separated by an insulating barrier 10-30Å thick formed by oxidizing the bottom strip prior to deposition of the top electrode. The homogeneity and durability of the oxide barrier depend critically on the nature of the electrodes and the manner in which the oxide is formed. Using proper techniques,[9] it is possible to form barriers of a quality sufficient to reduce the ratio of non-tunneling current to total current to $< 10^{-3}$. For many purposes, the evaporated film junction may be analyzed theoretically as two infinite bulk electrodes separate by a uniform potential barrier through which the electron tunneling current can flow.

This basic model was first applied to superconducting tunneling by Giaever and Megerle[10] who derived an expression for the quasiparticle current using a semiconductor junction type of single particle tunneling model.[11] The Giaever expression for the current as a function of bias voltage is

$$I = (G_{NN}/e) \int_{-\infty}^{\infty} N_\ell (E-eV)\, N_r(E)\, [f(E-eV) - f(E)]\, dE, \qquad (1)$$

where $f(E) = [\exp (E/k_BT) + 1]^{-1}$ and N_ℓ and N_r are the energy densities of states on the left and right hand sides of the barrier measured relative to the density of states at the Fermi energy. G_{NN} is the normal state conductance, given by the formula,

$$G_{NN} = (4\pi e/\hbar)\, |T|^2\, \rho_\ell(0)\, \rho_r(0)\, A, \qquad (2)$$

where $\rho_{\ell,r}(0)$ is the density of states at the Fermi energy, A is the junction area, and **T** is an average tunneling matrix element[12,13] which is proportional to the one electron barrier penetration probability and assumed to be constant. In the BCS constant energy gap model, the reduced density of states function is given by the expression,[14]

$$\begin{aligned} N_i(E) &= 0 && |E| \leq \Delta_i \\ &= |E|/(E^2 - \Delta_i^2)^{1/2} && |E| \geq \Delta_i \end{aligned} \tag{3}$$

where $i = \ell, r$, and Δ_i is the temperature dependent BCS energy gap parameter. Equation (1), together with the density of states factors given by Eq. (3), predicts quite accurately the major features of the temperature dependent I-V characteristics of superconductor-insulator-normal (S-I-N) and superconductor$_1$-insulator-superconductor$_2$ (S_1-I-S_2) junctions. Examples of normalized I-V characteristics for a Sn-I-Pb and a Sn-I-Sn junction are shown in Figs. (1a) and 1(b) respectively. The major features of the I-V characteristic are a cusp like peak at $V = \Delta_2 - \Delta_1$ (for a junction composed of non-identical superconductors) and the discontinuous jump in the current at $V = \Delta_1 + \Delta_2$. The $\Delta_2 - \Delta_1$ peak is theoretically a logarithmic singularity,[15] while the current jump at $\Delta_1 + \Delta_2$ is predicted to have magnitude,

$$\begin{aligned} \delta I &= (\pi G_{NN}/4e)\ (\Delta_1(T)\ \Delta_2(T))^{1/2}\ [\tanh\ (\Delta_1(T)/2k_BT) \\ &+ \tanh\ (\Delta_2(T)/2k_BT)] \end{aligned} \tag{4}$$

Both the peak and the discontinuity are consequences of the square root singularity of the BCS model density of states at $E=\Delta$. In models with a continuous density of states function the cusp at $\Delta_1 - \Delta_2$ will become rounded and the slope of the I-V curve at $\Delta_1 - \Delta_2$ will be finite.[16,17]

In actual junctions, the conductance, dI/dV at $V = \Delta_1+\Delta_2$ is always finite, and typically has a value, $dI/dV\ (\Delta_1+\Delta_2) \simeq 15\ G_{NN}$. Figures 10 and 19 show examples of actual I-V characteristics for a Sn-SnO-Sn and Sn-SnO-Pb junction respectively compared to the predictions of the BCS model as calculated from Eq. (1). In each of the figures the curve designated $I_o(V)$ represents the measured I-V characteristic. At sufficiently low temperatures such that $\Delta_1(T) \simeq \Delta_1(0)$ and $\Delta_2(T) \simeq \Delta_2(0)$, where $\Delta_1(0)$ and $\Delta_2(0)$ are the zero temperature energy gaps, the width of the current increase at $V = \Delta_1+\Delta_2$ is typically $\delta V \simeq (\Delta_1+\Delta_2)/15$. Althought this width is often attributed to "thermal smearing", measurements by Giaever[16] and Zavaritskii[18] at temperatures down to 0.1 °K have shown that the width does not decrease with temperature as one would expect for thermal smearing effects, but instead remains constant for temperatures below which the energy gaps nearly equal their zero temperature values.

Various mechanisms have been proposed to explain the width of the current rise at $V = (\Delta_1+\Delta_2)/e$ in the tunneling characteristic. In an early study of quasiparticle tunneling by Townsend and Sutton,[19] the following mechanisms were proposed to explain the width: inhomogeneities and strains in the superconducting films, quasiparticle and electron-phonon lifetime effects, and anisotropy ($\underset{\sim}{k}$ dependence) of the superconducting energy gap. Any or all of these effects could in principle modify the BCS density of states in such a way as to introduce the finite width at $\Delta_1+\Delta_2$. We shall discuss each of these effects in turn and compare previous experimental results for energy gaps and widths of various types of junctions with our own results for Sn-SnO-Sn and Sn-SnO-Pb junctions.

Inhomogeneities or strains in the electrode surfaces could cause variations in impurity concentration or density to occur over distances large compared to the coherence length, ξ_0. These variations would in turn lead to regions of varying transition temperature and energy gap in the metal films. The net current would then be the result obtained by averaging Eq. (1) over the area of the junction. If inhomogeneity is an important contributor to energy gap smearing, then it might logically be expected that measured I-V characteristics would vary from sample to sample, and that the value of the average gap and its width would be strongly dependent on conditions of sample preparation. Significant variations in the average gap have in fact been observed in junctions with aluminum[16,18-21] and niobium[19] bottom electrodes, although some of the spread in reported values of the energy gap for a given material must be attributed to inequivalent methods of determining Δ from experimental I-V graphs. We have used a method described by McMillan and Rowell[22] in determining experimental values of $2\Delta_{Sn}$ and $\Delta_{Pb}+\Delta_{Sn}$, and have found less than 1% variation in zero temperature gap values for all junction which showed well defined quasiparticle tunneling characteristics. There was also no noticeable variation in the shape of the I-V curves from sample to sample in the region of the maximum conductance. From this evidence we are led to the conclusion that strain broadening of the gap, while possible, is probably not responsible for the energy gap smearing seen in Pb and Sn films.

If electron-phonon lifetime effects were important mechanisms for energy gap smearing we would expect to observe a strong temperature

dependence in the broadening because the average number of phonons present is a rapidly varying function of temperature near $T = 0^{\circ}K$. No temperature dependence of the gap width is in fact observed after the temperature decreases to a value such that $T/T_c \lesssim 0.36$ (where $\Delta(T)/\Delta(0) \geq .99$). It is thus unlikely that this mechanism is responsible for Δ broadening. When lifetime effects are included in the BCS theory the quasiparticle energy levels, $E_{\underset{\sim}{k}}$, will be broadened by an amount $\delta E_{\underset{\sim}{k}} \sim \hbar/\tau_{\underset{\sim}{k}}$, where $\tau_{\underset{\sim}{k}}$ is the lifetime of the state associated with wave vector $\underset{\sim}{k}$. Recent calculations by Scalapino and Taylor[23] indicate that these lifetime effects are not large enough to explain the Δ width which is observed in nuclear spin relaxation measurements, and which is comparable in magnitude to that seen in tunneling experiments. We are thus left with gap anisotropy effects as the most probable candidate for the dominant mechanism causing broadening of the width of the current jump at the gap edge.

Wave vector dependence of the energy gap was predicted by the original BCS theory and is thought to be consequence of both Fermi surface and phonon spectrum anisotropies. A film composed of crystallites with linear dimensions greater than the coherence length ξ_0 might be expected to show behavior characteristics of a distribution of gaps centered about some average value. The detailed nature of the gap distribution function would depend on the distribution of crystallite orientations in the evaporated films. Tunneling experiments have been performed using junctions composed of a bulk single crystal electrode and evaporated film counter electrode. Results of measurements by Zavaritskii[24,25] on Sn-(single crystal)-SnO-Sn and by Blackford and March[26] on Pb (single crystal)-PbO-Pb junctions indicate that the energy gap is in fact a function of crystal orientation. Zavaritskii's measurements with Sn junctions

indicate a spread in Sn double gap values, $0.8 \lesssim 2\Delta_{Sn}(0) \lesssim 1.3$ me V, which is about six times larger than the gap width observed in thin film junctions (See Fig. 2). Blackford and March's measurements show a range of lead gap values, $2.36 \leq 2\Delta_{Pb}(0) \leq 2.78$ meV, a spread roughly twice the voltage width of the current rise observed in a single measurement at one crystal orientation. In addition, the Blackford and March measurements show the presence of structure corresponding to two energy gaps in Pb at all crystal orientations, as do experiments using evaporated film junctions with thick Pb counter electrodes[17,19,27].

Several explanations have been advanced to account for the observed two gap structure. Cambell and Walmsley[27] conjecture that the crystallites assume two preferential orientations in the evaporated film, resulting in the presence of two peaks in the effective gap distribution function for the film. Rochlin[17] has interpreted the structure as being the result of critical points in an energy gap distribution function, as predicted by Bennett's[28] theory of the Pb gap anisotropy, in which the phonon spectrum is considered to be the principle cause of the gap anisotropy. Blackford and March[26] have interpreted the two gap structures in lead as being a consequence of the presence of two different groups of tunneling electrons; one group from the second Brillouin zone hole surface and another group from the third zone electron surface. Our experiments with Sn-SnO-Pb samples produced no evidence of twin Pb gap behavior, even for junctions with Pb electrodes as thick as 10,000Å. The basic cause of energy gap structure, and smearing thus appears to be associated with gap anisotropy, but at this time there is no theory which predicts in detail the exact shape of the function I(V) for any thin film junction.

Although the exact shape of the quasiparticle I-V characteristic apparently cannot be predicted from first principles, several phenomenological models have been proposed which can produce reasonably good agreement with experimental characteristics. Giaever et al[16] modified the BCS density of states, Eq. (3) by introducing a breadth function, $\gamma(E-E')$ as suggested by Hebel and Slichter.[29] Using the density of states function,

$$N_T(E) = \int_{-\infty}^{\infty} N_{BCS}(E) \quad \gamma(E-E')\, dE' \tag{4}$$

with $\gamma(E-E')$ given by,

$$\gamma(E-E') = 1/(2\Delta(0)\epsilon) \qquad E - \Delta(0)\epsilon \leq E' \leq E + \Delta(0)\epsilon$$

$$\gamma(E-E') = 0 \qquad E' \text{ outside } [E - \Delta(0)\epsilon,\ E + \Delta(0)\epsilon],$$

they produced a reasonably good fit to an experimental Sn-SnO-Sn I-V trace by choosing $\epsilon = 0.03$. Most of the discrepancy between their calculated and experimental curves at voltages below $2\Delta_{Sn}(0)$ is probably due to the presence of nontunneling currents in the junction. Bennett[28] has proposed a more involved model for calculating the tunneling density of states. Using some results of the theory of strong coupling superconductivity,[30] he suggested the following expression for $N_T(E)$,

$$N_T(E) = \frac{\rho(0)}{4\pi} \int_{-1}^{1} d(\cos\theta) \times \int_{0}^{2\pi} d\phi \ \mathrm{Re}\left\{\frac{E}{[E^2-\Delta^2(E,\theta,\phi)]^{1/2}}\right\}, \tag{5}$$

where $\rho(0)$ is the density of states at the Fermi surface, θ and ϕ are the $\underset{\sim}{k}$ vector azimuthal and polar angles in the reciprocal lattice, and the energy dependence of Δ is described by strong coupling theory. If the energy dependence of Δ is neglected, Eq. (5) can be written in the form,

$$N_T(E) = \rho(0) \int_0^E \frac{E}{(E^2-x^2)^{1/2}} g(x)dx, \qquad (6)$$

with the gap distribution function g(x) given by

$$g(x) = (1/4\pi) \int_{-1}^{1} d(\cos\theta) \int_0^{2\pi} d\phi\ \delta(x-\Delta(\theta,\phi)) \qquad (7)$$

If we let $g(x) = \delta(x-\Delta)$ we recover the strong coupling theory equivalent of the BCS constant energy gap model,

$$N_T(E) = \rho(0)\ \mathrm{Re}\left\{\frac{E}{(E^2-\Delta^2)^{1/2}}\right\} \qquad (8)$$

Rochlin[17] has solved a simple model using a triangular distribution function given by the expression,

$$\begin{aligned} g(x) &= \frac{1}{\epsilon^2\Delta^2}\,[x-\Delta(1-\epsilon)] && \Delta(1-\epsilon) \le x \le \Delta \\ &= \frac{1}{\epsilon^2\Delta^2} = [\Delta(1+\epsilon)-x] && \Delta \le x \le \Delta(1+\epsilon) \\ &= 0 && \text{elsewhere,} \end{aligned} \qquad (9)$$

where ϵ is a gap spreading parameter such that the effective distribution width is $2\Delta\epsilon$, and Δ is the average gap. With the proper choice of ϵ the tunneling density of states derived from Eqs. (6) and (9) can be used in Eq. (1) to predict quite accurately a measured I-V characteristic.

At low bias voltages, $V \ll \Delta_1 + \Delta_2$, the observed current is usually somewhat larger than the current predicted by the BCS model. An example of this type of behavior for a Sn-SnO-Sn junction with a 1.31Ω normal state resistance is shown in Fig. 2. The rapid increase in current near $V = \Delta_{Sn}$ has been attributed to the onset of multiparticle tunneling processes[31,32] in which more than one electron is transferred across the barrier by the tunneling Hamiltonian interaction. A comparison of

single particle, double particle, and Josephson tunneling processes is shown schematically in Fig. 3 . Both double particle tunneling process illustrated in Fig.3c,d have a threshold energy $eV = \Delta$ for a symmetrical junction, but the theory of Schrieffer and Wilkins[31] predicts that the intensity of the total double particle current will be reduced by a factor of $\sim e^{-20}$ relative to the single particle current because of the presence of an additional factor of T^2 in the two particle current formulas.[33] The experimentally observed current increase at $eV = \Delta$ is often many orders of magnitude larger than that predicted by the multiparticle tunneling theory, and the width of the current rise is much larger than the width of the 2Δ rise. Similar effects have been observed in Pb-I-Pb junctions by Rowell and Feldmann.[34]

In order to obtain agreement between the theoretical and experimental two particle currents, Schrieffer and Wilkins postulated the existence of a distribution of low spots in the oxide through which most of the two particle current passed. However, our experimental studies of the response of the dc Josephson current to an externally applied magnetic field indicate that tunneling currents flow quite uniformly over the barrier area. Thus, there appear to be serious discrepancies between experiment and the multiparticle tunneling theory. Other processes which have been suggested to explain the Δ current rise include the excitation of collective modes in the superconducting electrodes[34] and the absorption of ac Josephson photons by the pair tunneling currents.[32] Neither of these processes has been theoretically analyzed to a point at which quantitative comparison with experiment can be made.

The background excess current evident in Fig. 2 at bias voltages $V < \Delta_{Sn}$ is of unknown origin, but could well be a result of ordinary transport currents flowing through shorts or weak spots in the oxide barrier. The magnitude of the excess current varied from sample to sample in our experimental studies, indicating that it is more dependent on the physical condition of the oxide barrier than on the details of the interactions in the junction. At voltages $V \gg \Delta_1+\Delta_2$, the small excess current is completely unnoticable and the theoretical current calculated with Eq. (1) will fit experimental results very closely if G_{NN} is used as an adjustable parameter determined by fitting experimental and theoretical currents at one value of bias voltage. Some extremely small deviations from Eq (1) occur because of strong coupling phonon induced structure[35] in the I-V characteristic , but these deviations will usually only be noticable in the derivative, dI/dV, since derivatives tend to magnify small sharp irregularities.

B. Josephson Tunneling

The phenomena of pair or supercurrent tunneling through the thin non-superconducting barrier was originally predicted theoretically by Josephson[6,7] and is essentially a consequence of long range phase coherence or phase locking of electron pairs in the superconducting state. Several excellent reviews have been given on the subject of Josephson tunneling[36-38] and so we shall simply set forth those results of the theory which are relevant to our experimental investigations.

The superconducting state may be described by a complex order parameter $\psi(r,t) = |\psi(r,t)|e^{i\theta(r,t)}$ which may be thought of as a wave-function characterizing the superconductor as a whole. The density of

paired electrons in the superconductor is given by $|\psi(r,t)|^2$ and the phase of the order parameter is specified by $\theta(r,t)$. For the ideal junction geometry illustrated in Fig. 4, the basic Josephson equations relate the fields and current density in the junction to the pair phase parameter $\phi(x,t)$, defined as,

$$\phi(\underset{\sim}{x},t) = \theta_2(\underset{\sim}{x},t) - \theta_1(\underset{\sim}{x},t) - \frac{2e}{\hbar c} \int_{P_1}^{P_2} \underset{\sim}{A}(\underset{\sim}{x},t)\cdot d\underset{\sim}{\ell}\,.$$

Here $\underset{\sim}{x}$ is the position vector in the x-y plane of the junction, $\underset{\sim}{A}$ is the vector potential, and P_1 and P_2 are positions with the same value of $\underset{\sim}{x}$ in the left and right hand electrodes respectively. The gradient of the phase parameter is given by

$$\phi(x,t) = (2ed/\hbar c)\, \underset{\sim}{H}(x,t) \times \underset{\sim}{n}, \tag{10}$$

where $\underset{\sim}{n}$ is a unit vector in the z direction H, is the magnetic field, and d is the effective magnetic field penetration length,

$$d = \lambda_1 + \lambda_2 + \ell, \tag{11}$$

as shown in Fig. 4. The time derivative of ϕ is related to the potential drop, $V(\underset{\sim}{x},t) = V_1(\underset{\sim}{x},t) \leq V_2(\underset{\sim}{x},t)$, across the barrier by,

$$\frac{\partial \phi}{\partial t}(\underset{\sim}{x},t) = \frac{2eV}{\hbar}(\underset{\sim}{x},t), \tag{12}$$

where the voltage is given by the expression,

$$V(\underset{\sim}{x},t) = 1/e\,[\mu(P_1) - \mu(P_2)] - 1/c \int_{P_1}^{P_2} \frac{\partial \underset{\sim}{A}}{\partial t} \cdot d\underset{\sim}{\ell}, \tag{13}$$

and μ is the chemical potential which for our purposes can be taken equal to the electrostatic potential.

The relation between the current density in the junction and the pair phase ϕ is, in general, quite complicated when fields of arbitrary strength are present in the barrier region. A full discussion of this

matter has been given by Werthamer[38] who has calculated the time dependent current in the framework of the BCS model. For most purpose, the current-phase relationship is well approximated by,

$$j_S(\underset{\sim}{x},t) = j_1 \sin\phi(\underset{\sim}{x},t) \qquad (14)$$

where j_S is the supercurrent component of the total current and j_1 is a constant, which in the BCS model for a junction composed of identical superconductors is given by,[38]

$$j_1 = (\pi\Delta(T)/2R_{NN}A)\tanh[\Delta(T)/2k_BT] \qquad (15)$$

with $R_{NN} = 1/G_{NN}$, the normal state resistance, and A = effective junction area. Equation (14) is most valid in the region where the time dependent voltage is small compared with $(\Delta_1+\Delta_2)/e$, at frequencies $\hbar\omega \ll (\Delta_1+\Delta_2)$, and dc bias voltages, $V_{dc} \ll (\Delta_1+\Delta_2)/e$.

The basic relations Eqs. (10), (12), and (14), when augmented by the Maxwell curl H equation written in the form,

$$\frac{\partial H_x}{\partial y} - \frac{\partial H_y}{\partial x} = \frac{4\pi}{c} j_z + \frac{1}{c}\frac{\partial D_z}{\partial t}, \qquad (16)$$

are sufficient in principle to solve for all this currents, voltage, etc. in the junction. In the case of the planar junction geometry we assume that the z component of the electric field is confined to the barrier region and that it is related to D_z by,

$$D_z(x,t) = \epsilon_s E_z(x,t),$$

where ϵ_s is the dielectric constant of the barrier region. Since the electric field is related to the voltage drop V(x,t) by,

$$V(\underset{\sim}{x},t) = \ell E_z(\underset{\sim}{x},t),$$

Eq. (15) may be rewritten in this form,

$$\frac{\partial H_x}{\partial y} - \frac{\partial H_y}{\partial x} = \frac{4\pi}{c}\left[j_{qp}(\underset{\sim}{x},t) + j_1 \sin\phi\,(\underset{\sim}{x},t)\right] + \frac{\epsilon_s}{c\ell}\frac{\partial V}{\partial t}, \tag{17}$$

where j_{qp} is the quasiparticle tunneling current density.

A single differential equation for either ϕ or V may be derived from Eqs. (10), (12), (14), and (17) by elimination of the other dependent variables. The equations for ϕ is given by

$$\nabla^2\phi - \frac{1}{v_J^2}\frac{\partial^2\phi}{\partial t^2} = \frac{1}{\lambda_J^2}\sin\phi \tag{18}$$

$$v_J = (\ell/\epsilon_s d)^{1/2}\, c \tag{19}$$

$$\lambda_J = [\hbar c^2/8\pi e d\, j_1]^{1/2} \tag{20}$$

v_J (often referred to as $\bar{c}$ in the literature) is the phase velocity of electromagnetic radiation propagating in the barrier region with a $\underset{\sim}{k}$ vector in the x-y plane. Using the typical values, $d \simeq 1000\text{Å}$, $\ell \simeq 30\text{Å}$, $\epsilon_s \simeq 4$, we find a typical value for v_J is c/12. The basic cause of the small value of v_J is the confinment of rf E fields to the thin barrier region of thickness ℓ while rf H fields can penetrate a distance $\lambda \simeq d/2$ into each superconductor. If electromagnetic radiation propagates down a stripline, the phase velocity is given by

$$v_p = 1/(LC)^{1/2} \tag{21}$$

where L and C are the inductance and capacitance per unit length of the line. For a line of width w and thickness t, L and C are given in esu by the expressions,

$$C = \epsilon w/4\pi t \tag{22}$$

$$L = 4\pi\mu t/c^2 w \tag{23}$$

Since C is related to the electric field and L to the magnetic field, we let $t = \ell$ in Eq. (22) and $t = d$ in Eq. (23). Then, taking $\mu = 1$, we obtain the result, $v_p = v_J$ by substituting (22) and (23) into Eq. (21).

The parameter λ_J is known as the Josephson penetration length because it represents a transverse screening length for the Josephson currents. For a junction with a width L larger than λ_J the magnetic field produced by the supercurrent will tend to screen out the current and confine it to a region of size λ_J at the edge of the junction. For the dc or zero-voltage Josephson current, V = 0, and from Eq. (12) $\partial\phi/\partial t = 0$. If the y dependence of $\phi(\underset{\sim}{x},t)$ is negligible, Eq. (18) may be written, $d^2\phi(x)dx^2 + (1/\lambda_J^2) \sin \phi(x) = 0$ (24)

Solutions to Eq.(24) have been obtained by Owen and Scalapino[39] for a range of values of L/λ_J. The static magnetic field H enters the problem through the boundary conditions on ϕ at the edges of the junction as discussed in Ref. (39). For a narrow junction (e.g. width $L < \lambda_J$) the magnetic field is approximately constant in the barrier region. The solution of Eq (10) for a field H_o in the y direction is then,

$$\phi(x) = \phi_o - kx \tag{25}$$

$$k = 2ed H_o/\hbar c \tag{26}$$

The current density from Eq. (14) is,

$$j = j_1 \sin (\phi_o - kx) \tag{27}$$

and the total current is then given by

$$I_J = j_1 A \times \frac{1}{L} \int_{-L/2}^{L/2} \sin(\phi_o - kx)\, dx$$

$$= j_1 A \sin\phi_o \sin[\pi \Phi/\Phi_o]/[\pi\Phi/\Phi_o] \qquad (28)$$

Φ is the magnetic flux in the junction, given by,

$$\Phi = H_o L d \qquad (29)$$

and Φ_o is the flux quantum, hc/2e. In cgs units, $\Phi_o = 2.07\times10^{-7}$ G-cm^2. The constant ϕ_o is determined in practice by the current supplied to the junction from the bias supply. When ϕ_o reaches the value $\pi/2$, the junction will be carrying the maximum possible zero voltage current and any further increase in current will cause the junction to make a transition to a non-zero voltage state. The zero-voltage current, I_J will be zero whenever the field H_o reaches a magnitude such that, $\Phi = n\Phi_o$ For a Sn-I-Sn junction with L = 0.2 mm and $\lambda \simeq 400$Å, the first zero of I_J occurs at a field, $H_o \simeq 1.3$G.

The value of the Josephson penetration depth, λ_J, given by Eq. (20) may be expressed in the practical units as,

$$\lambda_J(\text{mm}) = 11.5\,(j_1(\text{amp/cm}^2)\,\lambda_L(\text{Å}))^{-1/2}, \qquad (30)$$

where we have considered a junction composed of identical superconductors and neglected this oxide thickness ℓ in comparison with the London penetration length λ_L. For an 0.1Ω Sn-I-Sn junction with an area A = .2mm×.2mm the value of j_1 calculated from Eq. (15) is, $j_1 = 23.6$ A/cm^2, resulting in a value of λ_J, $\lambda_J = 0.12$ mm. For junctions with longer normal state resistance, λ_J will increase as $(R_{NN})^{1/2}$.

The detailed calculation of Owen and Scalapino[39] predict that for $L < 2\lambda_J$ the current density will be uniform across the junction and the field dependence of I_J for a rectangular junction will be governed by

Eq. (28). For larger values of L self-screening becomes important and the current and $\underset{\sim}{H}$ field tend to be excluded from the center region of the junction just as they are from a bulk superconductor. Experimental studies of the magnetic field dependence of I_J by Matisoo[40] and by Schwidtal and Finnegon[41] have verified the Owen and Scalapino predictions in great detail for a wide variety of geometries and L/λ_J ratios. We thus assume that Eq. (28) correctly predicts the magnitude of I_J in the region $L/\lambda_J \leq 2$, and that experimental deviations from this formula are caused by either barrier inhomogeneities or nonuniform transport current flow in the strip electrodes rather than by failure of the theory.

When there is a dc voltage bias V_o across the junction, which is much larger than any ac voltages present, Eqs. (10) and (12) have the approximate solution,

$$\phi(y,t) = \phi_o + \omega_o t - kx, \tag{31}$$

$$\omega_o = 2e V_o/\hbar. \tag{32}$$

The current density then becomes,

$$j = j_1 \sin(\phi_o + \omega_o t - kx) \tag{33}$$

indicating that an ac supercurrent of angular frequency ω_o will be generated by the presence of a finite dc bias voltage. In the case where large ac voltages are present, the approximations leading to Eq. (29) break down and a more careful analysis must be made. The nonlinearity of Eq. (17) and the unknown nature of the exact boundary conditions which should be placed on ϕ preclude exact solution of the general problem. Some of the approximate solutions which have been proposed for Eq. (17) will be discussed in the next section where we consider the interaction between rf fields and tunneling currents.

III. THEORY OF TUNNELING CURRENT-ELECTROMAGNETIC FIELD INTERACTIONS

A. Basic Theory

In this section we shall discuss the basic theory of tunneling in the presence of time varying electric and magnetic fields which may be either externally applied or self-generated by the ac Josephson currents. General discussions of tunneling in the presence of ac fields have been given by a number of authors. Riedel[43] has discussed the problem of a tunneling current in the presence of a spatially independent ac voltage of a single frequency. Larkin and Ovchinnikov[44] have studied the problem of a tunneling current interacting with a general time dependent but spatially independent scalar potential $V(t)$. Werthamer[38] has generalized these discussions to the case where a general time dependent field $\underset{\sim}{E}(\underset{\sim}{r},t)$ is present in the barrier region between the superconducting electrodes. We shall set forth the general results of Werthamer's discussion and then use these results to discuss photon assisted tunneling processes involving both the Josephson and the quasiparticle currents.

The problem of finding the time dependent current in the presence of applied and self-induced fields is essentially that of solving the electromagnetic wave equation,

$$(\nabla^2 - \varepsilon/c^2)\underset{\sim}{E}(\underset{\sim}{r},t) = \frac{4\pi}{c^2}\frac{\partial \underset{\sim}{j}}{\partial t}(\underset{\sim}{r},t) , \qquad (34)$$

subject to proper boundary conditions on $\underset{\sim}{E}$. The usual analytical method of attacking the problem is to express the current density $\underset{\sim}{j}(\underset{\sim}{r},t)$ as a functional of the time dependent electric field and static magnetic field. Eq. (34) can then be solved in some approximate manner subject

to an assumed set of boundary conditions. An exact specification of appropriate boundary conditions on $\underset{\sim}{E}$ is precluded by the complicated junction geometry and uncertainties concerning the oxide barrier structure. As a result, fairly sweeping assumptions and generalizations must be made before the fields can be calculated from Eq. (34). In problems involving only the Josephson current interacting with its self-generated fields, the current is sometimes calculated by solving various linearized forms of Eq. (18).[45-46] These methods are equivalent to solving Eq. (34) directly with the assumptions that,

$$V(\underset{\sim}{x},t) = \ell E(\underset{\sim}{x},t), \tag{35}$$

and that the relations between the current, voltage, and phase parameter are given by Eqs. (12) and (14).

The first step in solving Eq. (34) is to derive an appropriate form for $\underset{\sim}{j}(\underset{\sim}{r},t)$ from microscopic theory. By using thermodynamic Green's functions and first order perturbation theory within the tunneling Hamiltonian formalism, Ambegaokar and Baratoff[42] derived an expression for the current density in a junction with no time dependent fields present. Werthamer[38] has generalized this discussion to take into account time varying fields and has shown that the current in a junction with $L \lesssim 2\lambda_J$ can be calculated from the formula,

$$j(\underset{\sim}{x},t)=\mathrm{Im}\int_{-\infty}^{\infty} d\omega \int_{-\infty}^{\infty} d\omega' \Big\{ W(\omega)W^{*}(\omega')e^{-i(\omega-\omega')t}\, j_1(\omega'+\omega_o/2)$$

$$+W(\omega)W(\omega')e^{-i(\omega+\omega')t+i\phi+i\alpha}\, j_2(\omega'+\omega_o/2)\Big\}, \tag{36}$$

where the current amplitudes are given by,

$$J_1(\omega) = \frac{2e\pi}{\hbar} \sum_{\underset{\sim}{k}\underset{\sim}{q}\sigma} \int_{-\infty}^{\infty} d\omega_1 \int_{-\infty}^{\infty} d\omega_2 [f(\omega_1)-f(\omega_2)] |T_{\underset{\sim}{k}\underset{\sim}{q}}|^2 A_{\underset{\sim}{k}}(\omega_1) A_{\underset{\sim}{q}}(\omega_2)$$

$$\times [\omega_1-\omega_2-\omega+i0^+]^{-1} \tag{37}$$

$$J_2(\omega) = \frac{2e\pi}{\hbar} e^{-i\alpha} \sum_{\underset{\sim}{k}\underset{\sim}{q}\sigma} \int_{-\infty}^{\infty} d\omega_1 \int_{-\infty}^{\infty} d\omega_2 [f(\omega_1)-f(\omega_2)] T_{\underset{\sim}{k},\underset{\sim}{q}} T_{-\underset{\sim}{k},\underset{\sim}{q}}$$

$$\times |\bar{B}_{\underset{\sim}{k}}(\omega_1) B_{\underset{\sim}{q}}(\omega_2) [\omega_1-\omega_2-\omega-i0^+]^{-1} \tag{38}$$

$\underset{\sim}{k}$ and $\underset{\sim}{q}$ represent wavevectors on the left and right hand sides of the barrier respectively, σ is a spin index, and $f(\omega)$ is the Fermi function, $f(\omega)=[e^{\beta\hbar\omega}+1]^{-1}$. $A_{\underset{\sim}{k}}(\omega)$, $B_{\underset{\sim}{k}}(\omega)$ and $\bar{B}_{\underset{\sim}{k}}(\omega)$ are spectral weight functions, which in the BCS[47] approximation are given by

$$A_{\underset{\sim}{k}}(\omega) = \frac{1}{2}\{[1+(\varepsilon_{\underset{\sim}{k}}/E_{\underset{\sim}{k}})]\delta(\omega-E_{\underset{\sim}{k}}/\hbar) + [1-(\varepsilon_{\underset{\sim}{k}}/E_{\underset{\sim}{k}})]\delta(\omega+E_{\underset{\sim}{k}}/\hbar)\} \tag{39}$$

$$B_{\underset{\sim}{k}}(\omega) = -\frac{i}{2}\frac{\Delta_{\underset{\sim}{k}}}{E_{\underset{\sim}{k}}} [\delta(\omega-E_{\underset{\sim}{k}}/\hbar) - \delta(\omega+E_{\underset{\sim}{k}}/\hbar)] \tag{40}$$

$$\bar{B}_{\underset{\sim}{k}}(\omega) = (\Delta^*_{\underset{\sim}{k}}/\Delta_{\underset{\sim}{k}}) B_{\underset{\sim}{k}}(\omega). \tag{41}$$

$\varepsilon_{\underset{\sim}{k}}$ is a bare particle energy measured relative to the Fermi energy, and $E_{\underset{\sim}{k}}$ is a quasiparticle energy, defined as

$$E_{\underset{\sim}{k}} = (\varepsilon^2_{\underset{\sim}{k}} + \Delta^2_{\underset{\sim}{k}})^{1/2}, \tag{42}$$

where $\Delta_{\underset{\sim}{k}}$ is the energy gap parameter for wavevector $\underset{\sim}{k}$. The parameter ϕ in Eq. (36) is defined by the relation,

$$\phi(\underset{\sim}{x},t) = \omega_o t - kx, \tag{43}$$

where $\omega_o = (2e/\hbar)V_{dc}$ and k is defined by Eq. (26). The argument of the complex quantity $\bar{B}_{\underset{\sim}{k}} B_{\underset{\sim}{q}}$ has been made explicit in the phase α. The function $W(\omega)$ is defined in terms of the time varying electric field, $E_z(\underset{\sim}{x},t)$, by the relation,

$$W(\omega) = \frac{1}{2\pi} \int_{-\infty}^{\infty} dt e^{i\omega t} \exp\{(ie/\hbar) \int_{-\infty}^{t} dt' \int_{-\infty}^{\infty} dz\, E_z(\underset{\sim}{x},t')\}, \tag{44}$$

where it is assumed that $E_z=0$ in the electrode far from the barrier region.

The complexity of the current-field relationship, Eq. (36) precludes the possibility of finding a general solution for arbitrary applied fields. In Section B and C we shall discuss the response of the quasiparticle and Josephson currents to a known electric field which is periodic in time and may be represented by an equivalent voltage by a relation similar to Eq. (35). In Section D we shall examine some possible modifications of the basic theory discussed in B and C. These modifications may be caused by the external environment of the junctions such as the current biasing circuitry or by internal properties of the junction such as its capacitance and self inductance

B. Quasiparticle Photon Assisted Tunneling (PAT)

When a general time dependent electric field of the form,

$$E_z(t) = \sum_j E_j \cos(\omega_j t+\gamma_j), \tag{45}$$

which is spatially constant over the barrier region is present, it may by represented by an equivalent uniform voltage

$$V(t) = \int_{-\infty}^{\infty} dz E_z(t)$$

$$= \sum_j V_j \cos(\omega_j t+\gamma_j) \tag{46}$$

applied across the electrodes. $W(\omega)$ may then be calculated from Eq. (42) with the result,

$$W(\omega) = \prod_j \{ \sum_{n_j=-\infty}^{\infty} e^{-in_j(\gamma_j+\pi)} J_{n_j}(\alpha_j) \delta(\omega - \sum_j n_j\omega_j)\} \tag{47}$$

where,

$$\alpha_j = eV_j/\hbar\omega_j. \tag{48}$$

J_n is an ordinary Bessel function of the first kind of order n. In the special case where only one frequency is present, $W(\omega)$ reduces to the simple form,

$$W(\omega) = \sum_{n=-\infty}^{\infty} J_n(\alpha_1) \delta(\omega - n\omega_1), \tag{49}$$

where the applied voltage is $V_1 \cos \omega_1 t$.

The quasiparticle current contribution to the total tunneling current

arises from the first term in the integrand of Eq. (36) which contains the current amplitude $j_1(\omega'+\omega_o/2)$. If we substitute Eq. (49) into the first part of Eq. (36) and perform the ω and ω' integrations, we find the result,

$$I_{qp}(t) = \mathrm{Im} \sum_{n,n'=-\infty}^{\infty} J_n(\alpha)J_{n'}(\alpha)e^{i(n-n')\omega t}\, j_1(n'\omega_1 - eV/\hbar), \qquad (50)$$

where $V = V_{dc}$, $\omega = \omega_1$, and $\alpha = \alpha_1$. The time independent (dc) component of Eq. (48) arises from the term in which $n = n'$;

$$I_{dc}(V) = \sum_{n=-\infty}^{\infty} J_n^2(\alpha)\ \mathrm{Im} j_1(n\,\omega + eV/\hbar). \qquad (51)$$

The imaginary part of the current amplitude Eq. (37) can be evaluated with the aid of the relation,

$$(\omega' + i0^+)^{-1} = P(1/\omega') - i\pi\,\delta(\omega'), \text{ (P = principal value).}$$

After the spin summation is performed, the result is,

$$\mathrm{Im}\ j_1(\omega') = -\frac{4e\pi}{\hbar} \sum_{\underset{\sim}{k}\underset{\sim}{q}} |T_{\underset{\sim}{k}\underset{\sim}{q}}|^2 \int_{-\infty}^{\infty} d\omega''[f(\omega'') - f(\omega' + \omega'')]$$

$$\times A_{\underset{\sim}{k}}(\omega' + \omega'')\, A_{\underset{\sim}{q}}(\omega''). \qquad (52)$$

Eq. (52) is a general form for the single particle tunneling current.[13] If the tunneling matrix element $T_{\underset{\sim}{k}\underset{\sim}{q}}$ is considered to be constant, and Eq. (37) is used for $A_{\underset{\sim}{k}}(\omega')$, we may evaluate Eq. (50) by converting the sums over $\underset{\sim}{k}$ and $\underset{\sim}{q}$ to integrals and evaluating the k and ω'' integrals

as shown in Appendix A. This reduces Eq. (52) to the Giaever formula Eq. (1).

Using the above results, we can write Eq. (51) in the form,

$$I(V) = \sum_{n=-\infty}^{\infty} J_n^2(\alpha)\, I_o(V + n\hbar\omega/e), \tag{53}$$

where $I_o(V)$ is the quasiparticle current characteristic in the absence of radiation. This formula was originally derived by Tien and Gordon[2] using hueristic arguments about modulation of the densities of states by the applied rf voltage. Since the result of the microscopic theory is the same as that of Tien and Gordon, we shall designate the current in Eq. (53) as $I_{TG}(V)$. Using the relation, $J_{-n}(\alpha)=(-1)^n J_n(\alpha)$, Eq. (53) may be rewritten in the form,

$$I_{TG}(V) = J_o^2(\alpha) I_o(V) + \sum_{n=1}^{\infty} J_n^2(\alpha)[I_o(V + n\hbar\omega/e) + I_o(V-n\hbar\omega/e)]. \tag{54}$$

In the limits, $\hbar\omega \to 0$, $\alpha \to 0$, Eq. (54) becomes,[48]

$$I_{TG}(V) \approx I_o(V) + \frac{(V_{rf})^2}{4} \frac{d^2 I_o(V)}{dV^2}.$$

Since the rf power $P_{rf} \propto V_{rf}^2$, the low-power-level current deviation,

$$\Delta I(V) = I(V) - I_o(V), \tag{55}$$

is directly proportional to the applied rf power.

In the classical limit, $\hbar\omega \to 0$, $\alpha \to \infty$, V_{rf} finite, we would expect that I_{TG} would reduce to the correct classical expression for the average (dc) current,

$$I_{RF}(V) = \frac{\omega}{2\pi} \int_{o}^{2\pi/\omega} I_o(V + V_{rf} \sin \omega t)dt. \qquad (56)$$

That this is in fact the case is shown in Appendix B, and hence we can say that quasiparticle photon-assisted tunneling is simply the quantum mechanical analog of classical rf detection by a device with a nonlinear current-voltage characteristic.

In an attempt to explain their 36 GHz photon assisted tunneling measurements, Cook and Everett[3] proposed a modification of the Tien Gordon theoretical model by assuming that modulation of the densities of states occurred in both superconducting films. The expression proposed by Cook and Everett (CE) for the dc current in the presence of an rf field is given by,

$$I_{CE}(V) = \sum_{n,m=-\infty}^{\infty} J_m^2(\alpha) J_n^2(\alpha)\ I_o[V + (n-m)\ \hbar\omega/e]. \qquad (57)$$

After some manipulation, Eq. (57) may be rewritten in the form,

$$I_{CE}(V) = J_o^2(\alpha)\, I_{TG}(V) + 2 \sum_{m=1}^{\infty} J_m^4(\alpha) I_o(V)$$

$$+ \sum_{m,n=1}^{\infty} J_m^2(\alpha)[J_{m+n}^2(\alpha) + J_{m-n}^2(\alpha)] \times [I_o(V+n\hbar\omega/e)$$

$$+ I_o\,(V-n\hbar\omega/e)]. \qquad (58)$$

In the limit $\alpha \to 0$, $J_o(\alpha) \to 1$ while all the other J_n approach zero, and hence $I_{CE}(V) \to I_{TG}(V)$. As α becomes appreciably greater than 1, the difference between I_{CE} and I_{TG} becomes quite large, indicating that I_{CE} does not reduce to the correct classical limit when $\hbar\omega \to 0$.

The major assumption which has been made in deriving Eq. (53) is the representation of the rf electric field $E_z(\underset{\sim}{x},t)$ by a homogeneous voltage V(t). It might be expected that this assumption will cease to be valid when the wave length of the applied field in the barrier region becomes comparable with the length L of the junction. The wavelength in the barrier will be related to the free space wavelength λ_o by the relation,

$$\bar{\lambda} = \lambda_o(v_J/c), \qquad (59)$$

where v_J is given by Eq. (19). With typical values of junction parameters we estimate $\bar{\lambda} \sim .05\ \lambda_o$, and hence a condition for the validity of the TG formula, Eq. (53), can be stated as,

$$L \lesssim 0.05\ \lambda_o. \qquad (60)$$

If the time dependent voltage appearing across the junction is in the form of a standing wave,

$$V(x,t) = V_{rf}(x) \cos[\omega t + \gamma(x)], \tag{61}$$

Then a consideration of Eqs. (47)-(51) shows that the net dc tunneling current will be given by,

$$I_{TG}(V) = \sum_{n=-\infty}^{\infty} \left\{ \frac{1}{L} \int_{-L/2}^{L/2} J_n^2[\alpha(x)]dx \right\} I_o(V + n\hbar\omega/e) \tag{62}$$

$$\alpha(x) = V_{rf}(x)/\hbar\omega. \tag{63}$$

In principle, the function $V_{rf}(x)$ can be determined by solving the wave equation, Eq. (34), subject to the boundary condition that the electric field far from the junction position equal its value in the bare cavity or waveguide in which the junction is situated. In practice, exact solutions are rarely possible and hence some parameterized functional dependence for $V_{rf}(x)$ must be assumed.

C. Josephson - Photon Assisted Tunneling

The Josephson current response to an assumed field $E_z(\underset{\sim}{x},t)$ arises from the second term of Eq. (36) which contains the current amplitude $j_2(\omega)$. Again, the calculations are difficult, and hence various approximate solutions of the basic Josephson equations are usually considered. If we consider the case where there is an rf voltage, $V_{rf} \cos \omega_1 t$, applied to the junction, we can see from inspection of Eq. (49) that the function $W(\omega)$ contributes appreciably to the integral in Eq. (36) only at harmonics of ω_1, and then only up to a harmonic number $n_{max} \sim \alpha$, where $\alpha = eV_{rf}/\hbar\omega_1$. Thus, we only need the function $j_2(\omega' + \omega_o/2)$ in the integrand of Eq. (36) for values of its argument, satisfying the condition $|\omega' + \omega_o/2| \simeq |n_{max}\, \omega_1|$ or equivalently, $|\omega'| < |\omega_o/2 + n_{max}\omega_1|$. Another way of stating this condition is to say that the major contribution to the ω integral in Eq. (36) comes from the region where,

$$|\hbar\omega'/e| < |V_o + V_{rf}|. \tag{64}$$

Werthamer has calculated the functions $j_1(\omega)$ and $j_2(\omega)$ with the BCS constant energy gap model spectral weight functions, Eqs. (39)-(41), assuming $|T_{k',q}|^2$ to be constant and in the limit T = 0°K. The results for $j_2(\omega)$ in the case of identical superconductors is given by,

$$\begin{aligned} j_2(\omega) &= \left[\Delta/(e\, R_{NN} A)\right] K(x), \qquad 0 \leq x \leq 1 \qquad (65) \\ &= \left[\Delta/(e\, R_{NN} A x)\right] \left\{ K(1/x) + i\,\mathrm{sgn}(\omega)\, K\left[\left(\frac{x^2-1}{x^1}\right)^{1/2}\right] \right\}, \\ & \qquad\qquad x > 1. \end{aligned}$$

Here K is the complete elliptic integral of the first kind, $x = |\hbar\omega|/2\Delta$ and A is the junction area. The singularity in j_2 at x = 1 or equivalently at $\hbar|\omega| = 2\Delta$ was first pointed out by Riedel[43] and is a consequence of

the singularity in the BCS model density of states at a voltage Δ/e. For non-singular density of states functions, such as those discussed in section II-A in conjunction with gap anisotropy, we would expect the singularity to become a rounded peak of finite height. No model calculations have ever been performed to test this hypothesis, but the "width" of the distortion of j_2 from the BCS model prediction is probably comparable in size to the width of the quasiparticle current rise at $V_o = 2\Delta/e$. Since the function $K(x)$ is slowly varying until x becomes very close to 1, we can approximate $j_1(\omega)$ by a constant when the condition, $|V_o + V_{rf}| \ll 2\Delta/e$ is satisfied.

If the total voltage across the junction is given by,

$$V = V_o + V_{rf} \cos(\omega t + \theta), \tag{65}$$

then Eq. (12) relating the time derivative of ϕ to the voltage is ,

$$\partial\phi/\partial t = (2e/\hbar)[V_o + V_{rf} \cos(\omega t + \theta)]. \tag{67}$$

Integrating with respect to time, we obtain,

$$\phi = 2e\, V_o t/\hbar + (2e\, V_{rf}/\hbar\omega) \sin(\omega t + \theta) + \phi_o. \tag{68}$$

If we consider the current amplitude j_2 to be a constant, the approximate current-phase relation, Eq. (14) may be used to yield the current voltage relation,

$$I = I_1 \sin [2e\, V_o t/\hbar + (2\alpha) \sin(\omega t + \theta) + \phi_o]. \tag{69}$$

Since $I(t)$ is periodic in t with period $2\pi/\omega$, it may be expanded in a Fourier series. The result may be conveniently expressed by the formula,

$$I(t) = I_1 \sum_{n=-\infty}^{\infty} (-1)^n J_n(2\alpha) \sin(2e\, V_o t/\hbar - n\omega t - n\theta + \phi_o). \tag{70}$$

When the condition,

$$2e\, V_o/\hbar = n\omega, \tag{71}$$

is satisfied, the current has a dc component given by,

$$I_{dc} = I_1(-1)^n J_n(2\alpha)\sin(\phi_o - n\theta) \tag{72}$$

When the bias voltage V_o is given by (71), the current will be limited in absolute value to the region

$$0 \leq |I_{dc}| \leq I_1 J_n(2\alpha)\,|\sin\phi_o|, \tag{73}$$

where ϕ_o depends on the current supplied by the external bias circuitry. In the presence of a dc magnetic field Eq. (71) is modified by the addition of a multiplicative field dependent Fraunhofer factor, as specified by Eq. (28) for a narrow junction.

If the junction is biased by a constant current dc supply, the spikes in the constant voltage characteristic at the voltages specified by $2eV_{rf} = n\hbar\omega$ will appear as current steps at these same voltages. An example of this step like structure is shown in Fig.24 which illustrates the response of an Sn-SnO-Sn junction to 4GHz radiation.

When the small signal approximation, Eq. (64) is not valid we may calculate the dc current from the basic Werthamer formula, Eq. (36) in a manner strictly analogous to that used to determine the quasiparticle response, Eq. (51). Inserting the function $W(\omega)$ given by Eq. (49) in the second term of Eq. (36) and retaining the time independent terms we obtain,

$$J_{dc}(V_n) = \sum_{m=-\infty}^{\infty} \Big\{ J_m(\alpha)\, J_{n-m}(\alpha) \Big\{ \mathrm{Re}\left[j_2[(m-n/2)\omega]\right] \sin(kx + \phi_o) + \mathrm{Im}\left[j_2[(m-n/2)\omega]\right] \cos(kx + \phi_o) \Big\} \Big\} \tag{73}$$

with $V_n = n\hbar\omega/2e$ and ϕ_o used in place of α which appears in (36). At temperatures $T << T_c$, the second term inside the summation involving Im (j_2) is much smaller that the first term and may be neglected in computing j_{dc}. If the real part of j_2 is considered constant and taken outside the summation in Eq. (73), we can use the Bessel function identity,

$$\sum_{m=\infty}^{\infty} J_m(\alpha)\, J_{n-m}(\alpha) = J_m(2\alpha), \tag{74}$$

to show that j_{dc} from Eq. (73) reduces exactly to the approximate result, Eq. (71). In the case of arbitrarily large V_{rf} and ω_{rf}, $j_{dc}(V_n)$ must in general be computed numerically using Eq. (65) for $j_2(\omega)$. In the special case n=0 and V_n=0, Eq. (73) reduces to,

$$j_{dc}(0) = \left\{ J_o(2\alpha) + 2 \sum_{n=1}^{\infty} (-1)^n J_n^2(\alpha) \left[\frac{j_2(n\omega)}{j_2(0)} - 1 \right] \right\} \times j_2(0) \sin(kx + \phi_o), \tag{75}$$

where we have used the identity, $J_o(2\alpha) = J_o^2(\alpha) + 2 \sum_{n=1}^{\infty} (-1)^n J_n^2(\alpha)$. From Eq. (75) we can see that the response of the zero voltage Josephson current to an applied rf voltage will be proportional to $J_o(2\alpha)$ until terms in the summation in Eq. (75) become large. This will occur when α and ω satisfy the conditions $n\hbar\omega \simeq 2\Delta/e$ and $\alpha \sim n$. In our experiments conducted at frequencies $\nu \simeq 4$ GHz or $\hbar\omega/e \simeq 16$ μV, with Sn-I-Sn junctions these conditions imply that for values of $\alpha \simeq 75$, the Riedel singularity in $j_2(\omega)$ should cause one of the terms in the summation in (75) to contribute an observable magnitude to j_{dc}.

In the situation, where no applied rf field is present, the ac Josephson current oscillating at frequency ω_o can cause time varying $\underset{\sim}{E}$ and $\underset{\sim}{H}$ fields to be induced in the barrier region. The non-linear nature of both

the Josephson current-voltage relationship and quasiparticle characteristic can cause field and current harmonics to be generated at frequencies $\omega_n = n\omega_o$. For the thin film junction geometry shown in Fig. 4-6 the oxide barrier of height L and width ℓ forms an effective cavity or resonant structure in which electromagnetic fields may be confined. Although the ends of the cavity at x=0, L are not bounded by metallic walls, they do act to effectively confine the fields by causing a near total reflection of transverse waves traveling in the $\pm x$ directions. This reflection occurs because of the large mismatch between the wave propagation velocity v_J in the cavity and the speed of light in a vacuum The situation is analogous to the confinement of an E-M wave in an ordinary dielectric with a dielectric constant $\epsilon_{eff} = (c/v_J)^2$, or $\epsilon_{eff} \sim 200\text{-}400$. The modes with the highest Q, defined by the relation,

$$Q = \frac{\omega \times \text{Average stored energy}}{\text{Energy radiated per cycle}},$$

are those for which an integral number of half wavelengths fit in the cavity dimension in the plane of the barrier, i.e. those modes with propagation vectors satisfying,

$$kL = n\pi \tag{76}$$

or equivalently,

$$2L = n\lambda, \tag{77}.$$

where $\lambda = 2\pi v_J/\omega$. The electric field corresponding to the maximum Q condition in the n^{th} mode may be shown to have a spatial variation, $E_{nz} \propto \cos(n\pi x/L)$, corresponding to a magnetic field variation $H_{ny} \propto \sin(n\pi x/L)$. The functional form of the y component of the magnetic field is frequently taken to be a consequence of the vanishing of surface currents in the x direction at x = 0,L.[49,50] In most experimental junction geometries (such

as the crossed strip geometry illustrated in Fig. 5), it is far from obvious that these surface currents do in fact vanish, and hence it is worth noting that the vanishing of longitudinal surface currents is not a necessary condition for the specified E_z and H_z field variations.

For each cavity mode, designated by the integer n, there is a dc voltage V_n at which the ac Josephson frequency $2e\,V_n/\hbar$ equals the cavity mode frequency. Using Eq. (77) this condition may be expressed as,

$$V_n = n(\pi\hbar\, v_J/2eL). \tag{78}$$

These modes (commonly designated as "Fiske modes" after one of their principal discoverers[50]) may then be thought of as quasistationary oscillations in which the energy radiated away at the junction edges is supplied by the ac Josephson current. Explicit formulas for the time dependent electric field have been derived from linearized forms of Eq. (13). If we operate on Eq. (13) with the differential operator, $(\hbar/2e\ell)\,\partial/\partial t$ we can derive an equivalent equation for $E_z(x,t)$,

$$\nabla^2 E_z - (1/v_J)^2 \frac{\partial^2 E_z}{\partial t^2} = \frac{4\pi}{\epsilon_s v_J^2} \frac{\partial j_z}{\partial t} \tag{79}$$

The usual scheme[48,49] for solving Eq. (79) is to assume that j_2 may be approximated by Eq. (33) and that the time dependent field solution is of the form,

$$E_z(x,t) = \Sigma_n \cos(n\pi x/L)\, f_n(t). \tag{80}$$

This method of solution is equivalent to neglecting all time dependent voltages in the Josephson voltage phase relation, Eq. (12) and thus is most valid in the limit where $|V(x,t)| = |E_z(x,t)/\ell| \ll V_o$. A phenomenological damping term, $(\omega\ell/Q\, v_J^2)\,(\partial E_z/\partial t)$, is usually added to Eq. (79) to

represent radiative and skin effect losses. Since j_z is periodic in time with a period $\tau = 2\pi/\omega_o$, the functions $f_n(t)$ may written as, $f_n(t) = a_n \cos(\omega_o t + \theta_n) + b_n \sin(\omega_o t + \theta_n)$, and the constants a_n, b_n, θ_n, may then be determined by the standard methods of Fourier analysis. The result for this electric field is[49]

$$E_z(x,t) = \frac{4\pi j_1}{\epsilon_s \omega} \sum_{n=0}^{\infty} \cos\left(\frac{n\pi x}{L}\right) \times \frac{a_n \cos(\omega_o t + \theta_n) + b_n \sin(\omega_o t + \theta_n)}{\left\{\left[1 - (n\pi v_J/\omega_o L)^2\right]^2 + (1/Q_n)^2\right\}^{1/2}} \tag{81}$$

The coefficients a_n b_n are oscillatory functions of the static magnetic field strength with magnitudes; $|a_n|, |b_n| \leq 1$. At the Fiske mode voltages the Josephson frequency ω_o is given by, $\omega_o = n\pi v_J/L$, and hence the electric field has a magnitude, $|E_z| \cong 4\pi j_1 Q_n/\epsilon_s \omega$, where Q_n is the Q factor for the n^{th} mode.

The dc component of the total Josephson current may be calculated by computing the time and spatial average of the current density using Eqs. (12) and (14) to relate current and time dependent voltage, $V = \ell E_z(x,t)$

$$I_{dc} = (1/L) \int_o^L dz \, \frac{\omega_o}{2\pi} \int_o^{2\pi/\omega_o} dt \, I_1 \sin\phi(x,t) \tag{82}$$

If we write, $\phi = kx - \omega_o t + \delta\phi(x,t)$, where $\delta\phi$ is given by $\int^t (2e\ell/\hbar) E_z(x,t')\, dt'$, and then linearize the integrand of (82) by writing,

$$\sin\phi(x,t) \simeq \sin(kx - \omega_o t) + \delta\phi \cos(kx - \omega_o t)$$

we can perform the integration. Kulik[46] has graphed the first few step heights as a function of the dc magnetic flux threading the junction. They are also oscillatory functions of the dc magnetic field strength with the n^{th} step having a central maximum when $kL = n\pi$ where k is related

to H_o by Eq. (26). If H_o is adjusted for peak coupling to the n^{th} mode, the $n\pm 2m$ modes are not excited.

The major drawback of the linear theory described above is that the ac voltage amplitude at frequency ω_o is not in general small compared to the dc bias voltage. We can estimate the magnitude of the n^{th} Fiske mode ac voltage from Eq. (81). The result is, in practical units,

$$V_{rf}(n) \simeq \frac{60\pi}{R_{NN}(\Omega)} \left(\frac{Q_n}{\epsilon_S n}\right)\left(\frac{\ell/L}{v_J/c}\right) \times (\Delta/e) \qquad (82)$$

For a Sn-I-Sn junction with $\ell = 20\text{Å}$, $L = 1.6\times10^{-2}$ cm, $v_J/c = 0.1$, $\Delta/e = 0.6$ mV, $n = 2$, and $Q_n = 100$, Eq. (82) yields, $V_{rf}(n) \simeq 180$ μV. Since the corresponding dc bias voltage (V_2 from Eq. (78)) is $V_{dc} \simeq 390$ μV, it is immediately apparent that the small signal approximation linear analysis is invalid. Another shortcoming of the above analysis is that field spatial variation has been assumed to occur only in the x direction perpendicular to the externally applied dc magnetic field H_o. If the propagation vector quantization condition, Eq. (76) is generalized to include spatial variations in both the x and y directions for a square junction of side length L, the self resonant voltage mode relation, Eq. (78) will become,

$$V_{n,m} = (n^2+m^2)^{1/2} (\pi\hbar v_J/2eL). \qquad (83)$$

The bias voltage quantization conditions (78), or (83), are strictly a consequence of spatial boundary conditions imposed on the junction electromagnetic fields, and so they should not be affected by the nonlinearity of the junction response. However, we can expect that the magnitudes of the Fiske mode current steps will not be predicted accurately by the linear theory, although the general oscillatory dependence on H_o should remain.

When an external rf voltage is applied to the junction the nonlinear dependence of both the Josephson and quasiparticle currents on the total junction voltage leads to generation of harmonics of the applied frequency and to mixing of these harmonics with harmonics of the ac Josephson frequency ω_o. In the case of the quasiparticle current, mixing and harmonic generation are essentially a consequence of the nonlinear nature of the volt-amp characteristic, and are quantum analogues of the same phenomena which occur in classical nonlinear circuit elements. For Josephson currents, however mixing occurs not only via nonlinearity in the I-V characteristic, but also through the basic non-linearity of the Josephson current-phase relationship, Eq. (14).[51,52] All of these complex physical phenomena, however, are fundamentally consequences of the basic current-voltage relationship, Eq. (36).

D. Modifications of the rf Voltage Coupling Theory

In Section III-B,C above we have considered the response of tunneling currents to known applied rf voltages. In actual experimental situations, the junction's environment as well as its physical properties will affect the magnitude of the induced rf voltage for a given applied rf electric field. A property of special interest for evaporated film junctions is the capacitance since the capacitive reactance can be appreciable relative to the dynamic resistance of the junction. For example, a square junction with side length L = 0.16 mm, a plate separation ℓ = 20Å, and a dielectric constant ε_s = 4 has a capacitance C ≃ 400 μμF. At a frequency $\omega/2\pi$ =4GHz, the reactance X_C is $9.3\times10^{-2}\Omega$. This value of X_C is roughly the same as the gap region dynamic resistance of a junction with a normal state resistance R_{NN} ≃1Ω. Other important properties are the geometrical arrangement and physical nature of the junction's bias circuitry wiring since this wiring can act as an antenna in the presence of an rf field.

McCumber[53] has analyzed the response of a thin film junction when considered as a lumped circuit combination of a Josephson junction shunted by a linear conductance representing the quasiparticle current path and a capacitance. Although his model seems reasonable from a physical point of view, it does have the property that an applied rf voltage of any frequency and amplitude will appear undiminished across the junction despite the presence of the capacitance. The junction response will then be the same as it is in the unshunted case since, by Eq. (51) and Eq. (72), the dc current flowing in the junction is a property only of the magnitude and frequency of the rf signal voltage.

In an attempt to explain some experimental data which indicate that V_{rf} is not a constant which is independent of dc bias voltage, we have studied the properties of some alternate simple lumped circuit junction models.

If we consider a junction biased by a high resistance dc current source, one of the simplest circuits which can be devised that includes the effect of an rf electric field as an equivalent voltage source is shown in Fig. 7. All of the externally supplied dc current passes through the junction and all of the rf current circulates internally in the junction as shown, since the dc current source is assumed to have a very large series resistance. The function $I_o[V(t)]$ represents the quasiparticle tunneling characteristic, Eq. (50). At frequencies low compared to $e\delta V/\hbar$, where δV = gap width, we can approximate $I_o[V(t)]$ by the measured bare current characteristic. When the total time dependent voltage V(t) is known, the dc current at the bias voltage V_o may be calculated from the formula,

$$I_{dc} = \frac{\omega}{2\pi} \int_o^{2\pi/\omega} I_o[V(t)]dt. \tag{84}$$

The circuit equations describing the circuit shown in Fig. 7 are

$$\begin{aligned} I_{dc} &= I_o(V) - i_c \\ i_c &= \frac{d}{dt}(V_{rf} \sin \omega t - V) . \end{aligned} \tag{85}$$

If we write, $I_{dc}=\gamma_o/R$ and $I_o(V)=\gamma(V)/R$, where R is the normal state

resistance, then Eq. (85) may combine to yield a single integro-differential equation in the dimensionless variable $p=\omega t$,

$$\frac{dV}{dp} = \frac{1}{\kappa} \{\gamma_o - \gamma[V(p)]\} + V_{rf} \cos p, \tag{86}$$

with $$\kappa = \omega RC .$$

If we assume the form for $V(p)$,

$$V(p) = V_o + V_{rf} \sin p + \phi(p), \tag{87}$$

then Eq. (86) becomes,

$$\frac{d\phi(p)}{dp} = \frac{1}{\kappa} \{\gamma_o - \gamma[V_o + V_{rf} \sin p + \phi(p)]\}, \tag{88}$$

with γ_o given by,

$$\gamma_o(V_o) = \lim_{p_o \to \infty} \{ \frac{1}{2\pi} \int_{p_o}^{p_o+2\pi} \gamma[V(p)]dp\}. \tag{89}$$

Before discussing the mathematical problem of solving Eqs. (88)-(89), we can note that the same equations apply to the problem of a tunnel junction shunted by a capacitance and driven by a shunt rf <u>current</u> source in parallel with the dc source if we make the replacement, $V_{rf} \to (R/\kappa) i_{rf}$ in Eq. (88), where i_{rf} is the current source strength. More complicated model circuits can of course be devised, but they will require additional circuit elements which enter the problem as unknown parameters. Since there is no microscopic or experimental justification at this time for the introduction of additional parameters we shall confine our attention

to the simple circuit shown in Fig. 7 and described by Eqs. (87)-(89).

The essential difficulty in solving Eq. (88) is the high degree of nonlinearity introduced by the quasiparticle characteristic $\gamma(V)$. If the magnitude of the driving term, V_{rf}, satisfies the condition, $V_{rf} << \delta V$, $\gamma(V)$ can be approximated by a piecewise linear model and Eq. (88) can then be solved analytically. This approximation results in I_{dc} being given by Eq.(54), the TG formula, with V_{rf} given by,

$$V_{rf} = [\kappa_s/(1+\kappa_s^2)^{1/2}]V_{rf_o} \tag{90}$$

with $$\kappa_s = \omega C[dV/dI]_{V_o} .$$

From Eq. (90) we can see that the magnitude of the rf voltage is enhanced in regions of high dynamic resistance and diminished in regions of low dynamic resistance. In practice, V_{rf} is usually not small compared to δV and hence the approximate solution has only qualitative significance.

Although the solution of Eq. (88) and Eq. (89) is strictly a mathematical problem, it is not one that is discussed in any of the literature known to us. Because of this lack of previous discussion on the subject we shall describe briefly one method of solving the system. If Eq. (88) is solved numerically subject to the initial conditions that at p=0, $\phi=\phi_o$, then in general $\phi(p)$ will contain both a transient and a periodic part. The transient solution will decay with a time constant κ, and thus for practical purposes, p_o in Eq. (89) may be taken as $p_o \simeq 5\kappa$. However, the solution must also be self-consistent, i.e., the initially assumed value of γ_o must be the same as the one finally calculated from

Eq. (89) after solving Eq. (88). Since κ can be quite large relative to 2π, this method of solution in general is quite impractical.

An alternate method of solution which we have used involves converting Eq. (88) to an infinite system of nonlinear algebraic equations and then solving a truncated set of these equations by iteration. Since the desired part of $\phi(p)$ is periodic in p with period 2π and has zero average value, it can be represented as a Fourier series,

$$\phi(p) = \sum_{n=1} [(a_n \sin(np) + b_n \cos(np)]. \tag{91}$$

Substituting Eq. (91) in Eq. (88) and using the familiar Fourier orthogonality integrals we find that the coefficients a_n and b_n are given by the transcendental equations,

$$\begin{aligned} a_n &= -(1/n\kappa\pi) \int_o^{2\pi} \gamma[V(p)] \cos(np)dp \\ b_n &= (1/n\kappa\pi) \int_o^{2\pi} \gamma[V(p)] \sin(np)dp, \end{aligned} \tag{92}$$

with,

$$V(p) = V_o + V_{rf} \sin p + \sum_n [a_n \sin(np) + b_n \cos(np)]. \tag{93}$$

When a self-consistent set of coefficients satisfying Eq. (92) is found, the dc current can be computed from the formula,

$$\gamma_o(V_o) = (1/2\pi) \int_o^{2\pi} \gamma[V(p)]dp. \tag{94}$$

In practice, the utility of this method depends on the magnitudes of κ, V_{rf}, and V_o. In general, convergence is worst for small κ, large V_{rf}, and when V_o is in the gap region. The major numerical problem which is encountered is the selection of a rapidly convergent iteration procedure since the computation time varies directly as the product of the number of iterations times the maximum value of n used. For values of κ satisfying the condition $\kappa \geq 7$, we have found that convergence can be obtained, in from 4 to 15 iterations, at any values of V_o and V_{rf} when $n_{max}=4$ and when the iteration procedure for a_n or b_n at the k+1st iteration is given by,

$$a_n(k+1) = 1/2 \{g_n[\underset{\sim}{a}(k),\underset{\sim}{b}(k)] + a_n(k)\}$$

$$b_n(k+1) = 1/2 \{h_n[\underset{\sim}{a}(k),\underset{\sim}{b}(k)] + b_n(k)\}.$$

The functions g_n and h_n are defined from Eqs. (92) as,

$$g_n(\underset{\sim}{a},\underset{\sim}{b}) = -(1/n\kappa\pi) \int_o^{2\pi} \gamma[V(\underset{\sim}{a},\underset{\sim}{b},p)] \cos(np)dp$$

$$h_n(\underset{\sim}{a},\underset{\sim}{b}) = (1/n\kappa\pi) \int_o^{2\pi} \gamma[V(\underset{\sim}{a},\underset{\sim}{b},p)] \sin(np)dp.$$

The function $V(\underset{\sim}{a},\underset{\sim}{b},p)$ is given by Eq. (93), and the column vectors $\underset{\sim}{a},\underset{\sim}{b}$ are defined by,

$$\underset{\sim}{a} = (a_1,a_2,\ldots,a_{n_{max}})$$

$$\underset{\sim}{b} = (b_1,b_2,\ldots,b_{n_{max}}).$$

The initial values of $\underset{\sim}{a}$ and $\underset{\sim}{b}$ are taken as those predicted by the piecewise linear small signal model, $a_1 = V_{rf}/(\kappa_s^2+1)$, $b_1 = -\kappa_s V_{rf}/(\kappa_s^2+1)$, a_n, $b_n = 0$ for $n \neq 1$. κ_s is the "local" value of κ as defined by Eq. (90).

More sophisticated iteration schemes can of course be employed,[54] but any method involving increased function evaluation will rapidly increase the computation time. As κ decreases below 7, n_{max} and the number of iterations both must be increased, and even then, convergence is conditional on the value of V_o. We have not made an exhaustive study of the convergence problem since the major goal of our computation was to calculate theoretical current-voltage characteristics which apply to our own particular set of experimental data.

The major result of this section is that, within the framework of the simple model shown in Fig. 7, the junction capacitance can have a significant effect on the shape of the dc I-V characteristic when rf fields are present. In the case of quasiparticle tunneling, the relevant parameter is $\kappa = \omega R_{NN} C$. When $\kappa \lesssim 20$, the theoretical characteristics will start to deviate appreciably from $I_{RF}(V)$ as given by Eq. (56).

IV. EXPERIMENTAL METHODS

A. Junction Preparation

The Sn-SnO-Sn and Sn-SnO-Pb junctions used in our experiments were prepared by vacuum deposition of thin metallic strips onto microscope cover glass substrates 1.3×10^{-2} cm thick. The widths of the strip electrodes being deposited were delineated by thin aluminum masks located directly below the substrates. Evaporation pressures were in the range $(2\text{-}12) \times 10^{-7}$ Torr for Sn and $(1\text{-}5) \times 10^{-7}$ Torr for Pb and evaporation rates were in the ranges 5-10 Å/sec and 20-40 Å/sec for Sn and Pb respectively. There was no observable correlation between final junction quality and evaporation pressures or rates. All evaporations were performed at room temperature in a Varian VI-4C ion-pumped high vacuum system.

An 0.16 mm wide longitudinal strip of Sn $\approx$ 3000 Å thick was deposited first and then oxidized in pure oxygen at a pressure of approximately 1/3 atm. The oxidation time was varied from 12-36 hours and the oxidation temperature was controlled with heat lamps. Following oxidation of the bottom electrode, three 0.16 mm wide cross strip top electrodes were deposited in a perpendicular direction so as to form three crossed strip tunnel junctions on the same substrate (see Figs. 5, 6, 8). In general, for junctions with an area 0.16×0.16 mm^2, a 12-hour oxidation at 300°K would produce Sn-SnO-Sn junctions with 4.2°K normal state resistances in the milliohm range, while a 24-hour oxidation using two heat lamps (standard 250 W infra-red flood lights, approximately 3 ft. from the oxidation belljar) would produce resistances in the range 2-10 Ω. The resistances of the Sn-SnO-Pb junctions with

areas 0.16×0.16 mm^2 were all in the range 20-120 Ω. Junctions with normal state resistances in the range 20-40 Ω were produced by 18-hour oxidation with 1 heat lamp. The higher resistance junctions were produced by increasing the oxidation time but they would not be produced as reliably as the Sn-SnO-Sn junctions. As a general rule of thumb, we can conclude that junctions with Pb top electrodes will have resistances 1-2 orders of magnitude larger than those with Sn top electrodes when the oxidation time and temperature are identical. The thickness of a deposited metal strip was determined with a Sloan DTM-3 deposit thickness monitoring system. This system determines relative thickness by measuring the change in frequency of a resonating quartz crystal placed in close proximity to the substrate as the deposit builds up on the crystal surface. The crystal was calibrated by measuring the thickness of selected Sn and Pb films with a Varian 980-4000 multiple beam interferometer. The bottom Sn strips always had thicknesses ≈ 3000 Å while the thickness of the top strip was varied from sample to sample.

Following deposition of the top electrode, the substrate was installed in the microwave cavity and electrical leads were attached to the samples with silver conducting paint.[17] In general, the samples were installed and cooled down to liquid nitrogen temperature within 30-60 minutes after completion of deposition. When Sn-SnO-Sn junctions were left exposed to air at room temperature for a period of more than one day, they frequently showed signs of deterioration. Shorts appeared through the oxide film when the Sn electrodes were superconducting and the junctions displayed poor quasiparticle tunneling characteristics. The Sn-SnO-Pb junctions appeared to be much more stable. One junction,

with R_{NN} = 117 Ω, was left on the shelf for two months with no evidence of deterioration in that time. This stability is consistent with the generally higher resistances observed in the Sn-SnO-Pb junctions.

B. Cryogenics

Measurements were performed in a standard glass liquid-helium cryostat at temperatures between 4.2°K and 1°K. Temperatures were measured with a Solitron germanium thermometer which had been calibrated against a primary standard and which was mounted outside the microwave cavity but in close proximity to the sample. The temperature could be regulated to within a few millidegrees Kelvin with an ac wheatstone bridge temperature regulator.[56] The output of the regulator supplied current to a 100 Ω manganin wire heater coil wound around a shield can which surrounded the microwave cavity. The heater output was balanced by pumping on the helium bath through a small 1/8 inch line containing a needle valve. Most of the experiments were done at temperatures near 1.2°K in order to minimize the effects of microwave heating on the helium in the cavity. Below the λ-point the helium density changes only a small amount as the temperature increases and hence the helium dielectric constant (which varies linearly as the density) remains approximately constant. Above the λ-point the density varies rapidly with temperature, and the resultant dielectric constant variation can produce appreciable cavity detuning if the bath heats up during a run. Measurements could, however, be made above the λ-point as long as the microwave power dissipated in the cavity, P_D, was kept below 3×10^{-3} W.

C. Microwave and Cavity Systems

The microwave and resonant cavity systems used in our experiments

were designed to produce a large rf electric field at the position of sample for a given rf power input to the cavity. Two different microwave cavities were employed during the experiments, a coaxial reentrant cavity as shown in Fig. 8 and a rectangular cavity operating in the TE_{101} mode. The reentrant cavity was designed to resonant in a frequency range 3.5 - 4.1 GHz with the resonant frequency being controlled by the vertical position of the tuning plunger. The diameter of the cavity was 1.91 cm, the height 1.43 cm, and the diameter of the plunger was 0.96 cm. These dimensions were determined using design curves given by Moreno,[57] so as to provide adequate space for mounting the samples on the cavity endwall as shown in Fig. 8. On the axis of the cavity, directly below the tuning plunger, $\underset{\sim}{E}_{rf}$ is perpendicular to the plane of the junctions and $\underset{\sim}{H}_{rf}$ is zero when the cavity is excited in its fundamental mode. The substrate was located with its center on the cavity axis, and all three junctions on the substrate were close enough together so that $\underset{\sim}{E}_{rf}$ and $\underset{\sim}{H}_{rf}$ at the actual junction positions were the same as the axial values of the fields. The electrical wires connected to the junctions were run out of the cavity through small holes drilled in the cavity base in order to minimize antenna pickup in the leads.

The magnitude of the rf electric field on the cavity axis was determined indirectly from measurements of the cavity loaded Q, Q_L, and the VSWR at resonance. From measurement of the cavity bandwidth Δf, Q_L was calculated from the relation,

$$Q_L = f_o/\Delta f,$$

where f_o is the resonant frequency and $f_o \pm \Delta f/2$ are the points at which the reflected rf power has increased by 50% of its net change when the cavity is tuned far from resonance. With Q_L determined experimentally, the bare cavity Q factor, Q_o was calculated from the expression,

$$Q_o = Q_L(1+\beta), \tag{95}$$

where the coupling factor β is given by,

$$\beta = 1/(\text{VSWR})_{\text{resonance}},$$

for an undercoupled cavity.[58,59] The Q_o of our cavity when filled with liquid helium at 4.2°K with junctions in place was in the range Q_o=420-480, as compared to a value computed from Moreno's[57] design formulas, $Q_{o(\text{theor.})} = 1550$, using a brass skin depth $\delta = 2.2 \times 10^{-4}$ cm. Since the cavity was bolted together and had joints across which surface currents flowed, the observed reduction of Q_o below its design value seemed reasonable. With the experimental value of Q_o, the cavity shunt resistance R_o was calculated from the equation,

$$R_o = (R_o/Q_o)_{\text{theor.}} \times Q_o,$$

where $(R_o/Q_o)_{\text{theor.}}$ was determined from Moreno's formulas. R_o is defined for a reentrant cavity by,[58]

$$R_o = \left|\int_1^2 \underset{\sim}{E}_{rf} \cdot d\underset{\sim}{\ell}\right|^2 / 2P_D,$$

where P_D = power dissipated in the cavity and the line integral is taken along the cavity axis between base and plunger. The magnitude of the field could then be computed from,

$$E_{rf} = (2P_D R_o)^{1/2}/(\Delta z), \tag{96}$$

where Δz = height of plunger above the cavity base. The relation between E_{rf} and P_D determined in this manner was,

$$E_{rf}(\mu V/\text{Å}) = 8.48\times10^{-3}(P_D(\mu W))^{1/2}. \tag{97}$$

The major sources of error in determining the magnitude of the rf field arise from experimental errors in the determination of Q_o and P_D. The major source of uncertainty in the Q_o measurement arises from error in determination of the coupling factor β, while error in P_D measurement is caused by uncertainties in determining absolute values of incident and reflected power and coaxial cable attenuation between the directional coupler and the cavity (Fig. 9). The error from both sources was estimated to produce at most a factor of 1.5 error in the final computed value of the electric field.

In a later series of experiments with Sn-SnO-Pb junctions, a TE_{101} rectangular gold plated cavity was used. This cavity was 8.18 cm long, 1.27 cm high and 4.18 cm wide, with the rf electric field everywhere perpendicular to the large 8.18×4.18 cm^2 top and bottom cavity walls.

The cavity was excited by an adjustable coupling loop which terminated the coaxial input cable at one of the small 4.18×1.27 cm^2 end walls. Both the insertion depth and the orientation of the loop could be adjusted independently from outside the cryostat so as to achieve any desired magnitude of rf coupling. In practice, the cavity was normally operated in a critically coupled condition (β=1) in order to eliminate errors in Q_o determination and to maximize the magnitude of the rf field for given level of incident rf power. The substrate was installed at the center of the bottom face at the point of maximum $|\underset{\sim}{E}_{rf}|$, and the sample wiring was run out of the cavity along the bottom face so that it was always perpendicular to $\underset{\sim}{E}_{rf}$. We found experimentally that even very short (< 1 mm) sections of wiring parallel to $\underset{\sim}{E}_{rf}$ at the center of the cavity would reduce the cavity Q to a very small value relative to its empty cavity value. The value of Q_o measured with the substrate installed, was Q_o=1,250, as compared to a theoretical value, Q_o(theor.)=4070 computed using an rf skin depth $\delta = 1.55 \times 10^{-4}$ cm.

The magnitude of the rf field was determined from a measurement of incident rf power with the aid of the relation,

$$Q_o = \omega_o U/P_D \tag{98}$$

where ω_o=rf angular frequency and U= average stored energy. For a TE_{101} mode, $U = (\varepsilon/8)\, abd\, E_{rf}^2$, where a, b, d are cavity dimensions and $E_{rf} = |\underset{\sim}{E}_{rf}|$. Thus $E_{rf}=(4Q_o/\pi f_o \varepsilon\, abd)^{1/2} \sqrt{P_D}$, and with the actual values of Q_o, f_o, and cavity dimensions, E_{rf} is given by,

$$E_{rf}(\mu V/\text{Å}) = 3.28\times10^{-3}(P_D(\mu W))^{1/2}. \qquad (99)$$

The reason that the proportionality constant relating $P_D^{1/2}$ and E_{rf} is smaller for the rectangular cavity than for the reentrant cavity (Eq. 97) is that the rectangular cavity has a much larger effective volume for storing rf energy. Even though Q_o(rect.) $\simeq 4\ Q_o$ (reentrant), the volume effect more than compensates and so the reentrant cavity will produce larger fields at the sample position for a given value of P_D.

The remainder of the microwave system is illustrated schematically in Fig. 9. Microwave power produced by a tunable General Radio 1360-A microwave oscillator was supplied to the cavity via 0.141 inch semirigid coaxial cable. Incident and reflected rf powers were monitored with a Boonton 41A-R microwattmeter while junction data was being collected to insure that the microwave field strengths remained constant. When operating below the λ-point of helium, a value of $P_D \gtrsim$ 8-10 mW would result in relatively rapid cavity detuning due to the consequent decrease in helium density as the helium bath warmed up.

Static magnetic fields up to 20G could be applied with a small Helmholtz coil pair placed outside the microwave cavity but inside the helium bath. The cavity and magnet were both enclosed in a superconducting shield can to prevent interference from stray rf and magnetic fields, and additional magnetic shielding was placed outside the liquid nitrogen dewar in order to screen out the earth's field.

D. Electronics

The tunnel junction I-V characteristics were determined by sweeping the junction with a constant current biasssupply and measuring the junction

voltage using 4 terminal circuits such as the one shown schematically in Fig. 9. The motorized Helipot sweep and low pass filter were replaced by a Wavetek voltage controlled signal generator when oscilloscope display of the I-V characteristic was desired. The Wavetek generator could also be used to produce chart recordings of I-V characteristics when operating at sweep frequencies in the range 0.01-0.05 Hz. The junction bias current was determined by measuring the voltage drop across a nominal 1% tolerance resistor in series with the tunnel junction.

The junction dynamic resistance dV/dI as a function of voltage was determined by conventional phase-sensitive detection techniques.[17] The dynamic conductance dI/dV could also be determined directly by the use of a novel technique involving data acquisition with a RIDL 34-27 series multichannel analyzer. The junction was biased with the Wavetek generator operating in a linear (triangle wave) sweep mode thus producing a condition in which dI/dt=constant. Since the dynamic conductance can be expressed as

$$dI/dV = (dI/dt)/(dV/dt),$$

a quantity G(V) which is proportional to dI/dV can be determined from measurement of dt/dV. The voltage V was used to determine the analyzer memory address or channel in which input pulses from a 10 KHz pulse generator were to be stored. Since the voltage widths dV were also constant, the time dt(V) spent at each channel was proportional to G(V) and thus so was the number of counts stored in the channel corresponding to voltage V. The sensitivity of this technique compares favorably

with that found when using ac modulation and lock-in detection to measure dV/dI, and when rapid qualitative data was desired, the analyzer technique proved much the better of the two methods because stray short duration noise pulses picked up by the voltage measuring circuitry did not greatly affect the quality of the recorded data.

V. EXPERIMENTAL RESULTS

A. Quasiparticle PAT

The experimental response of the quasiparticle tunneling current to the perpendicular rf electric field was determined by measuring the junction I-V characteristic at a series of microwave power levels. The bare current $I_o(V)$ was taken to be the experimentally measured current with zero rf power applied (cf. Fig. 2), and the various theoretical characteristics were then calculated numerically from Eqs. (54) and (57) with α as a parameter, or from Eq. (56) with V_{rf} as a parameter. The experimental current deviations, $\Delta I = I(V)-I_o(V)$, were determined from I-V chart recording on which a group of I(V) graphs were superimposed on an $I_o(V)$ graph. Voltage differences were measured to an accuracy of $\pm$ 2μV using a horizontal scale of 50 μV/inch, while the current deviations, ΔI, were measured to an accuracy of approximately 3% of the maximum observed deviation at any given bias. The resistance parameter, $R=1/G_{NN}$, was determined for each junction by fitting the measured $I_o(V)$ for $V > 2\Delta/e + \delta V$ to the theoretical $RI_o(V)$ function calculated from Eq. (1). The value of $\Delta_{Pb} + \Delta_{Sn}$ or $2\Delta_{Sn}$ was determined using a method described by Rowell and McMillan[22] in which the sum of the energy gaps corresponds to the voltage at which the current has increased to approximately one half the value of the equivalent BCS current discontinuity (cf. Fig. 19). In calculating $RI_o(V)$ from Eq.(1), the transition temperature for the Pb films was taken as the measured bulk value, 7.19°K, while T_c for the Sn films was taken as the measured value (T_o=3.78±.03°K for all the Sn films). The zero voltage Josephson current, which was always observed for junctions with $R \lesssim 30\ \Omega$, was quenched with a dc magnetic

field while the quasiparticle characteristics were being measured.

The amount of non-tunneling or excess current flowing in the junction was measured by subtracting the theoretical thermally excited background current, calculated from Eq. (1), from the measured current at voltages $V < (\Delta_1 + \Delta_2)/e$, as illustrated in Fig. 2. The broad current rise at $V = \Delta_{Sn}/e$, discussed in Section I, is clearly evident in this figure. There was a general tendency for lower resistance junctions to have larger fractional excess currents but several exceptions to this rule were observed.

Typical graphs of the single particle tunneling current response for Sn-SnO-Sn junctions to a 3.93 GHz ($\hbar\omega/e = 16.3\mu V$) field are shown in Figs. 10,11, and 12. The data of Fig. 10 were taken at a reduced temperature $t=0.87$ while that of Figs. 11 and 12 were taken at $t=0.30$. The current deviations, ΔI, determined from Figs. 11 and 12 are plotted in Figs. 13 and 14 respectively, while $\Delta I(V)$ for a junction with a resistance between that of the junctions shown in Figs. 11 and 12 is shown in Fig. 15. The solid curves in Figs. 13-15 are graphs of $\Delta I_{TG}(V)$ derived from Eq. (54). The correspondence between the microwave power, P_D, and α was determined by fitting at only one point for each junction. If P_{Dm} was the microwave power dissipated in the cavity at the highest power level used, then α_m, the value of α corresponding to P_{Dm}, was determined by fitting the theoretical ΔI to the experimental ΔI at the point of maximum deviation. All succeeding theoretical $\Delta I(V)$ curves were then calculated by using α's determined from the relation,

$$\alpha(P_D) = \alpha_m (P_D/P_{Dm})^{1/2}. \tag{99}$$

The agreement between the TG theory and experiment is excellent in the limit of high junction resistance for all values of P_D, as can be seen from an inspection of Fig. 13. For Sn-SnO-Sn junctions with $R \gtrsim 2.5\ \Omega$, the exact point chosen to fit the data made little difference in the ultimate value of α_m determined from the fit. For the lower resistance junctions, agreement between experiment and the TG theory becomes progressively worse as R decreases, and hence the fitting procedure becomes somewhat ambiguous. In an attempt to improve agreement between theory and experiment for the low resistance junctions, we tried to determine α_m by fitting at low microwave power levels, as indicated by the dashed line in Fig. 15. Although this improved the small α agreement somewhat, the deduced fits for large α were then extremely poor. The agreement between theory and experiment improved at higher temperatures for the low resistance junctions, but for sufficiently small values of α deviations always occurred.

In Fig. 16 the data for the 6.35 Ω junction of Figs. 11 and 13 have been replotted to show $|\Delta I|$ as a function of P_D or α for various dc voltages measured from $V = 2\Delta_{Sn}/e$. The agreement between theory and experiment can be seen to be quite good, even in the limit of small α. Fig. 9 also indicates that the low rf power limit result, $|\Delta I| \propto P_D$, predicted by Eq. (55) is valid only in the range $\alpha \lesssim 1$. In Fig. 17 the α=1.8 data from Fig. 13 have been replotted together with theoretical ΔI_{TG}, ΔI_{RF}, and ΔI_{CE} curves calculated from Eqs. (54), (56), and (57) respectively. The very close agreement between the experimental points and ΔI_{TG} is clearly evident, as is the much poorer agreement between experiment and ΔI_{CE}. It can also be seen that $\Delta I_{RF}(V)$ is very close to

$\Delta I_{TG}(V)$, even at this low value of α. Numerical calculations indicate that I_{TG} and I_{RF} are approximately equal where $\alpha \gtrsim 10$ for 4 GHz microwaves.

In order to test the effects of finite junction capacitance, we calculated theoretical ΔI_{RF} characteristics for several of the low ($\lesssim 2\Omega$) resistance Sn-SnO-Sn junctions using the model discussed in Section III-D. The parameter κ defined in Eq. (86) was at first treated as an adjustable parameter since the junction capacitance was not precisely known. ΔI_{RF} was then calculated for a 0.59 Ω junction using a series of values for κ until substantial agreement between theoretical and experimental ΔI's was obtained. With κ determined, the capacitance was calculated from Eq. (86), and this value of C was subsequently employed to calculate κ for junctions with different values of R. In Fig. 18, ΔI_{RF} and ΔI_{TG} are shown for a junction with R=1.31 Ω and κ=11.3. The modified theory can be seen to fit the data very closely over most of the voltage range. The difference between ΔI_{RF} and the experimental points at $V-V_o \simeq 5\times10^{-2}$ mV is probably caused by using the classical formulas for calculating ΔI in lieu of the proper Tien-Gordon quantum mechanical formalism. A similar discrepancy between ΔI_{RF} and experiment is evident in Fig. 17 for a high resistance junction (R= 6.35 Ω, κ= 54.8). The experimental value of C for the junctions with a surface area A= 2.56×10^{-4} cm^2 was C= 350±10 $\mu\mu$F. With this value of C, the ratio of barrier thickness to dielectric constant, ℓ/ε_s, calculated from the expression $C= \varepsilon_s A/4\pi\ell$ is ℓ/ε_s= 6.5 Å, which is about twice as large as values of the same parameter derived from Eq. (19) and (78) with measured Fiske mode voltage spacing (See Section IV-B).

The validity of the CE theory was tested by comparing the measured response of high resistance Sn-SnO-Pb junctions to the response predicted by Eq. (58). Typical results are presented in Figs. 19 and 20 for a junction with $R \simeq 120\ \Omega$. Fig. 19 shows the measured I(V) characteristic compared with both I_{CE} and I_{TG}. Again, I_{TG} fits the data very closely while I_{CE} deviates appreciably from the experimental points. Fig. 20 shows the experimental current deviation compared to ΔI_{CE} and ΔI_{TG}. The variation of ΔI_{CE} from the data becomes smaller as α decreases, as predicted by Eq. (58). Fig. 17 shows a comparison of ΔI_{CE} and an experimental ΔI curve for a 6.35 Ω Sn-SnO-Sn junction at $\alpha = 1.8$. Even at this low value of α there is a large difference between ΔI_{CE} and ΔI_{TG}. In view of the detailed agreement between the predictions of the TG theory and the experimental data for low-frequency photon-assisted tunneling, it would appear that attempts[3,4] to explain the results of higher frequency tunneling measurements with Eq. (57) are incorrect.

At a fixed microwave power level, all samples of the same type would be expected to see the same rf voltage for a given value of P_D, since the magnitude of the induced voltage should depend only on physical parameters of the junction such as the barrier and electrode thicknesses. Since the barrier thickness ℓ is approximately constant for an order of magnitude change in normal state resistance,[60] there should not be a strong dependence of rf voltage on that parameter. Experimentally, there was a small spread in α values required to fit the quasiparticle I(V) data for the different junctions at the same microwave power level. For the experiments with Sn-SnO-Sn junctions in the reentrant cavity described in Section III-B, the effective values of α for $P_D = 10^{-4}$ W were

in the range, $\alpha_{eff}=1.9 \pm 0.6$. The experiments with the Sn-SnO-Pb junction in the rectangular cavity yielded, with one exception, an equivalent range of α_{eff} values, $\alpha_{eff} \simeq 4.2 \pm 0.7$ for $P_D=6.65\times10^{-4}$ W which is equivalent to $P_D=10^{-4}$ W in the reentrant cavity. The exact reason for the discrepancy in α_{eff} values between coaxial and rectangular cavities is not known, but it is within the margin of error of P_D measurement for the reentrant cavity as discussed in Section III-C. For the data relative to each cavity, there was no obvious correlation between the value of α_{eff} corresponding to a fixed P_D and junction normal state resistance or electrode film thicknesses. The average effective rf voltage calculated from $\alpha_{eff}\,\hbar\omega/e$ corresponding to $P_D=10^{-4}$ W in the coaxial cavity is $\langle V_{rf} \rangle \simeq 33$ μV. Using Eq. (97) to calculate the magnitude of the rf electric field present in the bare cavity, we find $|\underset{\sim}{E}_{rf}| = 8.48\times10^{-2}$ μV/Å, and thus the effective distance over which the rf voltage is developed should be $\langle V_{rf} \rangle/|\underset{\sim}{E}_{rf}| \simeq 390$ Å. This distance is an order of magnitude larger than a typical oxide barrier thickness, $\ell \simeq 20$ Å, indicating that the effective rf voltage is enhanced relative to the bare cavity voltage $\langle V_{rf} \rangle = |\underset{\sim}{E}_{rf}|\ell$ which is developed across a distance equal to the barrier thickness. Similar effects have previously been observed qualitatively in both quasiparticle[1,2,48] and Josephson[8] photon-assisted tunneling.

We can summarize the results of our quasiparticle PAT experiments by noting that we have observed excellent detailed agreement between experiment and the predictions of the TG theory when the parameter α is treated as an adjustable constant. Discrepancies which occur between the basic theory and experiment for low resistance junctions can be

explained by a model which includes the effects of junction capacitance. There remains, however, an order of magnitude discrepancy between the magnitude of V_{rf} necessary to fit the I-V data and the magnitude of V_{rf} which exists in the bare cavity along a distance equal to the oxide barrier thickness.

B. Josephson PAT

All the experimental measurements of Josephson tunneling phenomena were performed on the same Sn-SnO-Sn junctions which were used in the quasiparticle PAT experiments described in Section IV-A. The magnitude of the rf electric field was again determined from measurement of the incident and reflected microwave power. The magnitude of the static magnetic field was determined from measurement of the Helmholtz coil current using a calculated constant of proportionality between current and field. Due to some uncertainty in the value of the coil packing factor, magnetic field measurements were considered to be accurate only to within ± 10% of the theoretical design value.

A composite of two typical I-V graphs is shown in Fig. 21 for a 2.58 Ω junction with a length $L=1.6\times10^{-2}$ cm perpendicular to the dc magnetic field direction. The section of the graph marked I_{F1} indicates the current which flows in the first Fiske mode when the dc magnetic field has been set to produce the first zero in I_J. Fig. 22 illustrates a typical dependence of I_J on dc magnetic field for a junction with $1 \lesssim R_{NN} \lesssim 8\ \Omega$ as compared to the theoretical Fraunhoter type pattern prediction of Eq. (28) indicated by the dashed line. For lower resistance junctions ($R_{NN} \lesssim 0.1\ \Omega$), the field dependence of I_J agreed very closely with the theoretical prediction of Eq. (28), while for junctions with

larger values of R_{NN}, the magnitude of the sidelobes was usually less than the theoretical value, as indicated in Fig. 22. The magnetic field values at which $I_J=0$ were, however, always integer multiples of the field corresponding to the first zero in I_J, as predicted by Eq. (28).

As a standard of junction quality, we required that any junction being analyzed have a well defined I_J diffraction pattern with at least two sidelobes. Although all junctions had the same nominal length perpendicular to H_o, $L=1.6\times10^{-2}$ cm, there was an apparently random variation in the period, ΔH_o, between nulls in I_J. The cause of this variation cannot be completely determined since, according to Eqs. (28) and (29), measurement of ΔH_o yields only the product $Ld \simeq 2\lambda L$. If we assume that L is equal to its measured value, then the derived penetration lengths were in the range $\lambda_{Sn}(T=0°K) = 375 \pm 70$ Å, in reasonable agreement with the value $\lambda_{Sn}=400$ Å found by Matisoo[40] in measurements of Josephson junction critical currents. The observed temperature dependence of ΔH_o was also in reasonably good agreement with the theoretical inverse London penetration length temperature dependence,[61] $\lambda(0)/\lambda(T) = (1-(T/T_c)^4)^{1/2}$.

As another check of junction quality, we measured the temperature dependence of I_J for selected junctions and compared the measured $I_J(T)$ with the prediction of the Ambegaokar and Baratoff formula, Eq. (15). The ratios of the measured values of $I_J(T=0°K)$ to the theoretical value, $I_J(\text{theor.})=\pi\Delta(0)/2R_{NN}$, all fell within the range $0.79 \leqslant I_{rel} \leqslant 0.90$, where $I_{rel} = I_J(\text{meas.})/I_J(\text{theor.})$, with the average value of I_{rel} given by $\langle I_{rel} \rangle = 0.85$. This value is in reasonably good agreement with the

value $I_{rel} = 0.91$ for an Sn-I-Sn junction derived by Fulton and McCumber[62] in a calculation which included strong coupling superconductivity corrections to the basic Ambegaokar and Baratoff formalism. If $I_J(T=0°K)$ was taken as the experimentally measured value, the experimental $I_J(T)/I_J(0)$ function agreed very closely with the dependence predicted by Eq. (15).

Measurements of self-resonant or Fiske mode phenomena indicated that the amplitude dependence of the mode currents on H_o was complicated and not reproducible from sample to sample. A typical experimental I-V trace is shown in Fig. 23, where the arrows indicate the path traced for increasing or decreasing bias current. Fig. 22 indicates a typical experimental magnetic field dependence of mode currents on H_o, and is in general agreement with both the qualitative predictions of the linear theory described in Section III-C and similar measurements of Dimitrenko and Yanson.[62] The Fiske mode voltages V_n were usually spaced at equal intervals as predicted by Eq. (78). Although some examples of anomolous behavior were observed, they were neither reproducible, nor could they be correlated with the positions $V_{n,m}$ predicted by Eq. (83) for the case where wavevector quantization exists in both spatial dimensions in the plane of the junction. The average value of the Fiske mode spacing for our junctions was $\Delta V_n = 105\ \mu V$, yielding a value of $\ell/\varepsilon = 2.9$ from Eq. (78) if λ_{Sn} is taken as 500 Å, the value for pure tin.[63] With our value $\lambda_{Sn} \simeq 375$ Å derived from the measured average magnetic field dependence of I_J, we find $\ell/\varepsilon \simeq 2.1$. In Table I we list reported experimental value of ℓ/ε for Sn-SnO-Sn junctions and the methods by which they have been determined.

The predicted temperature dependence of the voltage interval between self-resonant modes as indicated by Eq. (78) is,

$$V_n(T)/V_n(0) = v_J(T)/v_J(0),$$

or, using Eq. (19) for v_J,

$$V_n(T)/V_n(0) = [1-(T/T_c)^4]^{1/4}. \qquad (100)$$

Although Dmitrenko and Yanson[62] have previously reported good agreement between the measured $V_1(t)$ and Eq. (100) for the first step, our measurements do not agree well with this theory. At reduced temperatures $0.6 < t \leq 1$, we find that $V_1(t)$ decreases more rapidly with increasing temperature than Eq. (100) predicts. Above a reduced temperature $t=0.73$ the spacing between the modes did not correspond to integral multiples of a fundamental spacing, as predicted by Eq. (78).

Ngai[64] has recently included the frequency dependence of the penetration depth (and hence the frequency dependence of v_J) in a calculation of $V_n(T)$. Although his theory predicts that the step spacing will become non-uniform for $t > 0.6$ because of the frequency ddependence of v_J, it also preducts that $V_n(T)$ will fall off <u>less</u> rapidly with increasing T than the rate predicted by Eq. (100), in contradiction with our experimental data.

The effect of the externally applied microwave field on the Josephson currents was determined by methods analogous to those used in the quasiparticle PAT experiments. The dependence of I_J on rf power

was determined for all the junctions used in the PAT experiments and the interaction of the external field with the Fiske mode currents was studied for selected samples. In general, we observed poor quantitative agreement with the theory discussed in Section III-C and large variations in measured quantities from sample to sample. For junctions with large excess current components, the effect of the rf electric field was to induce constant current steps at voltages $V_n = n\hbar\omega/2e$ as predicted by Eqs. (71) and (72). Although the step amplitudes were oscillatory functions of rf power, they did not vary as $J_n(2\alpha)$, as predicted by Eq. (72). A typical experimental I-V trace for a junction with excess current exposed to 4 GHz radiation is shown in Fig. 24. For the junctions used in our experiments which had small excess current components (cf. Fig. 2) the response to the rf field was quite different. The usual effect of the rf field was a monotonic decrease in I_J to zero. Thereafter, I_J usually remained zero for larger fields, but in some cases a small I_J would reappear at discrete values of P_D. Higher order induced steps could not be produced in these junctions, even at reduced temperatures near one where a large thermally excited quasiparticle current component existed.

The general nature of the measured dependence of I_J on $(P_D)^{1/2}$ is illustrated in Fig. 25. A $J_o(2\alpha)$ function has been fitted to the experimental curve at the points where $V_{rf}=0$ and where $I_J=0$ to indicate the usual nature of the discrepancy between theory and experiment. The small peak in the experimental graph near $V_{rf}=0$ was observed in all the samples, but the magnitude of the peak relative to the extrapolated value of I_J varied from sample to sample in the range $.03\ I_J \lesssim \delta I_J \lesssim 0.1\ I_J$. We

have assumed that this peak is caused by small short circuit current components flowing near the junction edges but no detailed analysis of the phenomena was performed. The experimental value of α for which the first zero of I_J occurred, α_J, was determined from Eq. (99) by using values of α_m and P_{Dm} determined from the single particle current response data, together with the measured P_D at which I_J=0. The values of α_J determined in this manner ranged from 0.19 to 10.4 as compared to the theoretical value of 1.2 at which $J_o(2\alpha)$=0. The experimental values of α_J appeared to vary randomly and were not correlated with either R_{NN} or the magnitude of the excess current component, even for junctions on the same substrate.

The rf detection sensitivity of the self-resonant mode currents was usually greater than the sensitivity of I_J. If the dc magnetic field was adjusted to maximize the first Fiske mode current, then the presence of external rf power would reduce I_{F1} to zero at a value $\alpha \simeq 0.1\ \alpha_J$. There was, however, no evidence of mixing between the external rf and the Fiske mode fields, i.e. no induced rf steps appeared superimposed on the Fiske steps.

In an attempt to obtain experimental evidence for the existence of the Riedel singularity in the Josephson current amplitude, we observed the response of I_J at large values of α, as determined from Eq. (99) with $\alpha_m = \alpha_J$. As discussed in Section III-C, Eq. (75) predicts that there should be an observable $I_J(\alpha)$ when the conditions $n\hbar\omega = 2\Delta$, $\alpha \simeq n$ are satisfied. In our case, n = 75 and, assuming $j_2(2\Delta/\hbar) \gtrsim 10\ j_2(0)$ we find that $I_J(\alpha=75) \simeq 0.1\ I_J(0)$. Although Eq. (75) predicts that the n ± 1 terms will contribute values of opposite sign

from the n^{th} term, the singularity in $j_2(\omega)$ as given by Eq. (65) is so sharp that $j_2(2\Delta/\hbar \pm \omega) \simeq 3.2 j_2(0)$, and hence the $n \pm 1$ terms will not cancel the n^{th} term when $\hbar\omega$ is an exact multiple of 2Δ. After stabilizing the junction temperature at $T \simeq 1.15°K$, the microwave frequency was adjusted slightly until $2\Delta/\hbar\omega = 75$. The dc Josephson current was then monitored as a function of rf power up to the highest rf powers attainable on two of our samples for which values of $\alpha > 75$ could be reached. No dc Josephson current was observed at large α within the experimental limit for these measurements, $\pm .01\ I_J(0)$.

VI. DISCUSSION AND CONCLUSIONS

The principal result of our low-frequency quasiparticle PAT measurements is the confirmation of the validity of the TG theoretical description of the process. In the limit where the parameter κ (defined by Eq. (86)) is large, the basic TG formula, Eq. (54), fits the data very closely for all values of $\alpha \leqslant 60$. At lower values of the parameter κ, the model described in Section III-D predicts the shape of the I-V characteristics quite accurately at low rf power levels where the basic TG theory fails. A consequence of this theory is that the external microwave field acts either as a voltage source in series with the junction capacitance or as a current source with a magnitude $i_{rf}/\omega C \propto \sqrt{P_D}/\omega C$ in parallel with both the capacitance and the quasiparticle nonlinear resistance. Although this model has been successful in explaining the measured data, we have not been able to derive it from the more general electromagnetic wave equation, Eq. (34). A secondary result obtained from comparison of model predictions and experimental data has been the indirect determination of junction capacitance at 4 GHz, resulting in an experimental value of ℓ/ε for Sn-SnO-Sn junctions, ℓ/ε=6.5 Å (see Table I). This value is about twice as large as most of the values previously determined from measurements of Fiske mode voltages (Table I), but considering the simplicity of our model, the agreement is felt to be quite good.

Since all the sample junctions were prepared in an identical manner, except for oxidation time, the variations in the actual strength of the coupling between the junctions and the rf field may be dependent on the condition of the oxide barrier at the edge of the

junction, which will vary from sample to sample in an unknown way, leading to a spread in experimental α values for a given rf power level. The order of magnitude discrepancy observed between calculated and actual microwave voltage across the junction has previously been ascribed to a large impedance mismatch between the microwave cavity and the junction.[38] However, if microwave power is reflected from the junction because of an impedance mismatch, we would expect that the effective rf voltage across the junction would be smaller than the rf voltage across a equivalent length of bare cavity. This would lead to $\alpha_{cav} > \alpha_{eff}$, where α_{cav} is determined from rf power measurement and α_{eff} from I-V curve fitting. Since experimentally, $\alpha_{eff} \simeq (20\text{-}50) \times \alpha_{cav}$, some alternative explanation is required. If one assumes that the bare rf voltage appears across the junction electrodes, then one must also assume that the junction barrier has an effective thickness $\ell \gtrsim 400$ Å to account for the observed values of α_{eff}.

In view of the detailed agreement between the predictions of the TG theory and the experimental data for low-frequency PAT, it would appear that recent attempts[3,5] to explain the results of higher frequency tunneling experiments with the CE theory (Eq. (57)) are incorrect. The results of a recent PAT experiment performed by Hamilton and Shapiro[65] at 70 GHz on Sn-SnO-Sn junctions have been explained by them in a semi-quantitative manner by including the effects of transverse spatial variation in the high frequency rf voltage, presumably by use of Eqs. (62) and (63). The major difficulty encountered in making a detailed comparison between theory and experiment at high frequencies is lack of detailed knowledge of the function

$V_{rf}(x)$ to be used in Eq. (62). Hamilton and Shapiro chose a conventional standing wave for this function, characterized by one parameter, the voltage standing wave ratio (VSWR), and then adjusted this parameter to fit experimental results to the theory. For our experiments the wavelength of 4 GHz radiation in the oxide barrier is estimated to be $\bar{\lambda} \simeq 3.7$ mm from Eq. (59), and since $\bar{\lambda} >> L$, the assumption of uniform rf voltage is certainly valid.

Our experiments on the interaction of Josephson currents with the rf field indicate that Josephson PAT is not well described by the basic theory outlined in Section III-C, even though the dependence of I_J on magnetic field and temperature agrees well with the dc theory of Section II-B. In particular, the functional dependence of I_J on α does not agree with the prediction of Eq. (75). The wide spread in α_J values for different samples indicates that sample variables (such as the microscopic condition of the junction boundary or film surface roughness) need to be accounted for. The deviation of α_J values from the theoretically predicted value of 1.2 and the large experimental spread of these values indicate that the quasiparticle and Josephson components of the current do not see the same value of rf voltage at the fundamental frequency ω for a given value of microwave power incident on the junction.

Another major discrepancy between experiment and theory has been lack of higher order induced steps in the I-V characteristics at voltages $\pm n\hbar\omega/2e$ for junctions with little or no excess current component. Although this may be due to a fundamental shortcoming of the theory, it could also be a result of instabilities in the junction

caused by noise voltages from the constant current bias circuitry. It may be noted, however, that for junctions with excess currents we could trace out the induced steps in the I-V characteristic with the dc sweep circuitry illustrated in Fig. 9, and it was possible to hold the voltage constant at any point on a step for long periods of time without the occurrence of a noise induced transition to the next step. It therefore seems likely that the presence of a nontunneling current component increases the inherent stability of the Josephson currents at the induced step voltages, and that the amplitudes of these currents are much smaller than those predicted by Eq. (75).

Experimental study of the interaction of external microwave radiation with the self-resonant mode currents produced no direct evidence for the existence of large rf voltages at the mixing frequencies $\omega_{n,m}=2eV_{n/\hbar} \pm n\omega_{rf}$, where V_n is the n^{th} Fiske mode voltage. The response of the Fiske mode currents to the external rf was similar to that of I_J although the rf voltage sensitivity was somewhat greater. Our search for experimental evidence of the Riedel singularity in the response of I_J likewise produced a null result, but this seems quite reasonable in view of the expected smearing of the Josephson current amplitude $j_2(\omega)$ near $\omega = 2\Delta/\hbar$.

APPENDICES

A. Derivation of BCS Model Current, Eq. (1) from Eq. (52).

The imaginary part of the current amplitude j_1, as given by Eq. (52) is,

$$\mathrm{Im}j_1(\omega) = \frac{4e\pi}{\hbar} \sum_{\underset{\sim}{k},\underset{\sim}{q}} |T_{\underset{\sim}{k},\underset{\sim}{q}}|^2 \int_{-\infty}^{\infty} d\omega' \, [f(\omega'+\omega)-f(\omega')] \times A_{\underset{\sim}{k}}(\omega+\omega') \, A_{\underset{\sim}{q}}(\omega'). \tag{A-1}$$

With the definition, $\omega_{\underset{\sim}{k}}=E_{\underset{\sim}{k}}/\hbar$, the spectral weight function $A_{\underset{\sim}{k}}(\omega)$ defined by Eq. (39) can be written,

$$A_{\underset{\sim}{k}}(\omega) = 1/2 \, \{[1+(\varepsilon_{\underset{\sim}{k}}/E_{\underset{\sim}{k}})]\delta(\omega-\omega_{\underset{\sim}{k}}) + [1-(\varepsilon_{\underset{\sim}{k}}/E_{\underset{\sim}{k}})]\delta(\omega+\omega_{\underset{\sim}{k}})\}. \tag{A-2}$$

To evaluate (A-1) in the BCS approximation, we use (A-2) for $A_{\underset{\sim}{k}}(\omega)$ and change the $\underset{\sim}{k}$ and $\underset{\sim}{q}$ summations to energy integrations via the prescription,

$$\sum_{\underset{\sim}{k}} \rightarrow \int N(\varepsilon_{\underset{\sim}{k}}) d\varepsilon_{\underset{\sim}{k}},$$

where $N(\varepsilon_{\underset{\sim}{k}})$ is the energy density of states for one spin. After performing the ω' integration we find,

$$\mathrm{Im}j_1(\omega) = \frac{e\pi}{\hbar} \int N_\ell(\varepsilon_{\underset{\sim}{q}}) d\varepsilon_{\underset{\sim}{q}} \int N_r(\varepsilon_{\underset{\sim}{k}}) d\varepsilon_{\underset{\sim}{k}} |T_{\underset{\sim}{k},\underset{\sim}{q}}|^2 F(\omega,\varepsilon_{\underset{\sim}{k}},\varepsilon_{\underset{\sim}{q}}), \tag{A-3}$$

where $F(\omega,\varepsilon_{\underset{\sim}{k}}, \varepsilon_{\underset{\sim}{q}})$ is defined by,

$$F(\omega,\underset{\sim}{\varepsilon_k},\underset{\sim}{\varepsilon_q}) = \{[-f(\underset{\sim}{\omega_q}+\omega) + f(\underset{\sim}{\omega_q})](1+\underset{\sim}{\varepsilon_q}/\underset{\sim}{E_q})$$

$$\times [(1+\underset{\sim}{\varepsilon_k}/\underset{\sim}{E_k})\,\delta(\omega+\underset{\sim}{\omega_q}-\underset{\sim}{\omega_k}) + (1-\underset{\sim}{\varepsilon_k}/\underset{\sim}{E_k})\,\delta(\omega+\underset{\sim}{\omega_q}+\underset{\sim}{\omega_k})$$

$$+ [-f(\omega-\underset{\sim}{\omega_q}) + f(-\underset{\sim}{\omega_q})](1-\underset{\sim}{\varepsilon_q}/\underset{\sim}{E_q})$$

$$\times [(1+\underset{\sim}{\varepsilon_k}/\underset{\sim}{E_k})\,\delta(\omega-\underset{\sim}{\omega_k}-\underset{\sim}{\omega_q}) + (1-\underset{\sim}{\varepsilon_k}/\underset{\sim}{E_k})\,\delta(\omega+\underset{\sim}{\omega_k}-\underset{\sim}{\omega_q})]\}. \qquad \text{(A-4)}$$

In the constant energy gap model, $\underset{\sim}{\Delta_k}=\Delta$ for all $\underset{\sim}{k}$, and thus,

$$\underset{\sim}{E_k} = (\underset{\sim}{\varepsilon_k}^2+\Delta^2)^{1/2}. \qquad \text{(A-5)}$$

In the evaluation of (A-3) we shall have to calculate integrals of the form $\int_{-\infty}^{\infty} g(\underset{\sim}{\varepsilon_k},\underset{\sim}{E_k})d\underset{\sim}{\varepsilon_k}$, where g is a function which contains factors such as $\delta(E-\underset{\sim}{E_k})$. In order to change the integration variable to $\underset{\sim}{E_k}$ we divide the original $\underset{\sim}{\varepsilon_k}$ integration into negative and positive parts,

$$\int_{-\infty}^{\infty} g(\underset{\sim}{\varepsilon_k},\underset{\sim}{E_k})d\underset{\sim}{\varepsilon_k} = \int_{-\infty}^{0} + \int_{0}^{\infty} g\; d\underset{\sim}{\varepsilon_k}. \qquad \text{(A-5)}$$

The integral over the negative $\underset{\sim}{\varepsilon_k}$ region can be rewritten

$$\int_{-\infty}^{0} g(\underset{\sim}{\varepsilon_k},\underset{\sim}{E_k})4\underset{\sim}{\varepsilon_k} = \int_{0}^{\infty} g(-\underset{\sim}{\varepsilon_k},\underset{\sim}{E_k})d\underset{\sim}{\varepsilon_k},$$

by changing the order of integration and then making the variable change $\underset{\sim}{\varepsilon_k} \rightarrow \underset{\sim}{\varepsilon_k}$. Since $\underset{\sim}{\varepsilon_k}=+(\underset{\sim}{E_k}^2-\Delta^2)^{1/2}$ for $\underset{\sim}{\varepsilon_k}>0$, $d\underset{\sim}{\varepsilon_k}/d\underset{\sim}{E_k}=\underset{\sim}{E_k}/\underset{\sim}{\varepsilon_k}$, Eq. (A-5) can

then be written as,

$$\int_{-\infty}^{\infty} g(\varepsilon_{\underset{\sim}{k}}, E_{\underset{\sim}{k}})d\varepsilon_{\underset{\sim}{k}} = \int_{0}^{\infty}[g(\varepsilon_{\underset{\sim}{k}}, E_{\underset{\sim}{k}}) + g(-\varepsilon_{\underset{\sim}{k}}, E_{\underset{\sim}{k}})]d\varepsilon_{\underset{\sim}{k}}$$

$$= \int_{0}^{\infty}[g(\varepsilon_{\underset{\sim}{k}},E_{\underset{\sim}{k}}) + g(-\varepsilon_{\underset{\sim}{k}},E_{\underset{\sim}{k}})] \frac{d\varepsilon_{\underset{\sim}{k}}}{dE_{\underset{\sim}{k}}} dE_{\underset{\sim}{k}}$$

$$= \int_{\Delta}^{\infty}[g(\varepsilon_{\underset{\sim}{k}},E_{\underset{\sim}{k}}) + g(-\varepsilon_{\underset{\sim}{k}},E_{\underset{\sim}{k}})] \frac{E_{\underset{\sim}{k}}}{|\varepsilon_{\underset{\sim}{k}}|} dE_{\underset{\sim}{k}}. \qquad \text{(A-6)}$$

With the aid of Eq. (A-6) we can easily evaluate the various integrals which appear in Eq. (A-3). All of the required integrals are of the form $\int_{-\infty}^{\infty} d\varepsilon_{\underset{\sim}{k}} 1/2(1\pm\varepsilon_{\underset{\sim}{k}}/E_{\underset{\sim}{k}})\ \delta(E_{\underset{\sim}{k}}-E)g(E_{\underset{\sim}{k}})$, and by using (A-6) we readily find

$$\int_{-\infty}^{\infty} d\varepsilon_{\underset{\sim}{k}}\ 1/2(1\pm\ \varepsilon_{\underset{\sim}{k}}/E_{\underset{\sim}{k}})\ \delta(E_{\underset{\sim}{k}}-E)g(E_{\underset{\sim}{k}}) = g(E)n(E), \qquad \text{(A-7)}$$

where n(E) is the BCS reduced density of states function,

$$n(E) = E/(E^2-\Delta^2)^{1/2} \qquad E \geqslant \Delta$$

$$= 0 \qquad E < \Delta. \qquad \text{(A-8)}$$

If we assume that the tunneling matrix element $T_{\underset{\sim}{k},\underset{\sim}{q}}$ and the normal metal densities of states are slowly varying functions of energy, then these factors may be taken outside the integrals in (A-3) and replaced by their average values. For this purpose, we define $|T_{\underset{\sim}{k},\underset{\sim}{q}}|^2 = T^2$ and $N(E) = N(0)\ n(E)$, where N(0) is the density of states at the Fermi surface. After performing the $\varepsilon_{\underset{\sim}{k}}$ integration and transforming the $\varepsilon_{\underset{\sim}{q}}$

integration with (A-6), we find that,

$$\mathrm{Im}j_1\left(\frac{eV}{\hbar}\right) = 4\,\frac{e\pi}{\hbar}\,N_r(0)N_\ell(0)T^2\int_0^\infty dE\; n_\ell(E)$$

$$\times\{[f(E)-f(E+eV)][n_r(E+eV) + n_r(-E-eV)]$$

$$+ [f(-E) - f(eV-E)]\,[n_r(eV-E) + n_r(E-eV)]\}. \qquad \text{(A-8)}$$

When $n(E)$ is redefined as $n(E) = |E|/(E^2-\Delta^2)^{1/2}$ in accordance with Eq. (3) and when the multiplicative constants in (A-8) are defined by Eq. (14), we find

$$\mathrm{Im}j_1(eV/\hbar) = G_{NN}\{\int_0^\infty dE\; n_\ell(E)\; n_r(E+eV)[f(E)-f(E+eV)]$$

$$+ \int_0^\infty dE\; n_\ell(E)\; n_r(E-eV)[f(-E) - f(eV-E)\}. \qquad \text{(A-9)}$$

If we make the change of variables $E \to -E$ in the second integral in (A-9) and also reverse the order of integration, (A-9) can be rewritten as,

$$\mathrm{Im}j_1(eV/\hbar) = G_{NN}\int_{-\infty}^{\infty} dE\; n_\ell(E)n_r(E+eV)[f(E)-f(e+eV)],$$

which, with the change of variable $E \to E-eV$, becomes the Giaever formula, Eq. (1).

B. Proof that $I_{TG}(V,\alpha) \rightarrow I_{RF}(V)$ in the Limit, $\alpha \rightarrow \infty$, $\hbar\omega \rightarrow 0$

In the classical limit, the average or dc current flowing in a nonlinear resistive element with characteristic $I_o(V)$ when biased at a voltage $V+V_{rf} \sin \omega t$ is,

$$I_{RF}(V) = \frac{\omega}{2\pi} \int_o^{2\pi/\omega} I_o(V+V_{rf} \sin \omega t)dt \qquad \text{(B-1)}$$

with the change of variable $p=\omega t$, (B-1) becomes,

$$I_{RF}(V) = \frac{1}{2\pi} \int_o^{2\pi} I_o(V+V_{rf} \sin p)dp$$

$$= \frac{1}{2\pi} \{\int_o^{\pi} [I_o(V+V_{rf} \sin p) + I_o(V-V_{rf} \sin p)]dp. \qquad \text{(B-2)}$$

By expanding the integrand in Eq. (B-2) in a Taylor in powers of $V_{rf} \sin p$ series about V and collecting terms we obtain,

$$I_{RF}(V) = \frac{1}{\pi} \sum_{n=0}^{\infty} \frac{1}{(2n)!} \left[\frac{d^{2n}}{dV^{2n}} \left(I_o(V)\right)\right] (V_{rf})^{2n} \int_o^{\pi} (\sin p)^{2n} dp, \qquad \text{(B-3)}$$

where the order of summation and integration has been reversed. With the aid of the formula,

$$\int_o^{\pi} (\sin p)^{2n} \, dp = \pi(2n)!/(2^n n!)^2,$$

we obtain

$$I_{RF}(V) = \sum_{n=0}^{\infty} \left(\frac{V_{rf}}{2}\right)^{2n} \frac{1}{(n!)^2} \frac{d^{2n}}{dV^{2n}}\left[I_o(V)\right]. \qquad \text{(B-4)}$$

In order to compare Eq. (B-4) with the limiting form of the TG formula, we expand the functions $I_o(V \pm n\hbar\omega/e)$ which appear in Eq. (54) in a Taylor series in powers of $n\hbar\omega/e$ about the point V. The resultant series may be expressed as,

$$I_{TG}(V) = \sum_{r=0}^{\infty} \frac{1}{(2r)!} (\hbar\omega/e)^{2r} \frac{d^{2r}}{dV^{2r}}\left[I_o(V)\right] \sum_{n=0}^{\infty} X_n \, n^{2r} J_n^2(\alpha), \qquad \text{(B-5)}$$

where

$$X_o = 1$$

$$X_n = 2, \qquad n > 0. \qquad \text{(B-6)}$$

Goldstein, Abeles, and Cohen[48] have shown that the summation over n may be expressed by the equation,

$$\sum_{n=0}^{\infty} X_n \, n^{2r} \, J_n^2(\alpha) = \frac{(2r)!}{(r!)^2 2^{2r}} \alpha^{2r} + \text{terms proportional}$$

$$\text{to } \alpha^{2r-2}, \; \alpha^{2r-4}, \text{ etc.} \qquad \text{(B-7)}$$

In the limit $\alpha \to \infty$, only the first term in Eq. (B-7) survives. When this term is inserted in Eq. (B-5) we find that the resultant series is the same as that for I_{RF} in Eq. (B-4).

For fixed values of r in Eq. (B-5), the summations over n can be calculated with the aid of various Bessel function sum rules. The

result through terms containing the fourth derivative of I_o can be written as,

$$I_{TG}(V) - I_o(V) = (V_{rf}/2)^2 \left\{ d^2I_o/dV^2 + \left(\frac{d^4I_o}{dV^4}\right) \frac{(\hbar\omega/e)^2}{12} \times \left[\alpha^2\left[\frac{3}{4} - J_o^2(\alpha)\right] - 2\alpha J_1(\alpha)J_o(\alpha) + 4J_1^2(\alpha) + 1 \right] \right\} \tag{B-8}$$

Thus, through terms with r=2,

$$\Delta I_{TG} - \Delta I_{RF} = \left(\frac{V_{rf}}{2}\right)^2 \frac{d^4I_o}{dV^4} \frac{(\hbar\omega/e)^2}{12} \left[-\alpha^2 J_o^2(\alpha) - 2\alpha J_1(\alpha)J_o(\alpha) + 4J_1^2(\alpha)+1\right] \tag{B-9}$$

$$= \frac{V_{rf}^4}{48} \left(\frac{d^4I_o}{dV^4}\right) \left[-J_o^2(\alpha) - \frac{2}{\alpha} J_1(\alpha)J_o(\alpha) + \frac{1}{\alpha^2}(4J_1^2(\alpha)+1)\right] \tag{B-10}$$

$$= \left(\frac{\hbar\omega/e}{48}\right)^4 \left(\frac{d^4I_o}{dV^4}\right) \left[-\alpha^4 J_o^2(\alpha) - 2\alpha^3 J_1(\alpha)\, J_o(\alpha) + \alpha^2(4J_1^2(\alpha)+1)\right]. \tag{B-11}$$

From Eqs. (B-10) and (B-11) we can observe the interesting fact that the difference between ΔI_{TG} and $\Delta I_{RF} \to 0$ not only in the limit when $\alpha \to \infty$ with V_{rf} finite, but also in the limit $\alpha \to 0$, $\hbar\omega/e$ finite.

ACKNOWLEDGEMENTS

I would like to thank Professor G. I. Rochlin for his enthusiastic support of this research project and for the invaluable assistance he provided in the design and construction of much of the cryogenic and electrical equipment used in my experiments. Thanks are also due to Professor J. Clarke and Dr. S. A. Sterling for many helpful discussions about the properties of Josephson junctions, and also to Professor L. M. Falicov for an informative discussion on problems in numerical analysis. I would also like to express my gratitude to Kathy Williams for the excellent job which she did in typing the manuscript of this thesis. Most especially, I would like to thank my wife, Mary, for the continued support and encouragement she provided throughout the duration of this research.

This work was performed under the auspices of the U. S. Atomic Energy Commission.

REFERENCES

1. A. H. Dayem and R. J. Martin, Phys. Rev. Letters 8, 246 (1962).

2. P. K. Tien and J. P. Gordon, Phys. Rev. 129, 647 (1963).

3. C. F. Cook and G. E. Everett, Phys. Rev. 159, 374 (1967).

4. D. Bonnet and H. Rabenhost, Phys. Letters 26, 174 (1968).

5. S. Teller and B. Kofoed, Solid State Comm. 8, 235 (1970).

6. B. D. Josephson, Phys. Letters 1, 251 (1962).

7. B. D. Josephson, Advan. Phys. 14, 419 (1965).

8. S. Shapiro, A. R. Janus, S. Holly, Rev. Mod. Phys. 36, 223 (1964).

9. W. L. McMillan and J. M. Rowell, in Superconductivity, edited by R. D. Parks (Marcel Dekker, Inc., N.Y., 1969), Vol. I, pp. 583-589.

10. I. Giaever and K. Megerle, Phys. Rev. 122, 1101 (1961).

11. An excellent discussion of the semiconductor analogy of metal-insulator-superconductor tunneling is given in, C. B. Duke, Tunneling In Solids, Solid State Physics, Suppl. 10 (Academic Press, N.Y., 1969) pp. 185-190.

12. M. H. Cohen, L. M. Falicov, and J. C. Phillips, Phys. Rev. Letters 8, 316 (1962).

13. W. L. McMillan and J. M. Rowell, in Superconductivity, op. cit., pp. 573-583.

14. J. Bardeen, L. N. Cooper, J. R. Schrieffer, Phys. Rev. 108, 1175 (1957).

15. S. Shapiro, P. H. Smith, J. Nicol, J. L. Miles, P. F. Strong, IBM Journal of Research and Dev. 6, 34 (1962).

16. I. Giaever, H. R. Hart, Jr., K. Megerle, Phys. Rev. 126, 941 (1962).

17. G, I. Rochlin, Phys. Rev. 153, 513 (1967).

18. N. V. Zavaritskii, Soviet Phys. JETP 14, 470 (1961).

19. P. Townsend and J. Sutton, Phys. Rev. 128, 591 (1962).

20. A summary of energy gap measurements made prior to 1964 is contained in: D. H. Douglass, Jr., and L. M. Falicov, Progress In Low Temperature Physics, C. J. Gorter, ed. (North-Holland, Amsterdam, 1964), Vol. 4, p. 177.

21. R. Meservy and B. B. Schwartz, in Superconductivity, op. cit., Vol. I, p. 141.

22. W. L. McMillan and J. M. Rowell, in Superconductivity, op. cit., Vol. I, pp. 595-597.

23. D. J. Scalapino, in Superconductivity, op. cit., Vol. I, pp. 555-557.

24. N. V. Zavaritskii, Soviet Phys. JETP 18, 1260 (1964).

25. N. V. Zavaritskii, Soviet Phys. JETP 21, 557 (1965).

26. B. L. Blackford, R. H. March, Phys. Rev. 186, 397 (1969).

27. C. K. Cambell and D. G. Walmsley, Can. J. Phys. 45, 159 (1967).

28. A. J. Bennett, Phys. Rev. 140, A1902 (1965).

29. L. C. Hebel and C. P. Slichter, Phys. Rev. 113, 1504 (1961).

30. J. R. Schrieffer, Theory of Superconductivity (W. A. Benjamin, Inc., N.Y., 1964), pp. 164-202.

31. J. R. Schrieffer and J. W. Wilkins, Phys. Rev. Letters 10, 17 (1963).

32. J. W. Wilkins, in Tunneling Phenomena in Solids, edited by E. Burstein and S. Lundquist (Plenum Press, N.Y., 1969) pp. 333-352.

33. Although the magnitude of T^2 depends on the way it is defined and the way in which the electrode wave functions are normalized, the ratio of the double to single particle current components is proportional to the single particle current transmission probability. For a uniform barrier of thickness d and height U_o, the transmission

probability is, $D \simeq \exp[-(2/\hbar)(m_e U_o)^{1/2} d]$. Using typical values for oxide barriers, $U_o \sim 1$ eV and $d \sim 30$ Å, we find that $D \simeq \exp(-20)$.

34. J. M. Rowell and W. L. Feldmann, Phys. Rev. 172, 393 (1968).

35. W. L. McMillan and J. M. Rowell, in Superconductivity, op. cit., Vol. I, pp. 561-611.

36. B. D. Josephson, in Superconductivity, op. cit., Vol. I, pp. 423-448.

37. C. B. Duke, Tunneling in Solids, op. cit., pp. 193-206; 230-250.

38. N. R. Werthamer, Phys. Rev. 147, 255 (1966).

39. C. S. Owen and D. J. Scalapino, Phys. Rev. 164, 544 (1967).

40. J. Matisoo, J. Appl. Phys. 40, 1813 (1969).

41. K. Schwidtal and R. Finnegan, J. Appl. Phys. 40, 2123 (1969).

42. V. Ambegaokar and A. Baratoff, Phys. Rev. Letters 11, 486 (1963) and erratum, 11, 104 (1963).

43. E. Riedel, Z. Naturforsch, 19A, 1634 (1964).

44. A. I. Larkin and Yu. N. Ovchinnikov, Soviet Phys. JETP 24, 1035 (1967).

45. R. E. Eck, D. J. Scalapino, B. N. Taylor, Phys. Rev. Letters 13, 15 (1964).

46. I. O. Kulik, Soviet Phys. JETP Letters 2, 84 (1965).

47. J. R. Schrieffer, Theory of Superconductivity (W. A. Benjamin, Inc., N.Y., 1964) p. 123.

48. Y. Goldstein, B. Abeles, and R. W. Cohen, Phys. Rev. 151, 349 (1966).

49. D. J. Scalapino, Tunneling in Solids, op. cit., pp. 477-518.

50. D. Coon and M. Fiske, Phys. Rev. 138, A744 (1965).

51. N. R. Werthamer and S. Shapiro, Phys. Rev. 164, 523 (1967).

52. C. C. Grimes and S. Shapiro, Phys. Rev. 169, 397 (1968).

53. D. E. McCumber, J. Appl. Phys. 39, 3113 (1968).

54. E. Isaacson and H. B. Keller, Analysis of Numerical Methods (John Wiley and Sons, Inc., N.Y., 1966), pp. 109-123.

55. R. C. Jaklevic, J. Lambe, E. Mercereau, and A. H. Silver, Phys. Rev. 140, A1628 (1965).

56. G. I. Rochlin, J. Appl. Phys. 41, 73, (1970).

57. T. Moreno, Microwave Transmission Design Data (Dover Publications, N.Y., 1948) pp. 210-241.

58. E. L. Ginzton, Microwave Measurements (McGraw-Hill Book Co., N.Y., 1957) Chapter 9, 10.

59. E. D. Reed, Proceedings of the National Electronics Conference 7, 162 (1951).

60. I. Giaever, in Tunneling Phenomena in Solids, op. cit., pp. 20-23.

61. J. R. Schrieffer, Theory of Superconductivity, op. cit., p. 12.

62. I. M. Dmitrenko and I. K. Yanson, Soviet Phys. JETP 22, 1190 (1966).

63. A. B. Pippard, Proc. Roy. Soc. (London) A203, 98 (1950).

64. K. L. Ngai, Phys. Rev. 182, 555 (1969).

65. C. Hamilton and S. Shapiro, Bull. Am. Phys. Soc. 15, 320 (1970).

Table I. Experimental value of ℓ/ε for Sn-SnO-Sn Tunnel Junctions.

ℓ/ε(Å)	Method of Measurement	Reference
6.5	Quasiparticle PAT measurement of $\kappa=2\pi fRC$	This work
2.1-2.9	Measurement of Fiske mode positions	This work
2.7	" " " " "	R. E. Eck (a)
3.5	" " " " "	J. Matisoo (b)
1.5-2	" " " " "	D. D. Coon and M. D. Fiske (c)
4.3	" " " " "	I. M. Dmitrenko, I. K. Yanson (d)
7.14	" " " " "	A. J. Dahm et. al (e)

(a) R. E. Eck, Ph.D. Thesis, Univ. of Penn. (1966), unpublished

(b) J. Matisoo, J. Appl. Phys. 40, 2091 (1969)

(c) D. D. Coon and M. D. Fiske, Reference 50

(d) I. M. Dmitrenko and I. K. Yanson, Reference 62

(e) A. J. Dahm, A. Denenstein, T. F. Finnegan, D. N. Langenberg, and D. J. Scalapino, Phys. Rev. Letters 20, 859 (1968).

FIGURE CAPTIONS

Fig. 1. (a) Normalized I-V characteristic for an Sn-I-Pb junction calculated from Eq. (1) with the BCS density of states function Eq. (3). Energy gap parameters used were $\Delta_{Sn}(0)=0.6$ mV, $\Delta_{Pb}(0)=1.4$ mV.

(b) Normalized I-V characteristic for an Sn-I-Sn junction calculated from Eq. (1). $\Delta_{Sn}(0)=0.6$ mV.

Fig. 2. Bare current $I_o(V)$ for a 1.31 Ω Sn-SnO-Sn junction with no microwave power applied. The current scale has been expanded as indicated. The dashed line labeled BCS shows the theoretical thermal background current predicted by Eq. (1).

Fig. 3. Schematic illustration of Josephson (a), single particle (b), and double particle (c) and (d) tunneling between two BCS superconductors with gap parameters Δ_L and Δ_R. In the Josephson (supercurrent) tunneling, the electrons are condensed into pairs in both electrodes, so the current flows only if there exists zero bias between electrodes. In single-particle tunneling, a pair is broken up and one of the two electrons tunnels. For non-identical electrodes, the threshold for this process is $eV=\Delta_L+\Delta_R$. In one kind of double-particle tunneling, both of the electrons that comprise a single pair tunnel through the barrier into quasi-particle states. The threshold voltage for this process is $eV=\Delta_R$ as shown in (c). Another two-particle tunneling process shown in (d) occurs when two pairs are broken in the left electrode and one member of each pair tunnels through the barrier and then recondenses in the right electrode. The threshold for this process is $eV=\Delta_L$.

Fig. 4. Schematic diagram of an "ideal" superconductor junction. The insulator is a planar slab of width ℓ and the electrodes are considered to be much longer than either of the penetration lengths, $\lambda_{1,2}$.

Fig. 5. Sketch of actual crossed-strip junction geometry showing junction in the presence of an rf electric field perpendicular to the plane of the junction. The dc magnetic field is in the y direction parallel to the edge of the bottom electrode.

Fig. 6. End and side views of crossed-strip tunneling junction showing directions of rf electric and dc magnetic fields.

Fig. 7. Schematic of lumped circuit junction model discussed in Section III-D. The rf electric field is considered to act as a voltage source in series with the junction capacitance. I_{dc} is the current supplied by the dc bias and $I_o[V(t)]$ is the total time dependent current flowing in the junction.

Fig. 8. Microwave reentrant cavity with tunnel junction samples installed. At the sample position, the rf electric field is perpendicular to the sample and the rf magnetic field is zero. A static magnetic field can be applied parallel to the common longitudinal strip.

Fig. 9. Schematic of microwave and electronic equipment used to measure the sample characteristics as a function of rf power.

Fig. 10. Bare current $I_o(V)$ and photon-assisted tunneling current for a 2.52 Ω Sn-SnO-Sn junction at a reduced temperature t=0.865. The dashed line indicates the BCS theoretical current calculated from Eq. (1).

Fig. 11. Current I(V) with microwave power applied for a 6.3 Ω

Sn-SnO-Sn junction. The numbers 1-7 of the graphs correspond to α values of 1.8, 4.0, 5.7, 8.0, 11.3, 15.0, and 18.0 respectively. α=18 corresponds to $P_D=5.3\times10^{-3}$ W dissipated in the cavity.

Fig. 12. Current I(V) with microwave power applied for a 0.35 Ω Sn-SnO-Sn junction. The numbers 1-4 of the graph correspond to α values of 3.2, 5.5, 8.4, and 12.3 respectively. α=12.3 corresponds to $P_D=7.95\times10^{-3}$ W dissipated in the cavity.

Fig. 13. $\Delta I(V,\alpha)$ derived from the I(V) curves in Fig. 11. The solid lines are theoretical curves calculated from Eq. (54). V_o is an arbitrary voltage near $V=2\Delta$ chosen for convenience in data reduction. The correspondence between α and P_D was determined by fitting curve 7 of Fig. 4 at one point.

Fig. 14. $\Delta I(V,\alpha)$ corresponding to the I(V) curves in Fig. 12. The solid lines are theoretical curves calculated from Eq. (54). V_o is an arbitrary voltage near $V=2\Delta$ chosen for convenience in data reduction. The correspondence between α and P_D was determined by fitting the graph for α=12.3 at the point where $V-V_o=-.04$ mV.

Fig. 15. $\Delta I(V,\alpha)$ for a 0.69 Ω Sn-SnO-Sn junction. The solid lines are theoretical curves calculated from Eq. (54). The curve for α=12.6 was fitted to the experimental $P_D=5.3\times10^{-3}$ W data at $V-V_o=-.05$ mV. The dashed line indicates the theoretical α=2.7 graph fitted to the $P_D=.53\times10^{-3}$ W data at $V-V_o=-.03$ mV.

Fig. 16. $|\Delta I(V,\alpha)|$ vs P_D for the junction of Figs. 11 and 13 plotted for various values of $\Delta V=V-V_o$ as indicated. The dashed lines are theoretical and the solid curves are experimental. The α range covered in this graph is $0 \leq \alpha \leq 5.4$. The linear power

dependence of $|\Delta I|$ on P_D is approximately correct for $\alpha \lesssim 1$.

Fig. 17. $\Delta I(V,\alpha)$ for a 6.35 Ω Sn-SnO-Sn junction at α=1.8. $\Delta I_{RF}(V)$ has been calculated from Eq. (56) using $V_{rf}=1.8\ \hbar\omega/e$. The points are experimental values.

Fig. 18. $\Delta I(V,\alpha)$ for a 1.31 Ω Sn-SnO-Sn junction. The solid lines have been calculated using the finite capacitance model of Section III-D and κ=11.3. The dashed lines are the TG theory predictions from Eq. (54).

Fig. 19. Typical I-V characteristic for a Sn-SnO-Pb junction at voltages near $\Delta_{Pb}+\Delta_{Sn}$. $I_o(V)$ is the measured bare current. $I_{TG}(V)$ was derived from Eq. (54) using α=19, and $I_{CE}(V)$ was derived from Eq. (57) for the same value of α. The points are experimental. $I_{BCS}(V)$ is the current predicted by the BCS constant Δ model.

Fig. 20. $\Delta I(V,\alpha)$ derived from the measured I-V graphs for the junction of Fig. 19. α was scaled as $(P_D)^{1/2}$ after fitting a theoretical $\Delta I_{TG}(V)$ to measured data at P_D=19.5 mW (not shown).

Fig. 21. Composite I-V graph of 2.58 Ω Sn-SnO-Sn junction at T=1.2°K showing zero voltage Josephson current I_J in zero magnetic field and current in the first Fiske mode I_{F1} at a magnetic field value for which I_J=0. The arrows indicate the path by which the characteristic is traced when biased by a current source.

Fig. 22. I_J vs dc magnetic field for a 2.17 Ω Sn-SnO-Sn junction. The dashed line is the theoretical pattern for junction with $L < 2\lambda_J$ predicted by Eq. (28). I_{F1} and I_{F2} are the currents observed in the first two Fiske modes.

Fig. 23. Experimental I-V graph showing Fiske mode constant current

steps. Arrows indicate the path by which the characteristic is traced when the junction is biased by a current source.

Fig. 24. Microwave induced steps for a junction in the presence of 4 GHz radiation. This junction has a large non-tunneling current component which can be seen at bias voltages $|V| > 40\mu V$.

Fig. 25. I_J vs $(P_D)^{1/2}$ for a 2.17 Ω Sn-SnO-Sn junction. The solid line is the experimentally measured graph and the dashed line represents a $J_o(2\alpha)$ function fitted at both ends of the experimental trace.

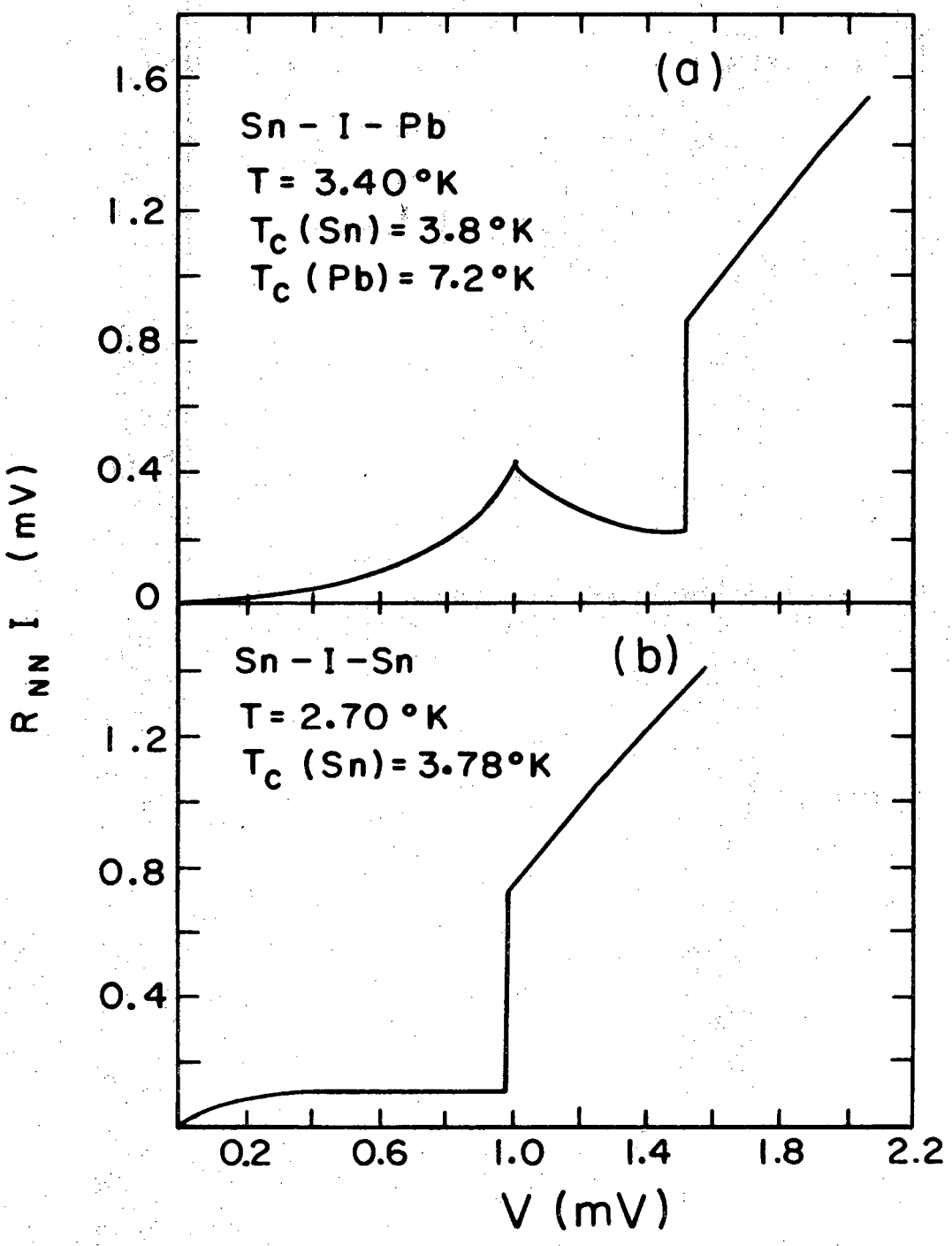

XBL706-3232

Fig. 1

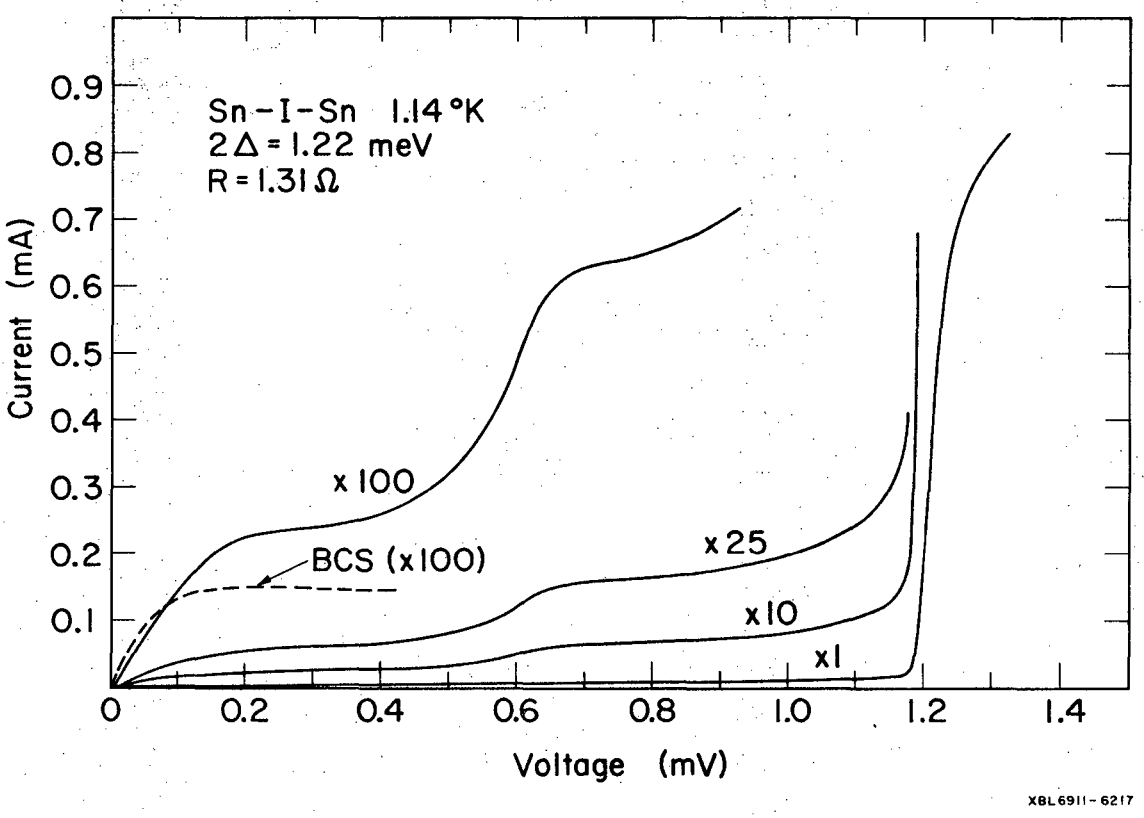
Sn-I-Sn 1.14°K
2Δ = 1.22 meV
R = 1.31 Ω
x 100
BCS (x100)
x 25
x 10
x 1
Current (mA)
Voltage (mV)
0.9
0.8
0.7
0.6
0.5
0.4
0.3
0.2
0.1
0
0.2
0.4
0.6
0.8
1.0
1.2
1.4
XBL6911-6217

Fig. 2

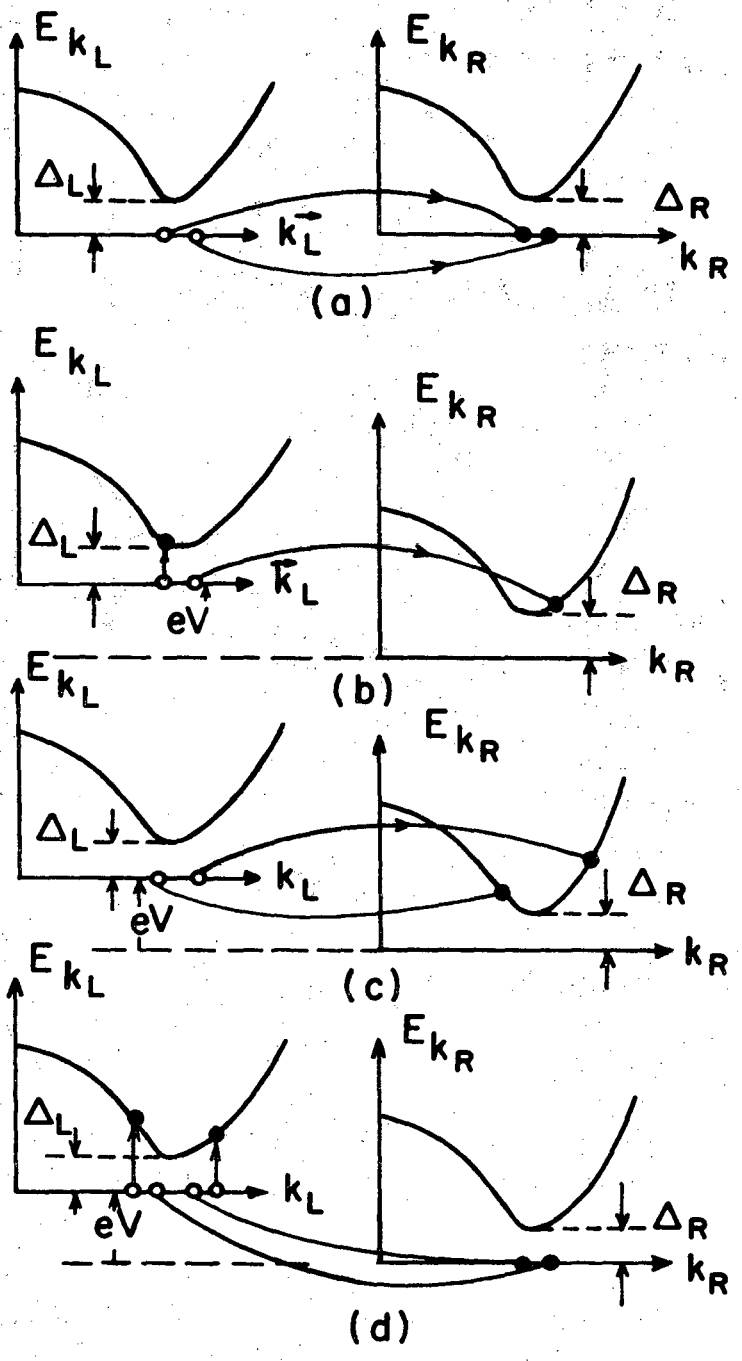

XBL706-3231

Fig. 3

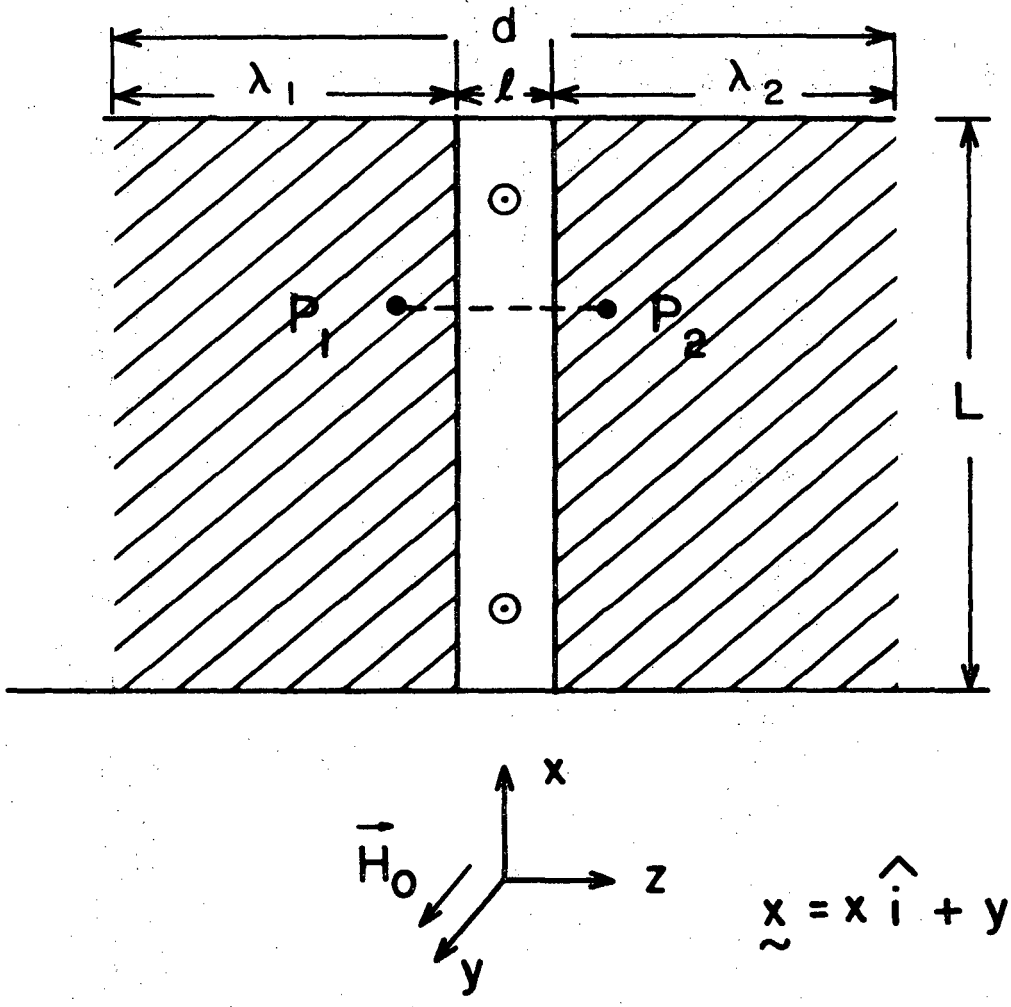

XBL706-3233

Fig. 4

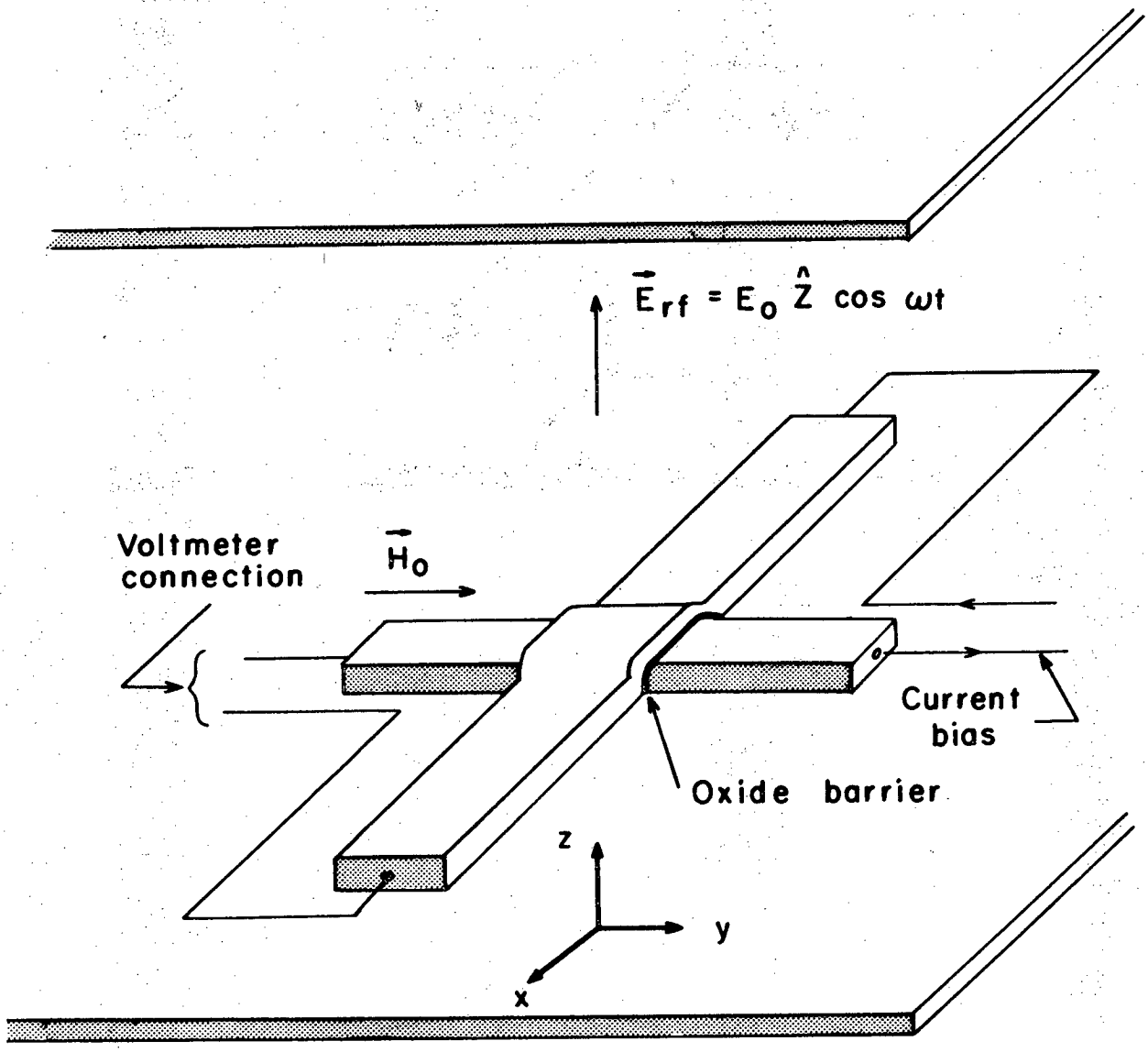

XBL706-3229

Fig. 5

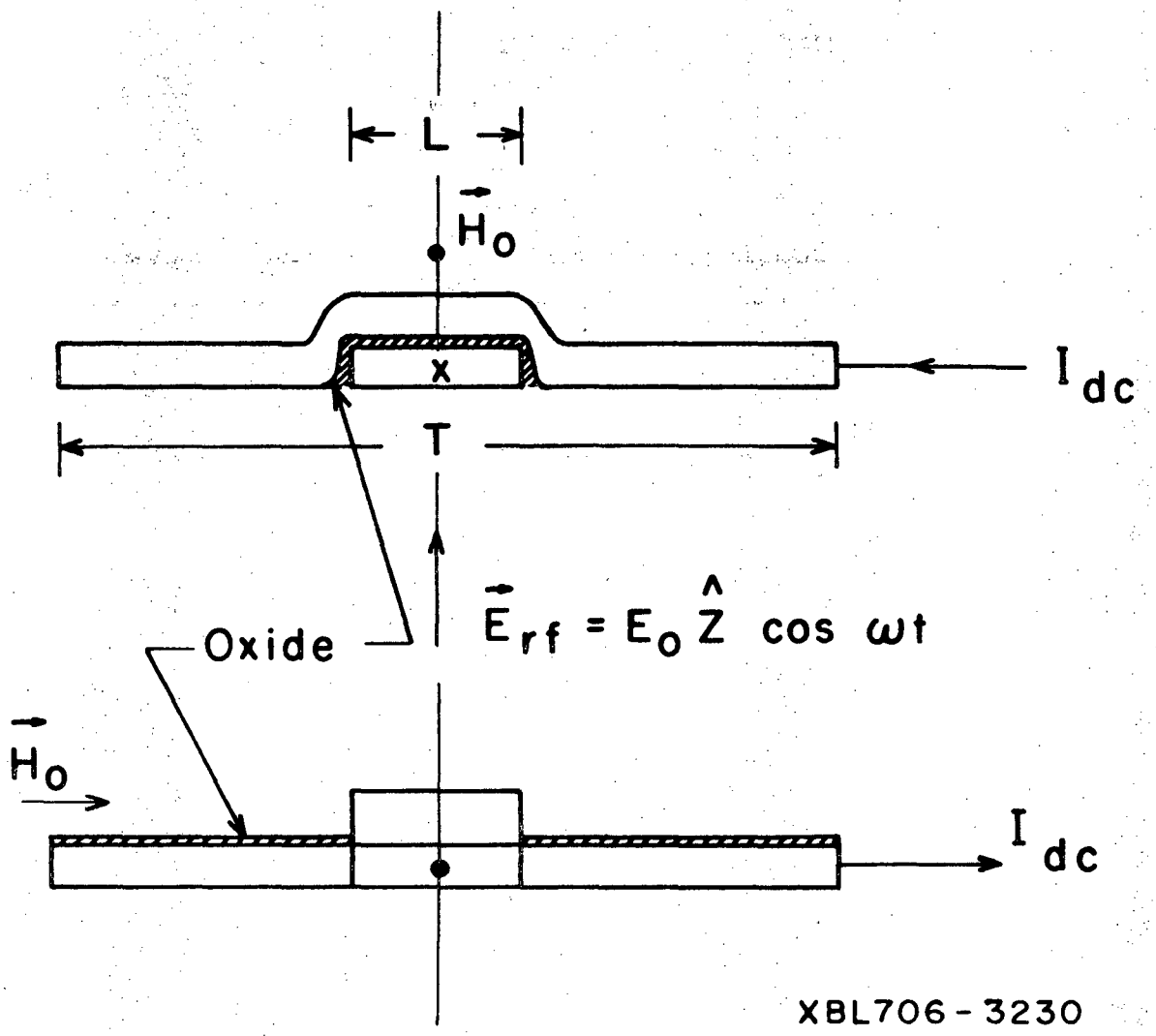
L
$\vec{H}_o$
x
I_{dc}
T
$\vec{E}_{rf} = E_o \hat{Z} \cos \omega t$
Oxide
$\vec{H}_o$
I_{dc}
XBL706-3230

Fig. 6

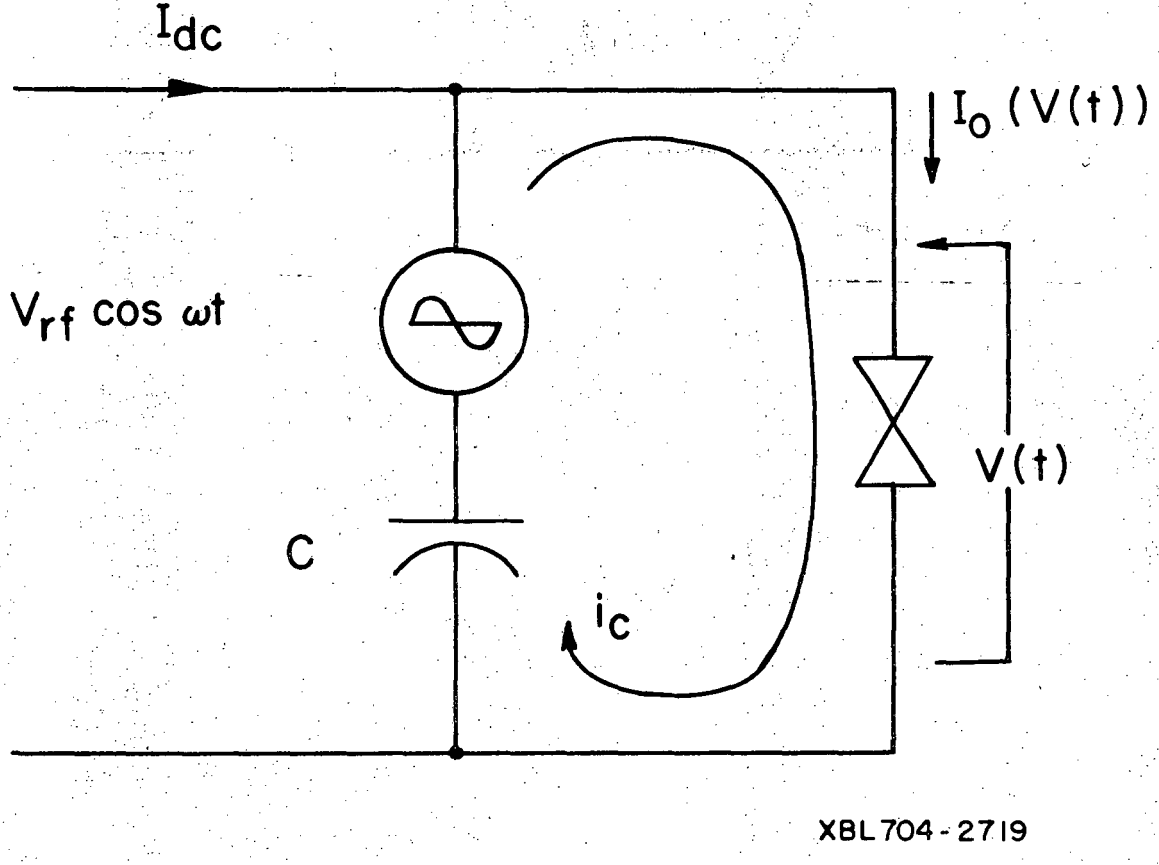

Fig. 7

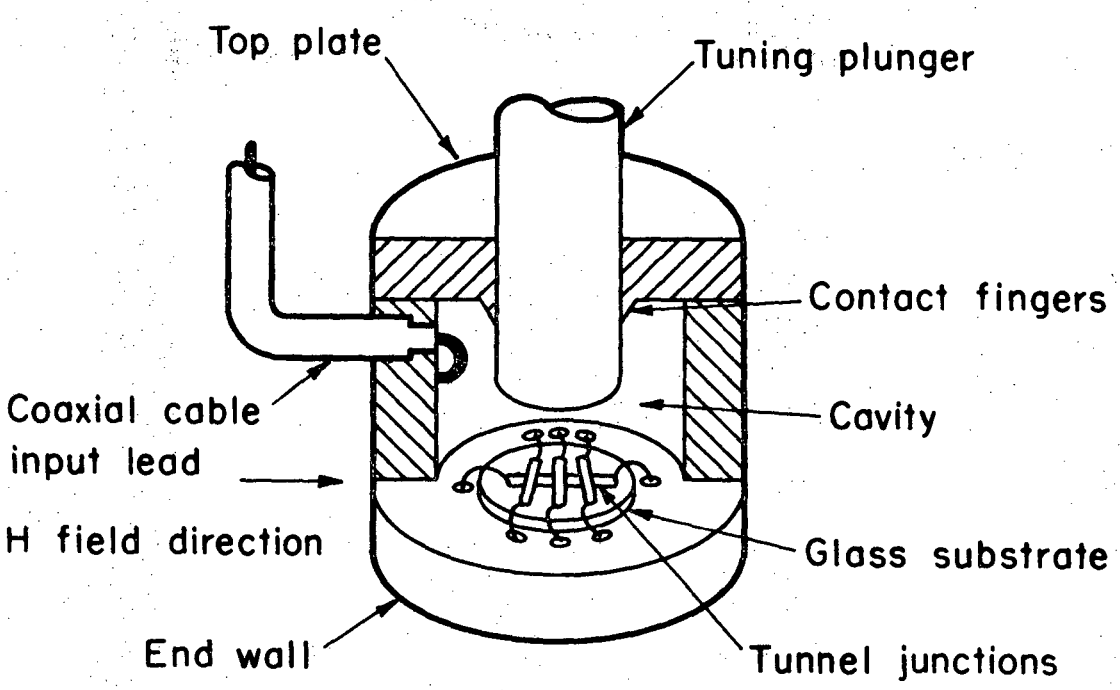
Top plate
Tuning plunger
Contact fingers
Coaxial cable
input lead
Cavity
H field direction
Glass substrate
End wall
Tunnel junctions
XBL 6911-6212

Fig. 8

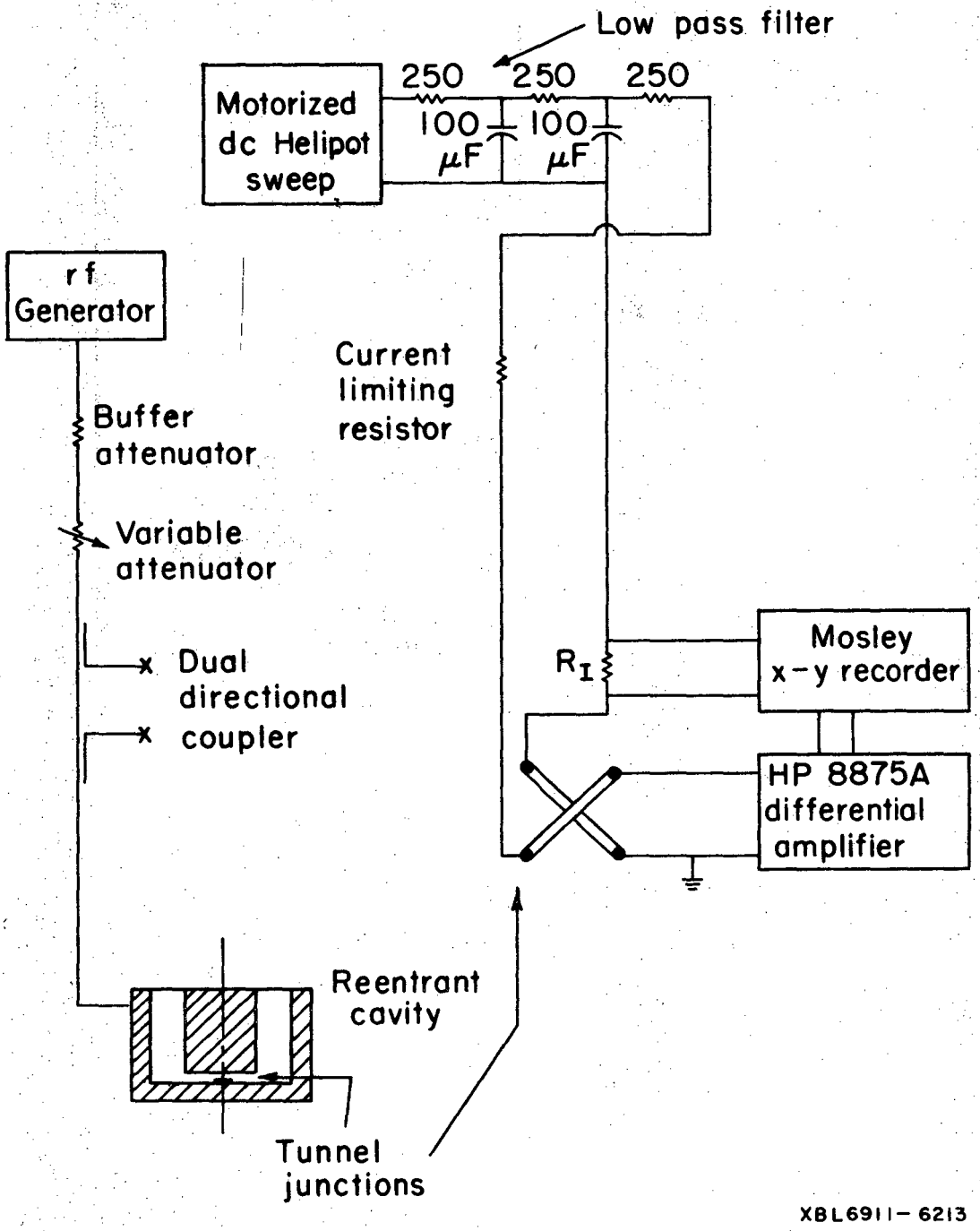
Low pass filter
Motorized dc Helipot sweep
250
250
250
100 μF
100 μF
r f Generator
Current limiting resistor
Buffer attenuator
Variable attenuator
Dual directional coupler
R_I
Mosley x-y recorder
HP 8875A differential amplifier
Reentrant cavity
Tunnel junctions
XBL6911-6213

Fig. 9

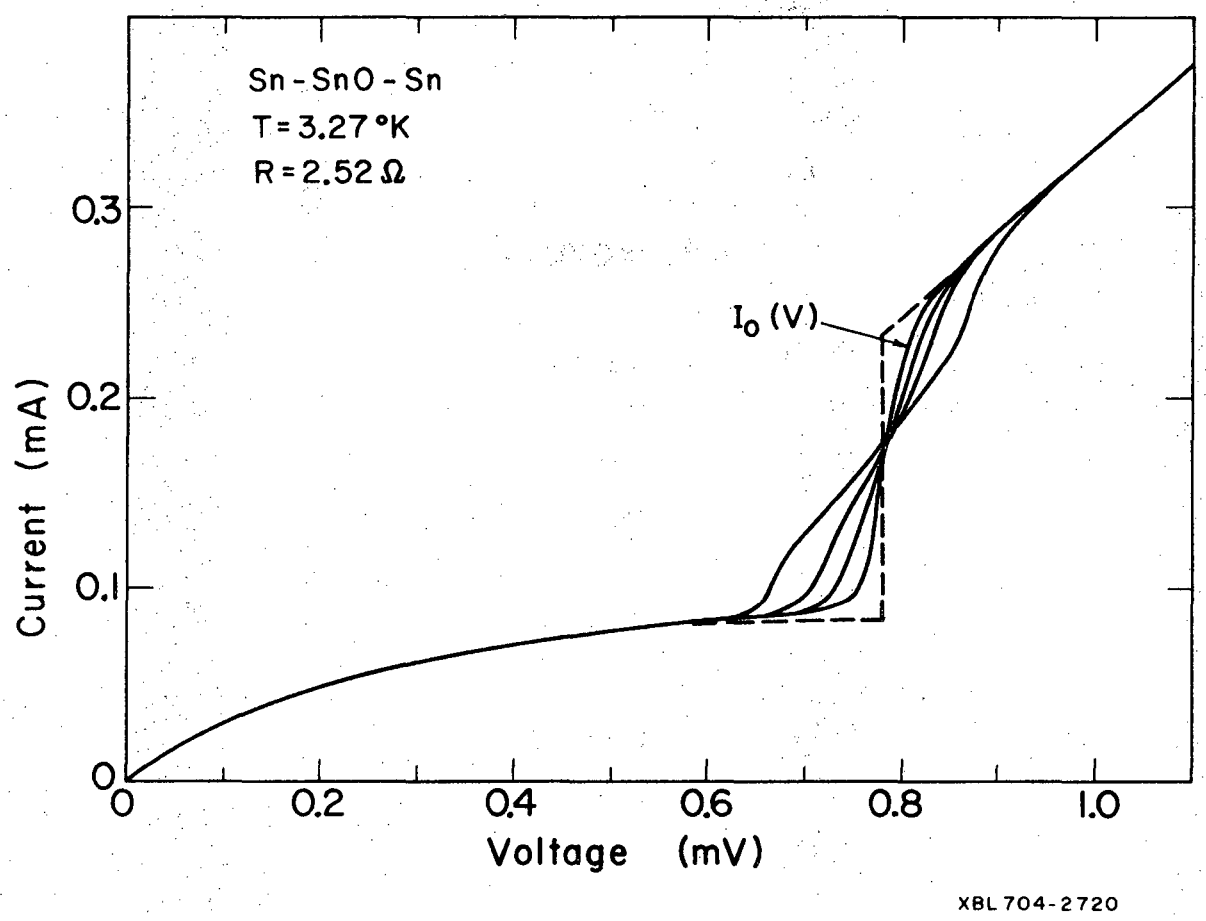
Sn - SnO - Sn
T = 3.27 °K
R = 2.52 Ω
I_o (V)
Current (mA)
0
0.1
0.2
0.3
0
0.2
0.4
0.6
0.8
1.0
Voltage (mV)
XBL 704-2720

Fig. 10

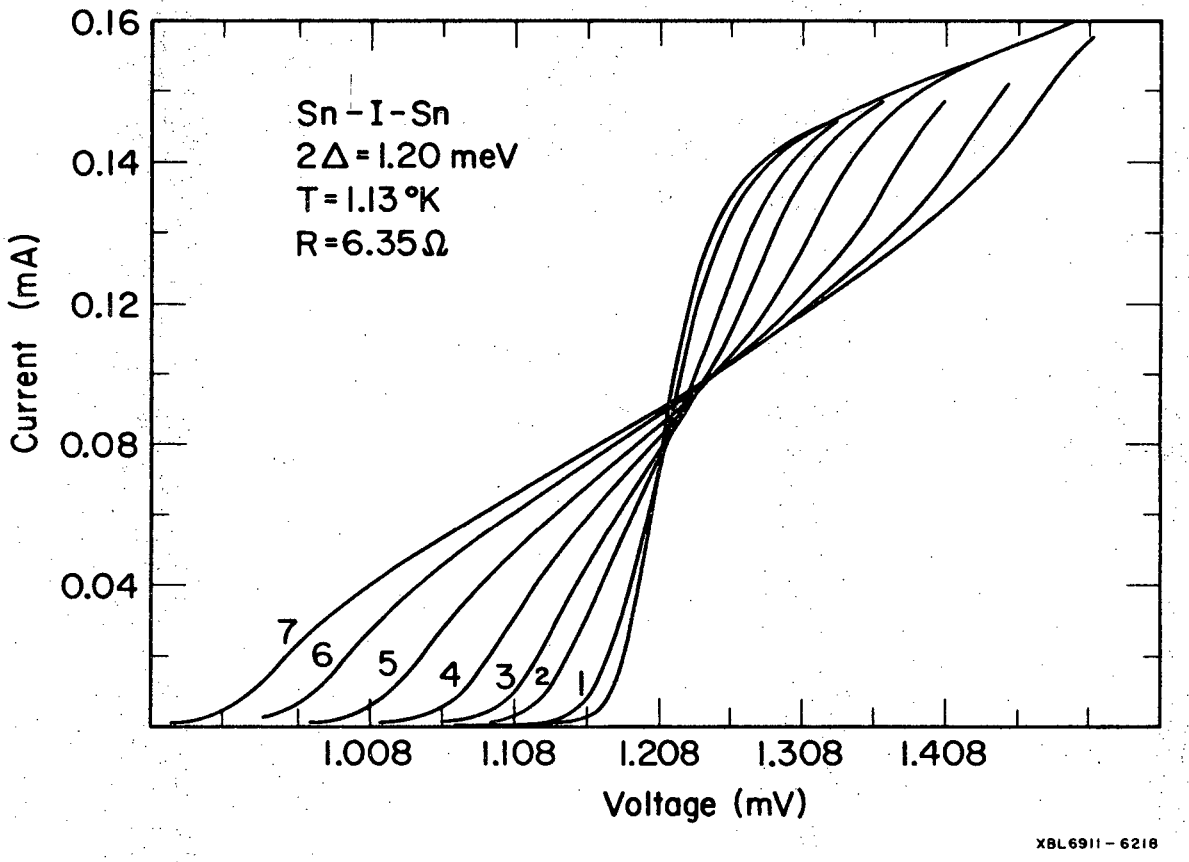
Sn - I - Sn
2Δ = 1.20 meV
T = 1.13 °K
R = 6.35 Ω
Current (mA)
0.16
0.14
0.12
0.08
0.04
1.008
1.108
1.208
1.308
1.408
Voltage (mV)
7
6
5
4
3
2
1
XBL6911 - 6218

Fig. 11

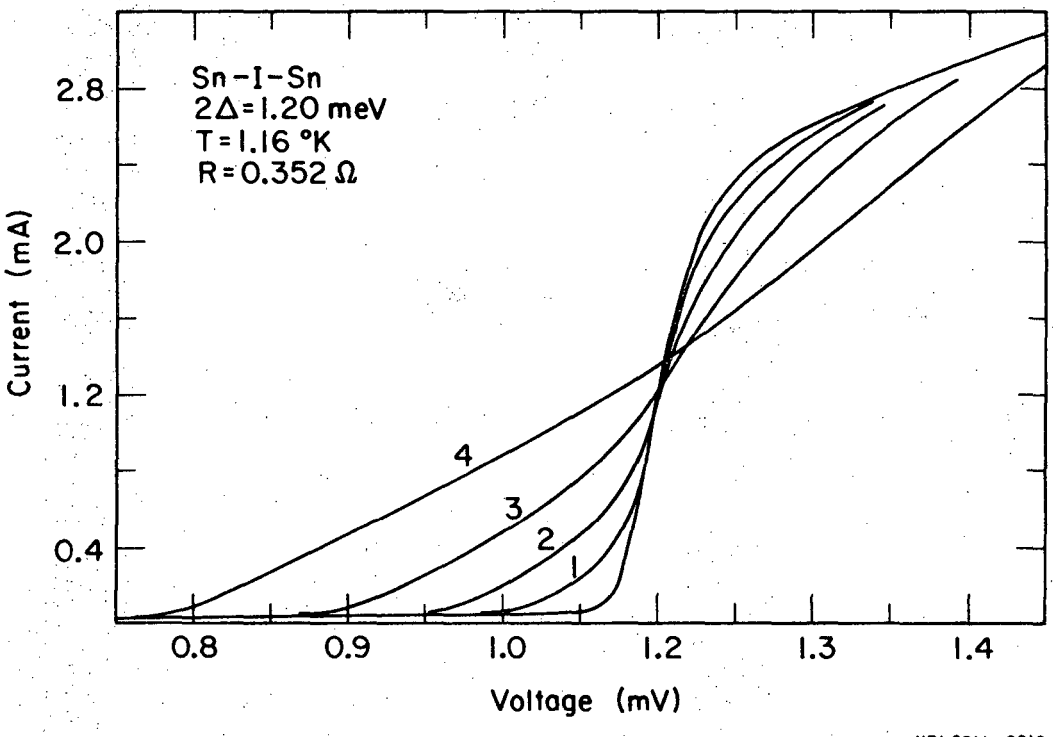
Sn-I-Sn
2Δ=1.20 meV
T=1.16 °K
R=0.352 Ω
Current (mA)
2.8
2.0
1.2
0.4
0.8
0.9
1.0
1.2
1.3
1.4
Voltage (mV)
4
3
2
1
XBL6911-6216

Fig. 12

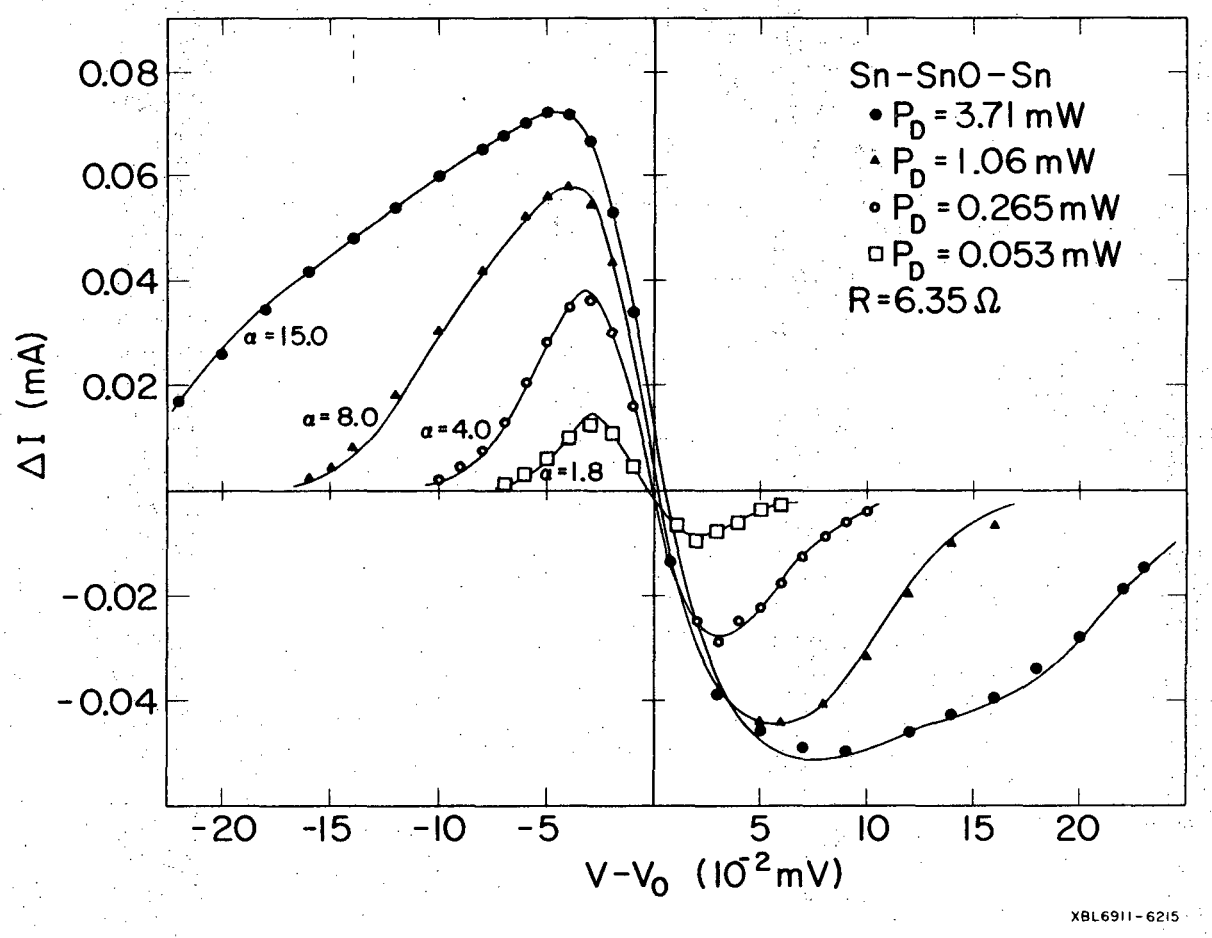
Sn-SnO-Sn
P_D = 3.71 mW
P_D = 1.06 mW
P_D = 0.265 mW
P_D = 0.053 mW
R = 6.35 Ω
α = 15.0
α = 8.0
α = 4.0
α = 1.8
ΔI (mA)
0.08
0.06
0.04
0.02
-0.02
-0.04
-20
-15
-10
-5
5
10
15
20
V-V$_0$ (10^{-2}mV)
XBL6911-6215

Fig. 13

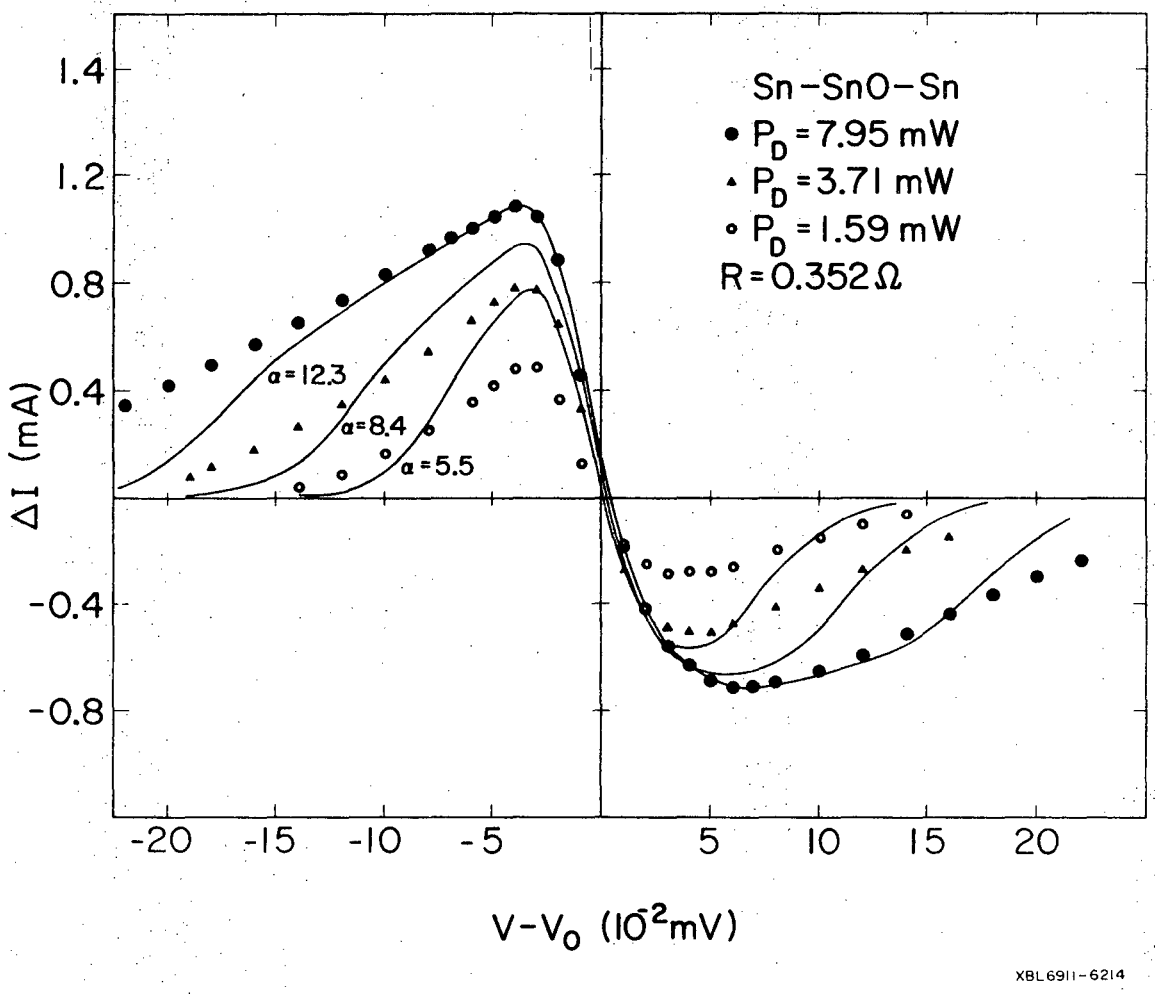
Sn-SnO-Sn
● P_D = 7.95 mW
▲ P_D = 3.71 mW
○ P_D = 1.59 mW
R = 0.352 Ω
α = 12.3
α = 8.4
α = 5.5
ΔI (mA)
1.4
1.2
0.8
0.4
-0.4
-0.8
-20
-15
-10
-5
5
10
15
20
V-V$_0$ (10^{-2}mV)
XBL6911-6214

Fig. 14

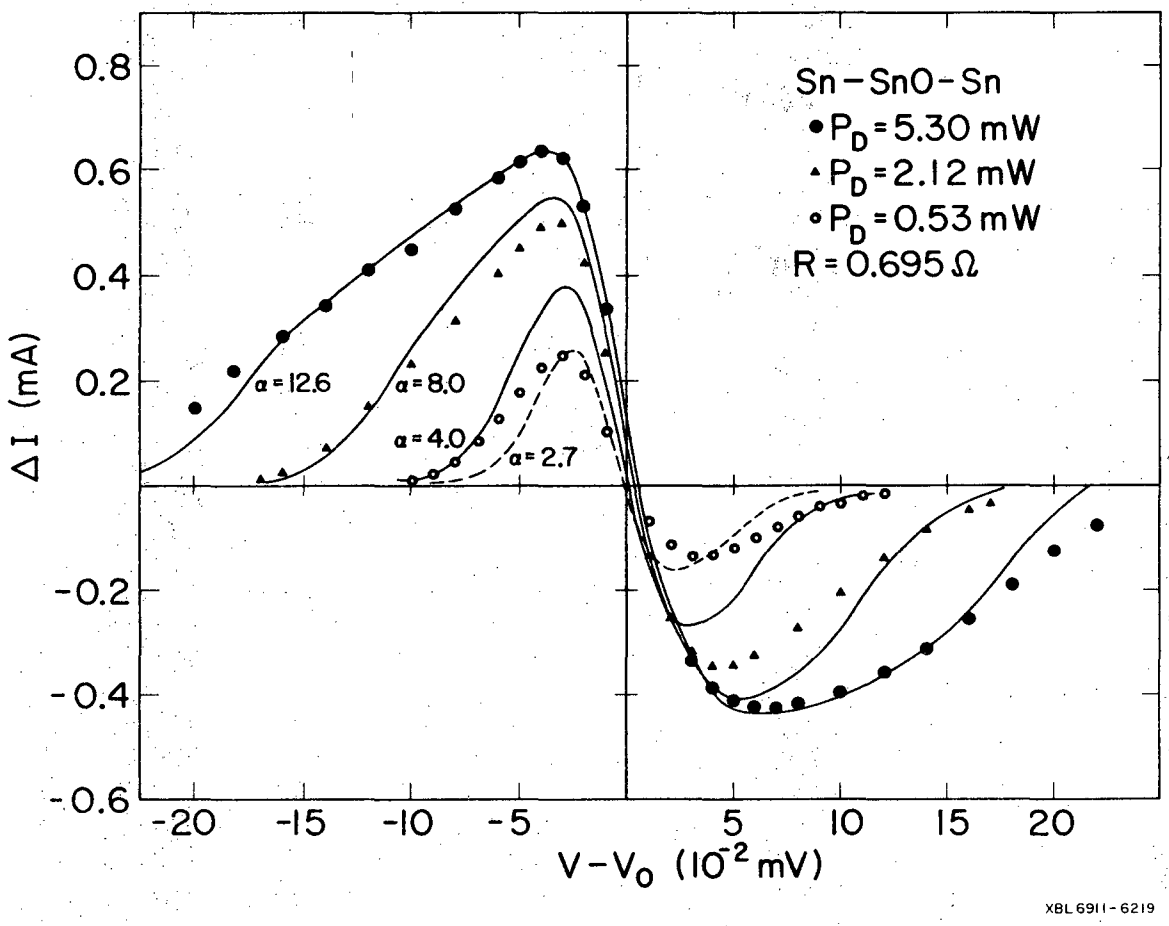
Sn – SnO – Sn
● P_D = 5.30 mW
▲ P_D = 2.12 mW
○ P_D = 0.53 mW
R = 0.695 Ω
α = 12.6
α = 8.0
α = 4.0
α = 2.7
ΔI (mA)
0.8
0.6
0.4
0.2
-0.2
-0.4
-0.6
-20
-15
-10
-5
5
10
15
20
V – V₀ (10⁻² mV)
XBL 6911 - 6219

Fig. 15

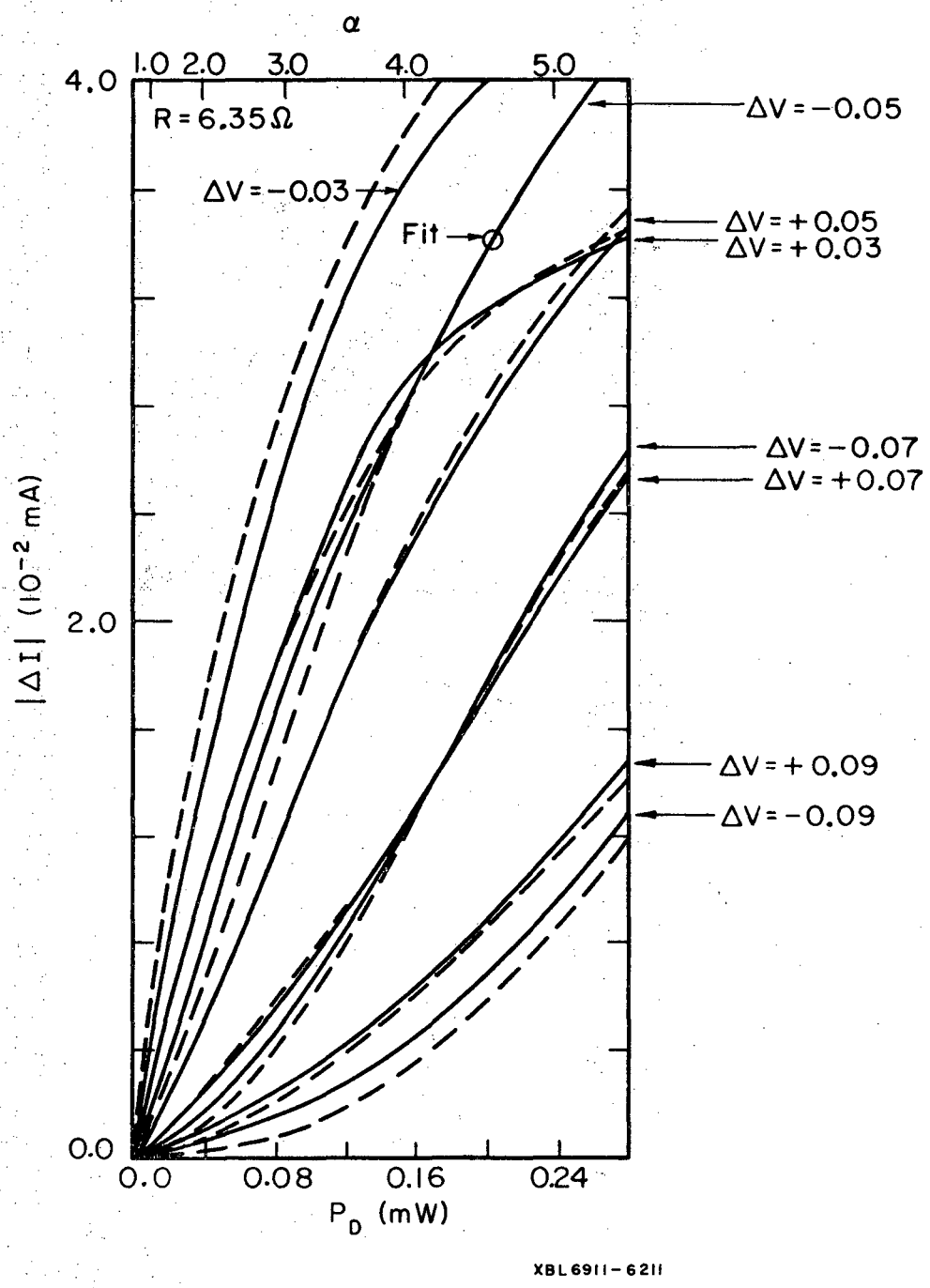
α
1.0 2.0 3.0 4.0 5.0
4.0
R = 6.35 Ω
ΔV = −0.05
ΔV = −0.03
Fit
ΔV = +0.05
ΔV = +0.03
ΔV = −0.07
ΔV = +0.07
ΔV = +0.09
ΔV = −0.09
|ΔI| (10⁻² mA)
2.0
0.0
0.0 0.08 0.16 0.24
P_D (mW)
XBL6911-6211

Fig. 16

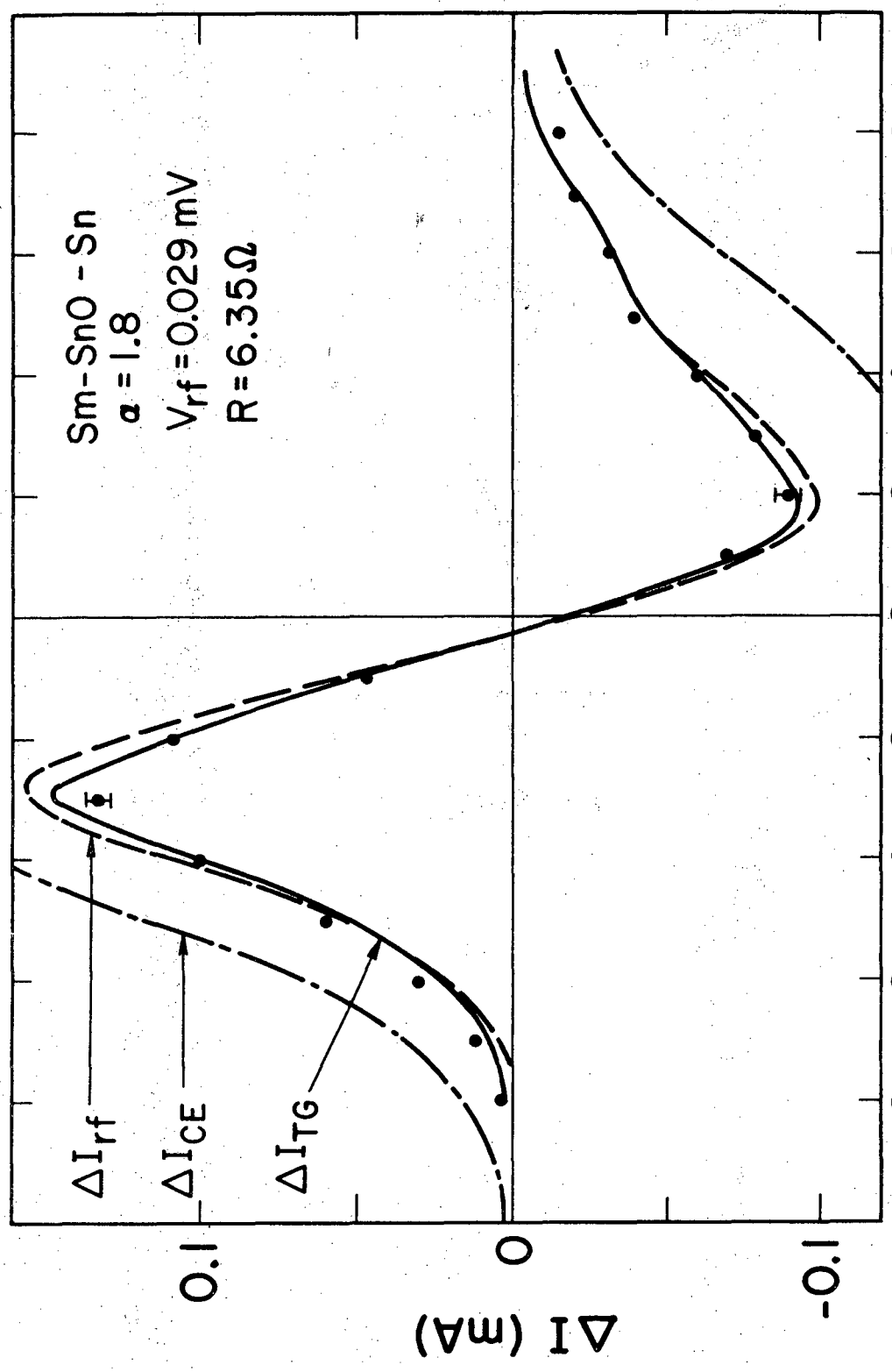

XBL 704-2725

Fig. 17

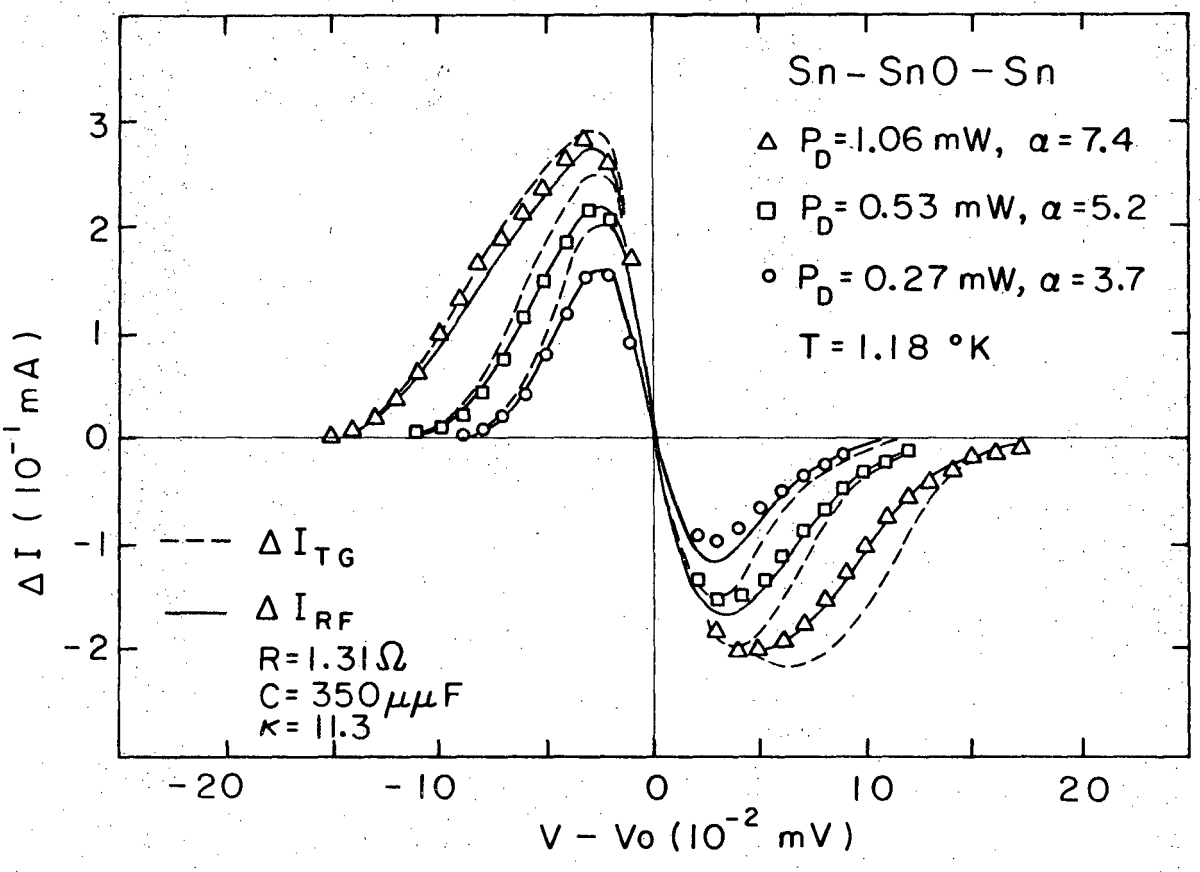

XBL707-3318

Fig. 18

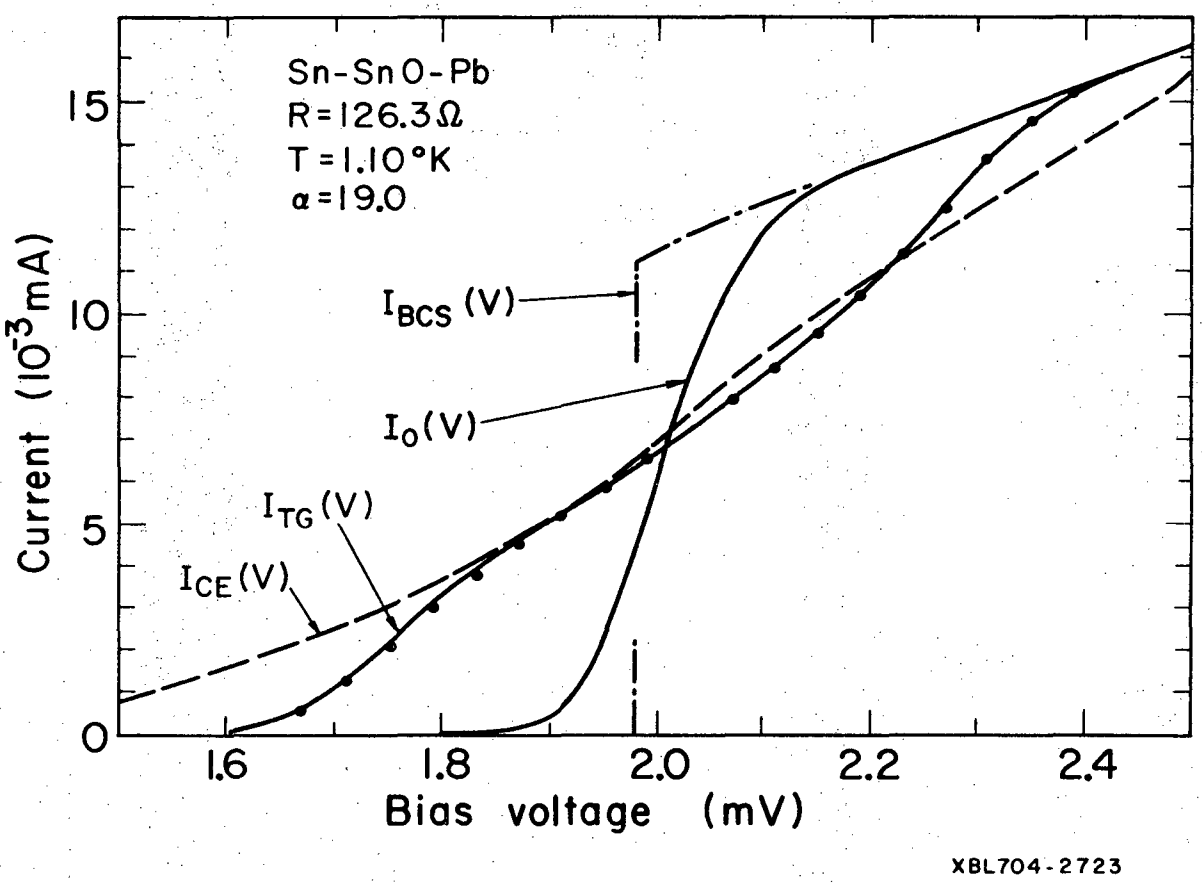
Sn-SnO-Pb
R=126.3Ω
T=1.10°K
α=19.0
I_{BCS} (V)
I_0(V)
I_{TG}(V)
I_{CE}(V)
Current (10^{-3}mA)
0
5
10
15
1.6
1.8
2.0
2.2
2.4
Bias voltage (mV)
XBL704-2723

Fig. 19

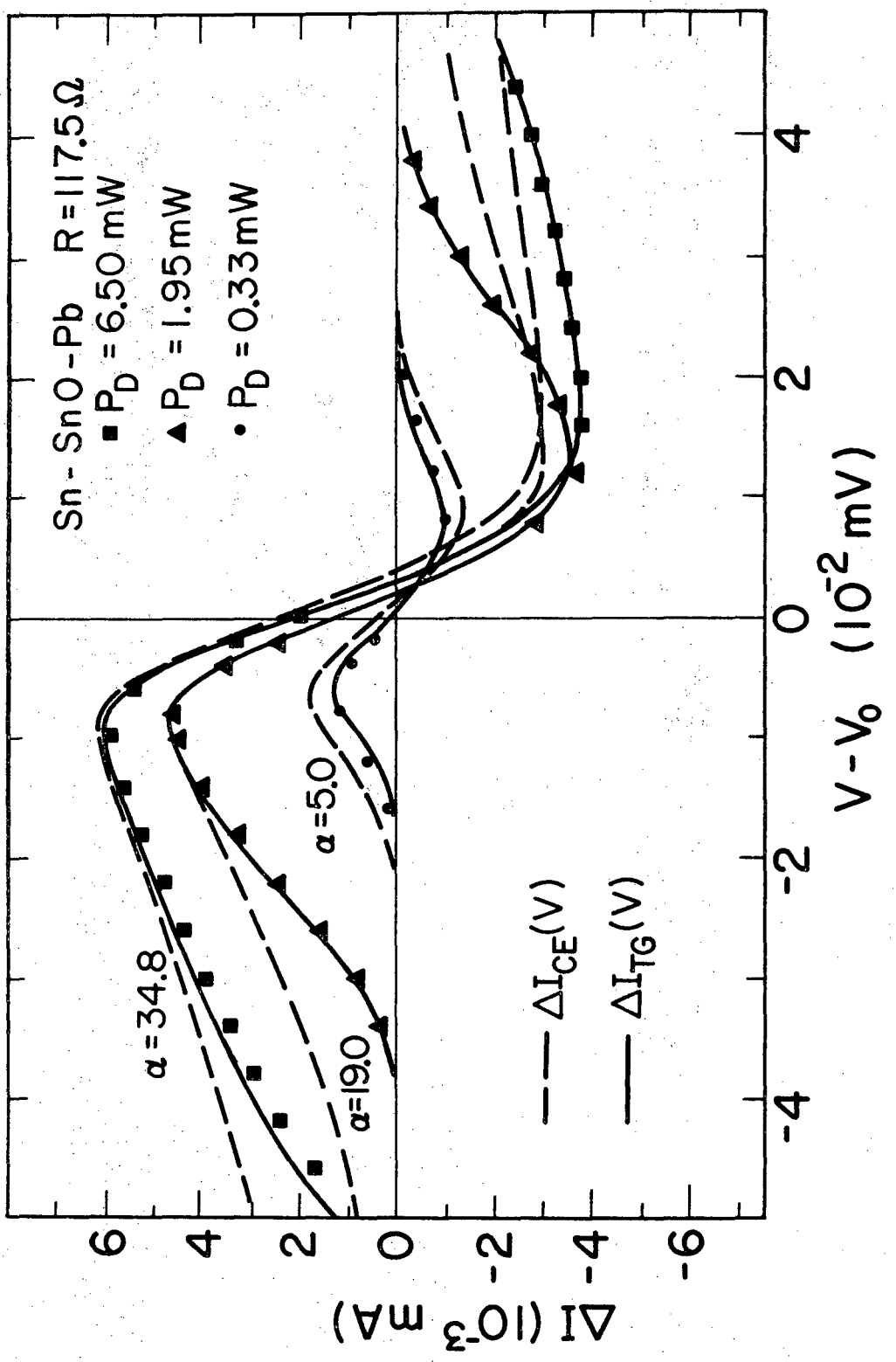

XBL704-2724

Fig. 20

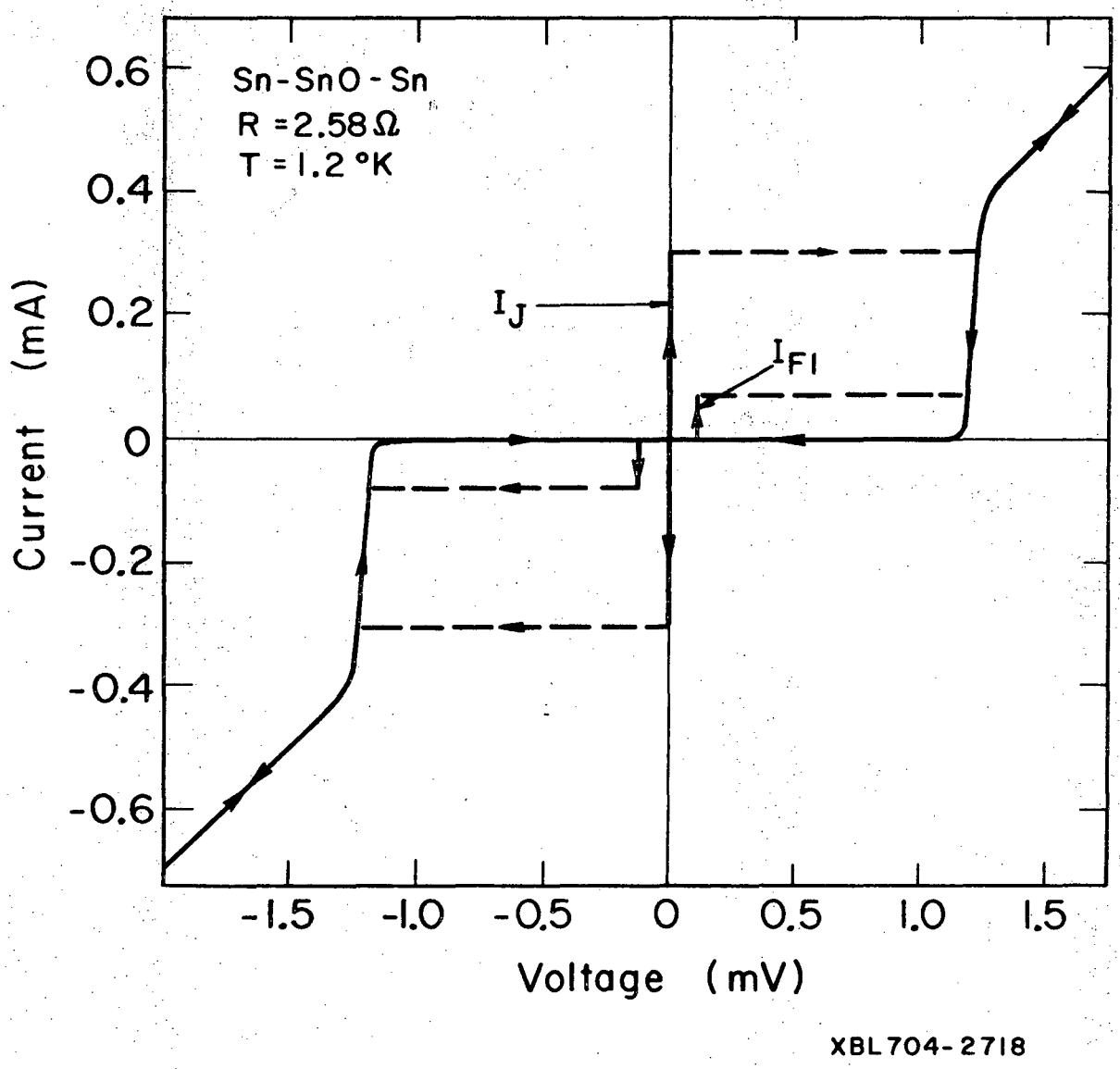
Sn-SnO-Sn
R = 2.58 Ω
T = 1.2 °K
I_J
I_{FI}
Current (mA)
0.6
0.4
0.2
0
-0.2
-0.4
-0.6
-1.5
-1.0
-0.5
0
0.5
1.0
1.5
Voltage (mV)
XBL704-2718

Fig. 21

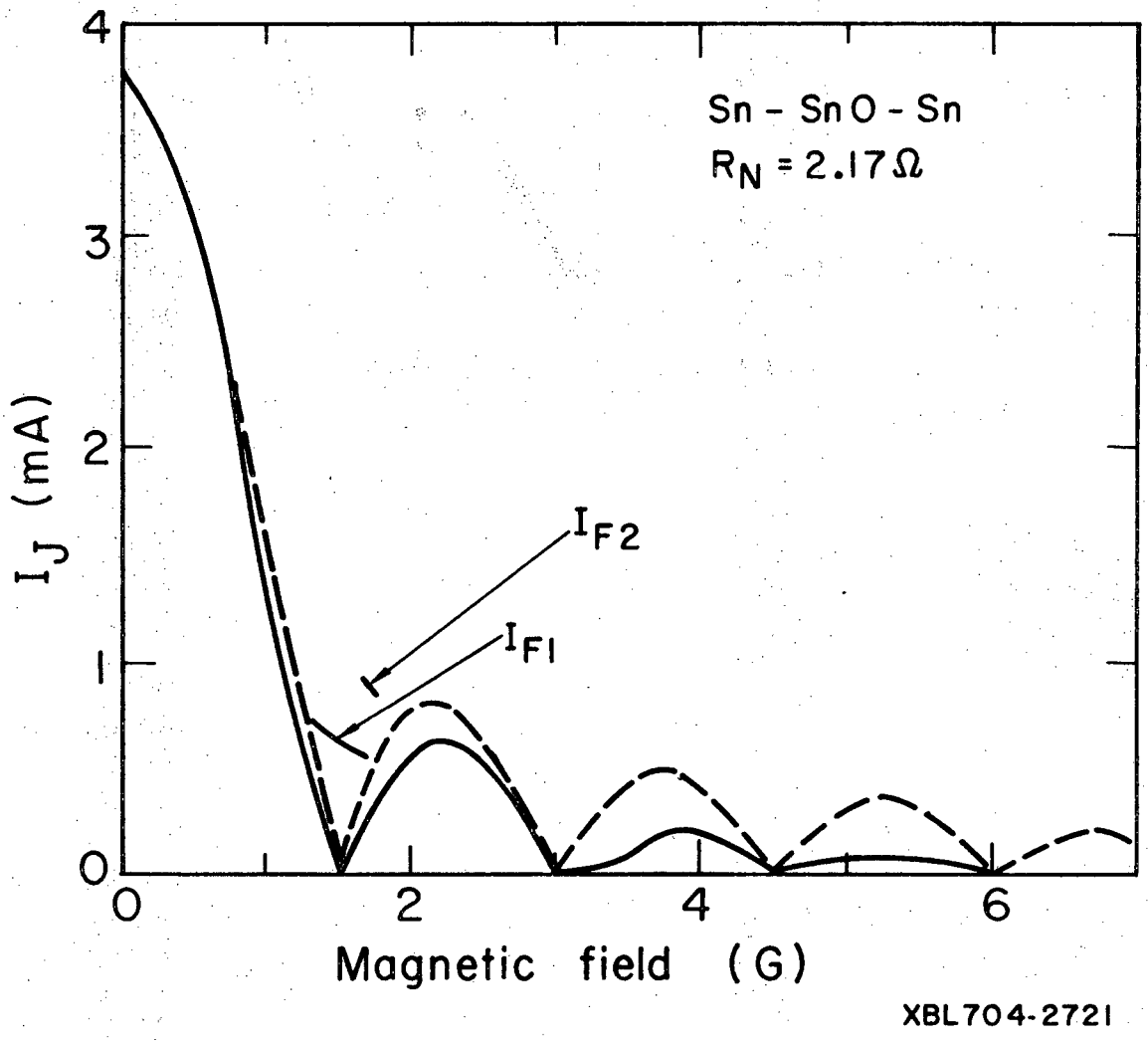
Sn - SnO - Sn
$R_N = 2.17\,\Omega$
I_{F2}
I_{F1}
I_J (mA)
Magnetic field (G)
0
1
2
3
4
0
2
4
6
XBL704-2721

Fig. 22

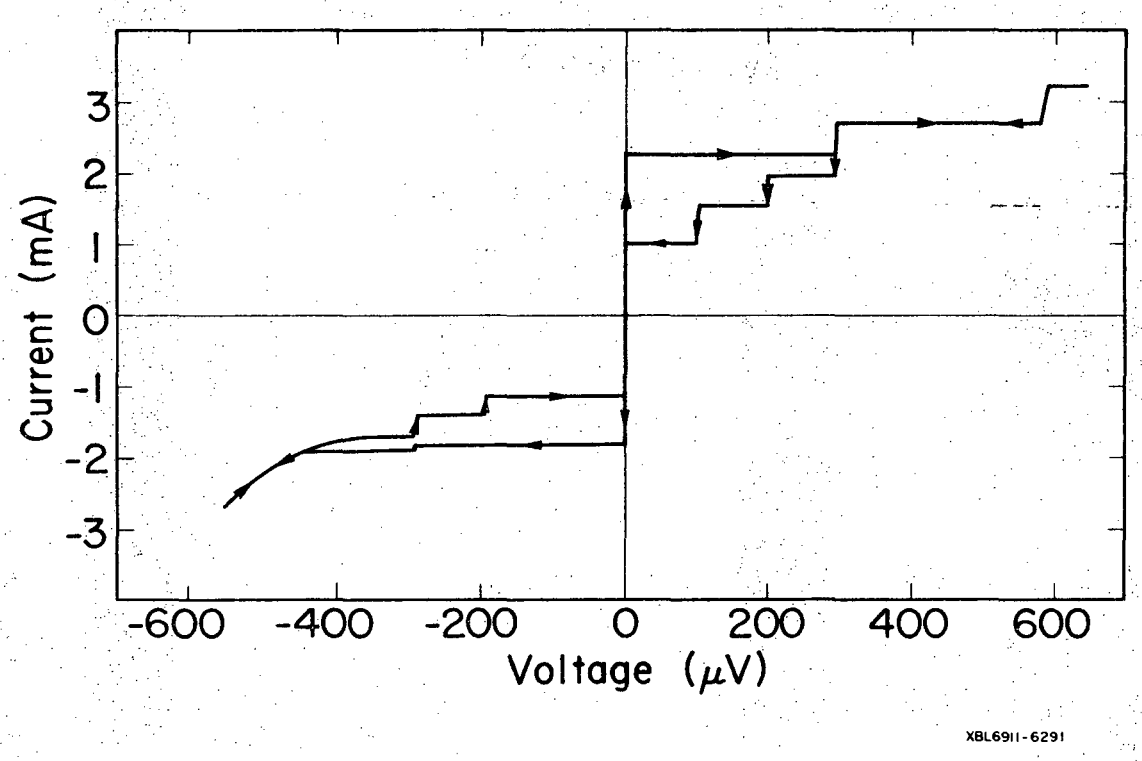
Current (mA)
3
2
1
0
-1
-2
-3
-600
-400
-200
0
200
400
600
Voltage (μV)
XBL6911-6291

Fig. 23

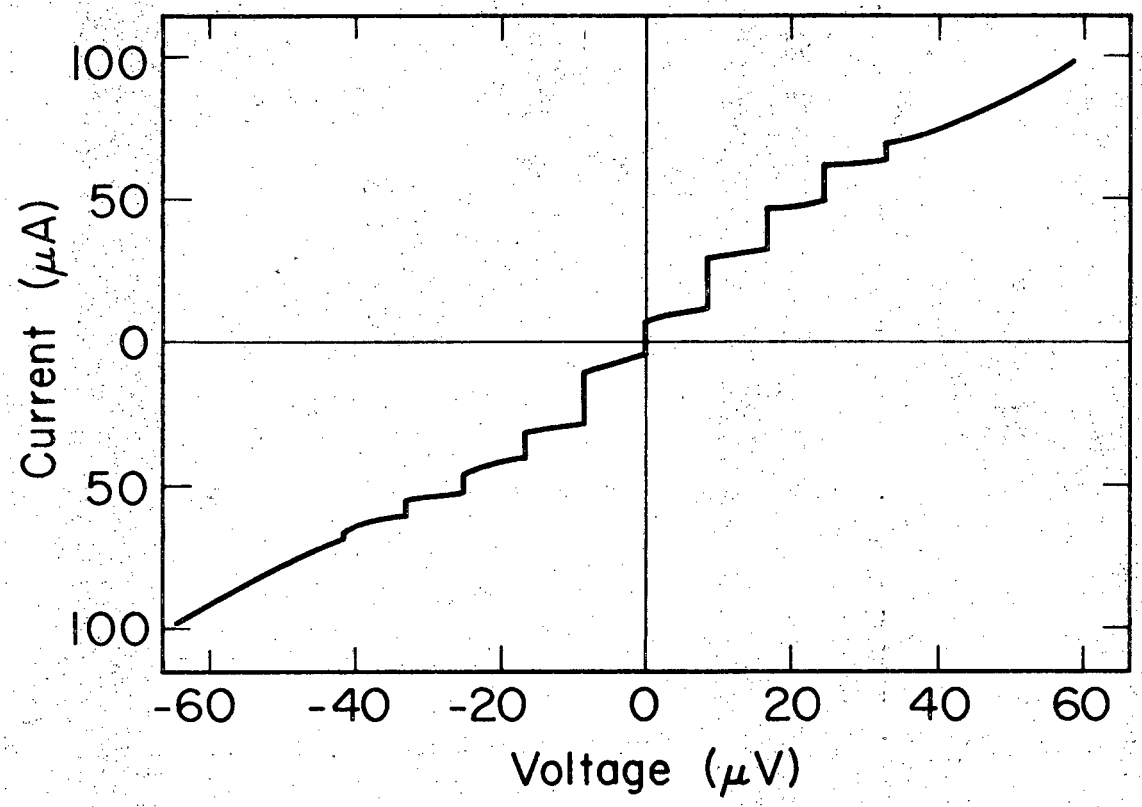

XBL6911-6288

Fig. 24

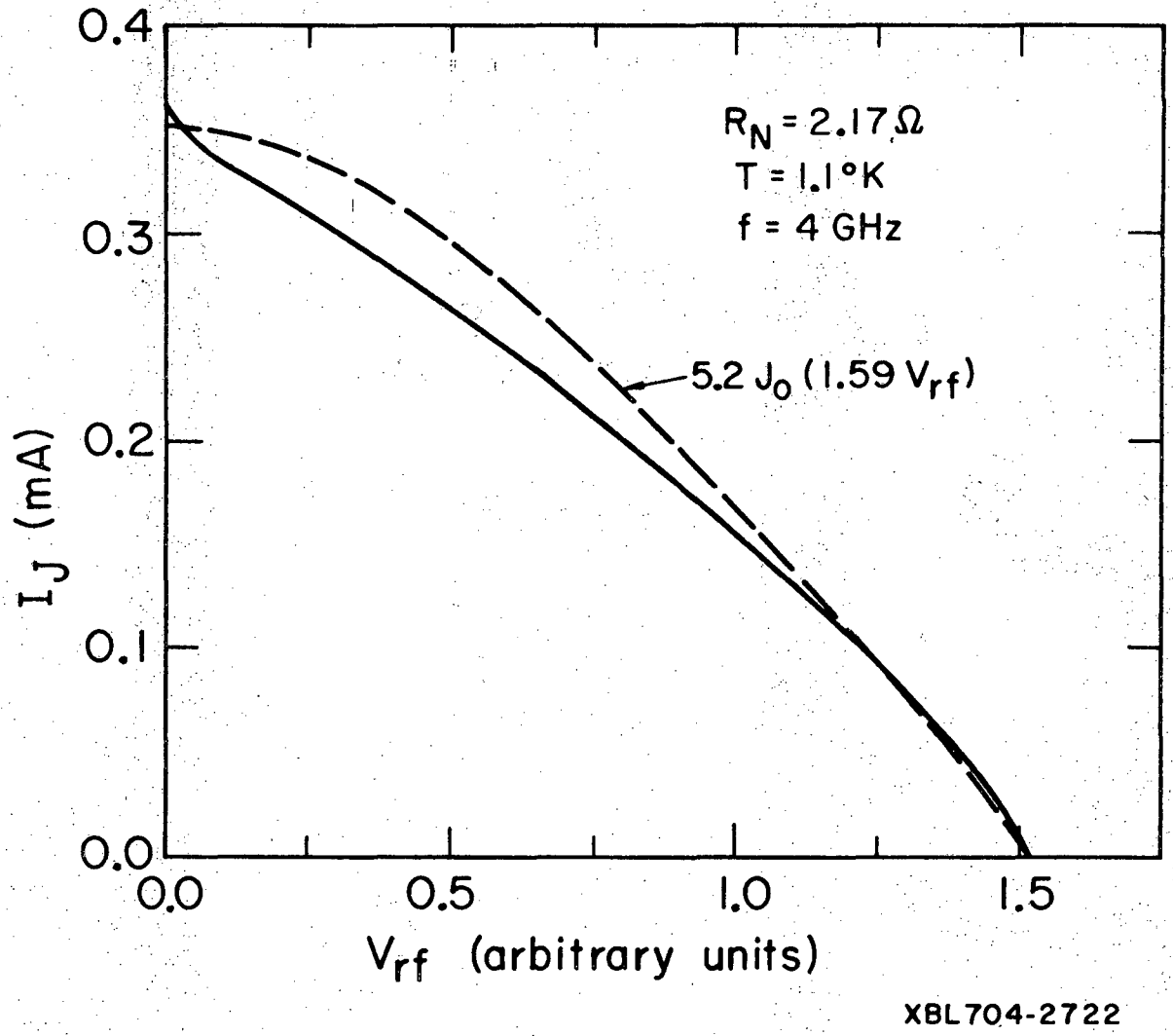
0.4
0.3
0.2
0.1
0.0
I_J (mA)
$R_N = 2.17\,\Omega$
T = 1.1°K
f = 4 GHz
$5.2\,J_0\,(1.59\,V_{rf})$
0.0
0.5
1.0
1.5
V_{rf} (arbitrary units)
XBL704-2722

Fig. 25

TECHNICAL INFORMATION DIVISION
LAWRENCE RADIATION LABORATORY
UNIVERSITY OF CALIFORNIA
BERKELEY, CALIFORNIA 94720